ORIGIN, TRANSPORT AND BURIAL OF ORGANIC MATTER IN THE WHITTARD CANYON, NORTH-EAST ATLANTIC

A thesis submitted in partial fulfilment of the requirements of Liverpool John Moores University for the degree of Doctor of Philosophy

NOVEMBER, 2020

CATHERINE ELIZABETH KERSHAW

CONTENTS

LIST OF TABLES

LIST OF FIGURES

ABSTRACT

The Whittard submarine canyon (Celtic Sea, North East Atlantic) is one of the largest (~100km across, down to 4500m depth) and most complex underwater features in the North-Western European Margin having several branches all converging to the main channel. It is located >200km from the nearest coast, affected by complex hydrodynamics and is home to an array of diverse benthic ecosystems. Little is known about how submarine canyons differ from typical open-ocean environments. This study aims to improve the understanding of the canyon's underlying role in biogeochemical cycling and carbon storage in relation to the sedimentological regime and specific geomorphic features. This study hypothesizes that the highly heterogeneous nature of the canyon's physical landscapes may influence organic matter spatial patterns and the potential for carbon burial. This project attempted to assess this gap in knowledge by examining morphological (slope analysis, ruggedness), grain size characteristics, and biogeochemical properties (organic carbon, nitrogen, $\delta^{13}C$ and $\delta^{15}N$ isotopes) of 46 short cores (0-10cm) from a variety of depths, across nine main locations (Western, Western Middle, Acesta, Eastern Middle, Eastern Middle 2, Intersection, Eastern, Explorer and the Main channel branches). Grain sizes often appear multimodal, with a sandy/silty/clay predominance, with coarse material present at depths exceeding 1000m, indicating that diverse processes are at play within the system. Surficial mean molar C/N ratios are variable but often higher than typical marine ranges; 22 ± 15.62, given the distance from land, this is likely a consequence of reworking. Organic carbon contents generally exceeded the typical range expected from the deep-sea (>~0.5% of dry

sediment) but are similar to other canyon systems that are closer to land, this may indicate an increased potential for carbon storage within the Whittard Canyon (Tyler et al., 2009b; Masson et al., 2010a). All samples within the central channel (Main Channel) at depths >3700m were organically enriched (>1.25%), this is likely an accumulation of organic material, funnelled from the upper canyon reaches. However, at one site of the Eastern branch (CE14009-005-450m), the lowest TOC content of 0.33% was recorded, indicating reduced input or the efficient recycling of organic matter. The majority of $\delta^{13}C‰$ values fell within the lighter isotopic range of ~-24‰ and ~-22‰, indicating phytoplankton and zooplankton derived organic matter. However, a heavier value was recorded at the connecting shelf of the Acesta and Eastern Middle branch CE16006-030-PSH12-511.37m (-12.76), indicating sulfide-oxidized carbon which is associated with the form II Rubisco pathway (Fry and Sherr, 1984; Levin and Michener, 2002; Hunter et al., 2013a). A mean $\delta^{15}N$ signature of 3.32‰ ± 0.84 falls just below the deep-water average of ~5‰ value associated with internal cycling and assimilation by marine primary producers (Sigman and Casciotti, 2001). This is in line with previous research within the Whittard Canyon, where values of 4.09‰ ± 2.42 and 3.94‰ ± 0.67 for West and Eastern branches were recorded (Hunter et al., 2013a). Statistical analyses were carried out to decipher influences of morphology, location (i.e. branch), depth and potential anthropogenic activity. Previous research has indicated that the Eastern branch displays high biodiversity and faunal abundance, results from all disciplines explored in this study confirmed that the Eastern branch was the most heterogeneous, which may explain this phenomenon (Amaro et al., 2015; Gunton et al., 2015). Recent work suggests that anthropogenic (i.e. fishing) activities may impact natural processes, possibly affecting material transport, deposition and ecological functions within the Acesta and Eastern Middle branches, that would take many years to recover (Wilson et

al., 2015). Because of this, this study proves useful as it provides one of the highest resolution accounts of recent conditions across this environmentally and biologically diverse canyon system.

DECLARATION

I declare that this thesis has been composed solely by myself and that it has not been submitted, in whole or in part, in any previous application for a degree. Except where states otherwise by reference or acknowledgment, the work presented is entirely my own carried out in the Faculty of Science, Liverpool John Moores University from 16th September 2014 to 14th November 2020, under the supervision of Doctor Kostas Kiriakoulakis.

Catherine Elizabeth Kershaw 12/11/20

ACKNOWLEDGMENTS

Firstly, I would like to express my most profound appreciation to my supervisor Dr. Kostas Kiriakoulakis. My life would have taken another path if it were not for you. You saw the biogeochemist in me that I did not know existed. While you trusted me to work independently, you offered wisdom, guidance, and support whenever I was in need. For these reasons, I will always be grateful.

Many thanks must go to Dr. Jason Kirby, Dr. Jon Dick and all the colleagues and lecturers I have had the pleasure to meet at Liverpool John Moores. Thank you for the many hours of feedback, advice, and comments you have provided. It has been invaluable to my research and you have helped me to become a better scientist. My sincere gratitude also extends to the School of Biological and Environmental Sciences at Liverpool John Moores for funding this project and making it possible for me to carry this research out.

I would also like to thank all who had an integral role in collecting and processing my data. Special thanks go to the principal scientists and crew of *RV Celtic Explorer* CE13008, CE14009, CE16006 and *RRS James Cook* JC125 cruises. Thank you to Dr. Louise Allcock and Dr. Martin White of the National University of Ireland Galway, for my first, and very positive, experience at sea. I was a dopey undergraduate at the time, but under your wings, I was inspired to do something I had never thought I was capable of. I would also like to express my deepest gratitude to Dr. Veerle Huvenne and all the academics at the National Oceanography Centre for collecting samples on my behalf and for welcoming me within the scientific community. Thank you also to Dr. Teresa Amaro for allowing me to contribute to my first scientific paper and for the valuable information that you provided.

I owe a great deal to all the senior technicians that made this study possible. Without your crucial role in helping me analyze my samples, I would not be able to submit this work. Thank you to Sabena Blackbird and Jim Ball for making me feel at home at the University of Liverpool. Thanks, must also go to Nicola Dempster of Liverpool John Moores. Thank you for training me to use the GC/MS, while my lipid work is not included in this study, the knowledge I have gained will undoubtedly be useful in the future. Likewise, I am incredibly grateful to Dave Williams and Hazel Clark who have become family during my time at Liverpool John Moores. During difficult times, your thoughtfulness and kindness often kept me going. Thank you to Dave for being a wizard on the Skalar and for keeping me company during some long stints of analysis. Hazel, I have learnt a lot during my time at university, but one of the things that have become evident is how much more I could learn from you. Thank you for the Lady Grey tea, for improving my grammar, for elevating me and pulling me up on things I may get wrong.

Special thanks must also go to the many beautiful friends I have made during my time at Liverpool John Moores. Dr. Emma Smith, thank you for showing me the ropes, for being a constant source of inspiration and for always being an uplifting presence. Thank you also to Hollie Ball and Tom Vincent for your advice and support, but also for just being “really sound”. Thank you for talking about things that are not always science-related and for being there when I needed a friend. Thank you to my dearest Irish loves, Dr. Jessica Franklin, Declan Morrisey, Morag Taite and Dr. Annette Wilson. You made my time at sea so enjoyable and I am forever grateful that we remained friends on land. Meeting friends like you was never guaranteed, but it was undoubtedly the icing on the cake.

I would also like to thank my friends and family for your support these last years. My sister

Frances deserves special mention. Thank you for your unfaltering love and encouragement during my doctoral studies. Thank you for being there when I am in crisis, for the endless cups of coffee, and mostly, thank you for looking after Marina when I need to write. To my parents, thank you for preparing me for this journey, which would not have been possible without you.

Lastly, thank you to my dear Ben. You have acted as the most supportive husband I could have hoped for. Thank you for chauffeuring me to and from university, discussing my research, putting up with my neurotic tendencies and for never doubting my ability. Pursuing a PhD requires a great deal of attention and there have been occasions where this has impacted our personal life. However, despite this, you have offered unwavering reassurance, love and comfort. While it may seem like I have done this PhD for myself, I want you to know that everything I have done is for you and our daughter Marina.

Chapter 1: Submarine canyons

1.1 Introduction

Submarine canyons are abundant and ubiquitous incisions found along continental and oceanic island margins, connecting the continental shelves to deep ocean basins (Shepard and Dill, 1966). Recent bathymetric data analysed by Harris and Whiteway (2011) revealed that there are 5,849 separate large submarine canyons in the world ocean, with active continental margins containing 50% more canyons than passive margins (Figure 1:1). Canyons are typically closely spaced, steeper, shorter and more dendritic on active than passive margins. The global distribution of all canyons is estimated to be over 9,000, covering approximately 11% of the continental margins (Harris et al., 2014a). They are complex, heterogeneous, topographic features, characterised as being broad, deep valleys with intricate relief and highly dynamic sedimentary and hydrodynamic characteristics. The complexity of canyons results in an environment that differs significantly from the majority of the deep-sea, with rich and varied biological communities being able to establish and thrive in many canyons globally (Tyler et al. 2009). Steep topography renders conventional shipboard mapping and sampling techniques inadequate, due to the inaccessibility of these sites, with the result that many questions regarding their global role in maintaining biodiversity/productivity and in storing and transporting minerals and organic matter remain largely unanswered. However, recent advances in technology, such as dynamic positioning of research vessels and precisely controlled remotely operated vehicles (ROVs), have rendered their study a possibility (Huvenne et al., 2011).

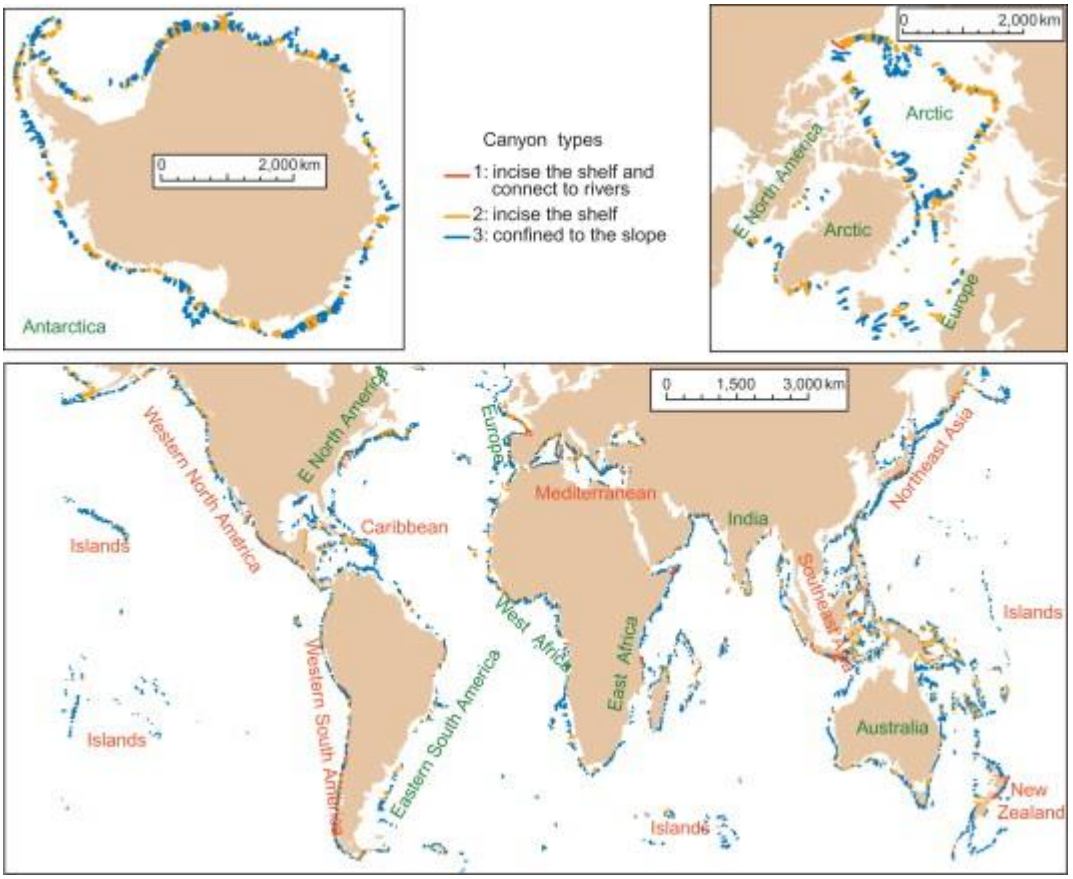

Figure 1:1 Global distribution of large submarine canyons, as classified by Harris and Whiteway (2011). Active continental margins are labelled in red, passive margins in green (figure courtesy of Harris and Baker, 2012).

1.1.1 Submarine carbon and ecosystems

The complexity of the physical environment of submarine canyons is often mirrored by rich and varied biological communities that inhabit them compared to continental slopes (Tyler et al., 2009a; Amaro et al., 2016a). This is likely to be a result of a localised increase in organic matter, food availability, and quality compared to other deep-water environments, in part due to the hydrodynamic regimes within some canyons.

Within the open ocean, the sinking of marine organic matter (OM) produced in the euphotic zone through the mesopelagic zone and down to deeper waters, is the primary pathway for transporting carbon and other vital biological elements to pelagic and benthic organisms (Henson et al., 2011; Boyd et al., 2019; Conte, 2019). However, the organic compounds are

almost entirely consumed, and remineralized to $C0_2$, by heterotrophic zooplankton and bacteria, this leaves a limited amount (5-15%) of organic matter to escape into the ocean interior, where it is mainly used as a food source for meso- and bathypelagic organisms. Subsequently, just a fraction (>0.5%) of organic matter reaches the sea-floor, where benthic organisms and bacteria continue to assimilate and respire it (Gordon, 1971; Emerson and Hedges, 1988, 2008; Wakeham and Lee, 1989; Aberle and Witte, 2003). Though, the presence of fauna may also affect benthic carbon burial, as carbon may be subducted into deeper layers through bioturbation (Kiriakoulakis et al., 2004). In areas of complex topography, such as submarine canyons, reports of organic-rich material being transported to the seafloor have been made, indicating that larger quantities of organic matter (>0.5%) may be available for carbon-recycling or burial (Kiriakoulakis et al., 2001).

Unique canyon morphology and distance from land are key influencers in the variability of ecosystem connectivity (Jannasch and Taylor, 1984; Gage and Tyler, 1992; Bergamaschi et al., 1997; Soliman and Rowe, 2008; DE Leo et al., 2010; Morris et al., 2013a). Indeed, some canyons are known hotspots for enhanced deep-sea sediment and water fluxes, through a variety of mechanisms such as gravity flows and dense water cascades and act as conduits and reservoirs for terrigenous deposits and organic material (Hotchkiss and Wunsch, 1982; Gardner, 1989; de Stigter et al., 2007; Arzola et al., 2008; Savoye. et al., 2009; Canals et al., 2009; Kiriakoulakis et al., 2011). Where internal tides dominate canyons, organic matter distribution may focus within the canyon walls. However, where canyons are dominated by down canyon hydrological circulation, organic matter will likely be transported to greater water depths (García et al., 2008)

1.1.2 Submarine canyon stresses

While the presence of submarine canyons may prove significant for deep-sea heterogeneity and biodiversity, stresses on submarine canyon systems have been recognised. Submarine hydrodynamics may enhance the transportation of litter and chemical pollutants from the continental shelf to the vulnerable deep-sea environments (Palanques et al., 2012). Additionally, while canyon morphology affects the circulation and transportation of water, sediment and particulate matter, climatic forcing factors exist too, although the spatial and temporal resolution is still relatively coarse (Pérenne et al., 2001; Bosley et al., 2004; Genin, 2004; Kiriakoulakis et al., 2011). The effects of climate change may alter the characteristics of water masses, changing the intensity of currents, which may have an impact on submarine species (Canals et al., 2009). Submarine canyons may also be subjected to direct anthropogenic stressors, such as fishing, oil and gas extraction (Harris et al., 2014a). The impact of bottom-trawl fishing on the continental slope and canyon flanks is known to negatively affect the benthic ecosystem more than any other anthropogenic activities combined (Benn et al., 2010). Covering a ground area of up to three-quarters of the world's continental shelves bottom-trawling is believed to transport as much sediment as global terrestrial fluvial systems and resulting sediment-laden gravity flows are known to occur, engulfing fauna in their wake (Watling and Norse, 1998; Kaiser et al., 2002; Puig et al., 2012; Wilson et al., 2015a). Upon impact with the seafloor dragged trawling gear leads to the smoothing of the seafloor at large scales and is responsible for the overturning, destruction of sediment fabric, causing bed armouring and sorting and layering of sediments (Martín et al., 2014; Oberle et al., 2016, 2017; Daly et al., 2018). With increasing particle density and a reduction in substratum heterogeneity there is believed to be a reduction in organic carbon

(OC) concentration in surficial sediments (Clark and Rowden, 2009; Puig et al., 2012; Martín et al., 2014).

Further to the physical alterations, trawling activity is also known to modify the biogeochemical composition of sediments (Lykousis et al., 2005; Pusceddu et al., 2005). Additionally, it has been noted that compositional changes observed from trawling activity exceed that of natural seasonal inputs of organic matter (Sañé et al., 2013). Previous work has revealed that trawled sites are commonly organic carbon impoverished as a result of the removal of recent, organic-rich sediments, and sediment stirring that increases oxygen penetration, thus enhancing remineralisation of buried organic matter (Paradis et al., 2019). Flocculent organic carbon may be winnowed, along with the fine sediment fraction, leaving the coarse, OC depleted, sediment behind (Martín et al., 2014). Ultimately, these changes may harm the structure and functioning of canyon communities, resulting in changes in nutrient supply to the deep-sea, biodiversity, carbon storage and burial; the latter is poorly studied but potentially large (Masson et al., 2010a). Thus, the understanding of both natural and anthropogenic drivers in canyon transformation requires further quantification for management and conservation purposes (Davies et al., 2007; Benn et al., 2010; Daly et al., 2018).

1.2 General aims and rationale

Specific aims and objectives can be found in each chapter. However, the overarching outcome of this work aims to support existing research by providing a better understanding of the function of submarine canyons and its variability from typical open-ocean settings. Three overall aims attempt to do this:

I. Canyon morphology: Geomorphometric measures may aid the understanding of the topography of each branch, providing valuable insight into slope stability, sediment and hydrodynamics.

II. Sedimentary characteristics: Particle analyses aim to characterise the canyon sediments down core and compare them with the adjacent slopes at different points along several canyon branches, to acquire a more representative spatial and temporal view of the processes that operate in the system.

III. Carbon and nutrient cycling potential: Using elemental (TOC, TN and C/N), and bulk stable isotope ($\delta^{13}C$ and $\delta^{15}N$) analyses, the origin, quantity, nutritional quality and burial potential of sedimentary organic matter (SOM) across the canyon branches will be examined.

1.3 Study site

I. *Site description*

The Whittard Canyon is located within the Celtic Margin; a WNW-ESE orientated passive margin that extends from the Goban Spur to the Berthois Spur, found within the Bay of Biscay (Figure 1:2 inset). While the adjacent continental shelf is vast, the continental slope is steep, averaging 8°. The extent of the margin is incised by approximately 35 submarine canyons, with the Whittard Canyon being the most westerly 300km south of Ireland (Amaro, de Stigter, Lavaleye, and Duineveld, 2015; Bourillet, Zaragosi, and Mulder, 2006; Morris, Tyler, Masson, Huvenne, and Rogers, 2013b).

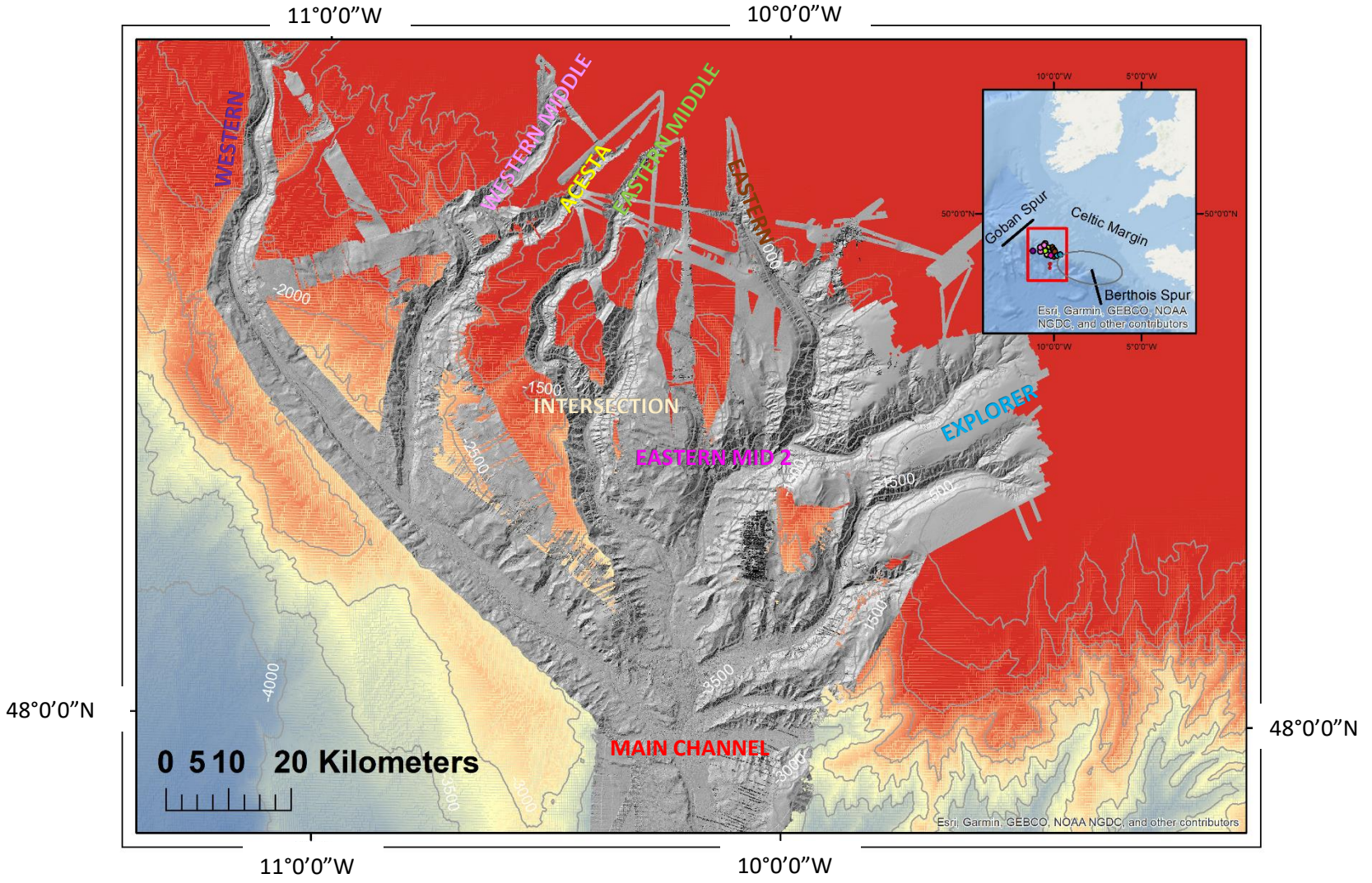

Figure 1:2 Main branches of Whittard canyon. Bathymetry data from Esri, Garmin, GEBCO, NOAA, NGDC and other contributors. (Inset map) Sidescan sonar map of the Whittard Canyon and proximal part of the Whittard Channel and adjacent slopes, showing all the stations used for this paper. Bathymetry courtesy of the RRS James Cook Cruise JC35, 7-19 Jun 2009 and RRS James Cook cruise JC125 13 Aug-09 Sept 2015. Projected coordinates (WGS84).

It is one of the largest and most complex dendritic canyon systems in European waters. Its morphology influenced by existing NNW-SSE trending fault systems, older buried canyons and natural depressions within the seafloor (Cunningham et al., 2005). The Celtic spurs and canyons are associated with the Grande Sole and Petite Sole submarine drainage basins. Both drainage areas feed the Celtic deep-sea fan via the Whittard and Shamrock Canyons (Bourillet et al., 2006).

Extending from the upper slope down to abyssal depths, the Whittard Canyon has four main V-shaped branches that converge downslope, connecting the shelf at 180-200m with the broad, flatbottomed, U-shaped Whittard Channel, that then flows out to the Celtic Fan 3600-4400m (Reid and Hamilton, 1990; Duineveld et al., 2001; Amaro et al., 2015) (Figure 1.2 main map). The orientation of the canyon branches at the shelf edge is primarily NNW-SSE and NNE-SSW with canyon slope angles rising to 40°, or potentially more, within the canyon head and flanks, forming cliffs and overhang features (Cunningham et al., 2005; Huvenne et al., 2011; Robert et al., 2015).

The upper flanks are characterised by complex gully networks, numerous headwall scars from slumps and slope failures which result from gravity-driven flows that widened the canyon through retrogressive canyon wall failure (Amaro et al., 2015). Due to the distance from land, the Whittard Canyon has reduced sediment input from fluvial processes. However, significant off-shelf sediment fluxes have been recorded. This is due to high overlying pelagic productivity and complex hydrological processes such as boundary currents and internal waves that generate sediment-laden nepheloid layers (Figure 1:3) (Morris et al., 2013a; Sharples et al., 2013; Wilson et al., 2015c; Hall et al., 2017). The seabed substratum is generally mixed on the interfluves with pelagic material and reworked

sediments from the outer shelf and canyon margins tending to be coarse, compared to the alternations of fine and coarse material found in the lower reaches (Cunningham et al., 2005; Duros et al., 2011; Stewart et al., 2014). Outcropping rocks are mainly limited to vertical walls, gullies and scars. To the East, reports of over 400 mini-mounds of dead cold-water coral fragments within the Explorer and Dangeard interfluves have been found between 250-410m deep (Reid and Hamilton, 1990; Cunningham et al., 2005; Stewart et al., 2014). In contrast to the morphologically diverse canyon walls, the canyon thalwegs are blanketed by flat areas of soft sediment (Robert *et al.*, 2015).

The Whittard Canyon was initiated in the Plio-Pleistocene era through headward erosion and retrogressive slope failure incising deeply into the underlying Miocene deltaic deposits and Cretaceous/Palaeocene chalks (Huvenne et al., 2011). The most recent phase of canyon incision occurred during several episodic sea-level low stands in the Plio-Pleistocene era (Bourillet et al., 2003). During this last glacial period, these canyons were linked to an active palaeovalley system (Bourillet et al., 2006; Toucanne et al., 2009). However, its activity is now reduced due to the distance from the current shoreline (Reid and Hamilton, 1990). Linear tidal sand ridges that developed on the outer continental shelf of the Celtic sea between ~ 20-12ka are proposed as sediment sources to the Celtic deep-sea fan. Due to the lowered sea level, rivers were connected to the Grande Sole and the Petite Sole drainage basins, resulting in multiple terrestrial sediment sources to the Celtic deep-sea fan at this time (Bourillet et al., 2003). Furthermore, with deglaciation of the British and European ice-sheets (~ 20-12ka) there was a significant eustatic change within the Grande Sole Basin, and hence the Whittard Canyon. It is suspected, with glacial-hydrostatic uplift of the British Isles, that this terrigenous input was prolonged until ~7000 years ago (Jean François Bourillet et

al., 2003; Lambeck, 1996). However, recent hydrological measurements and modelling results suggest the upward flow of sediment transport (Cunningham et al., 2005; Bourillet et al., 2006; Scourse et al., 2009; Praeg et al., 2015; Amaro et al., 2016b).

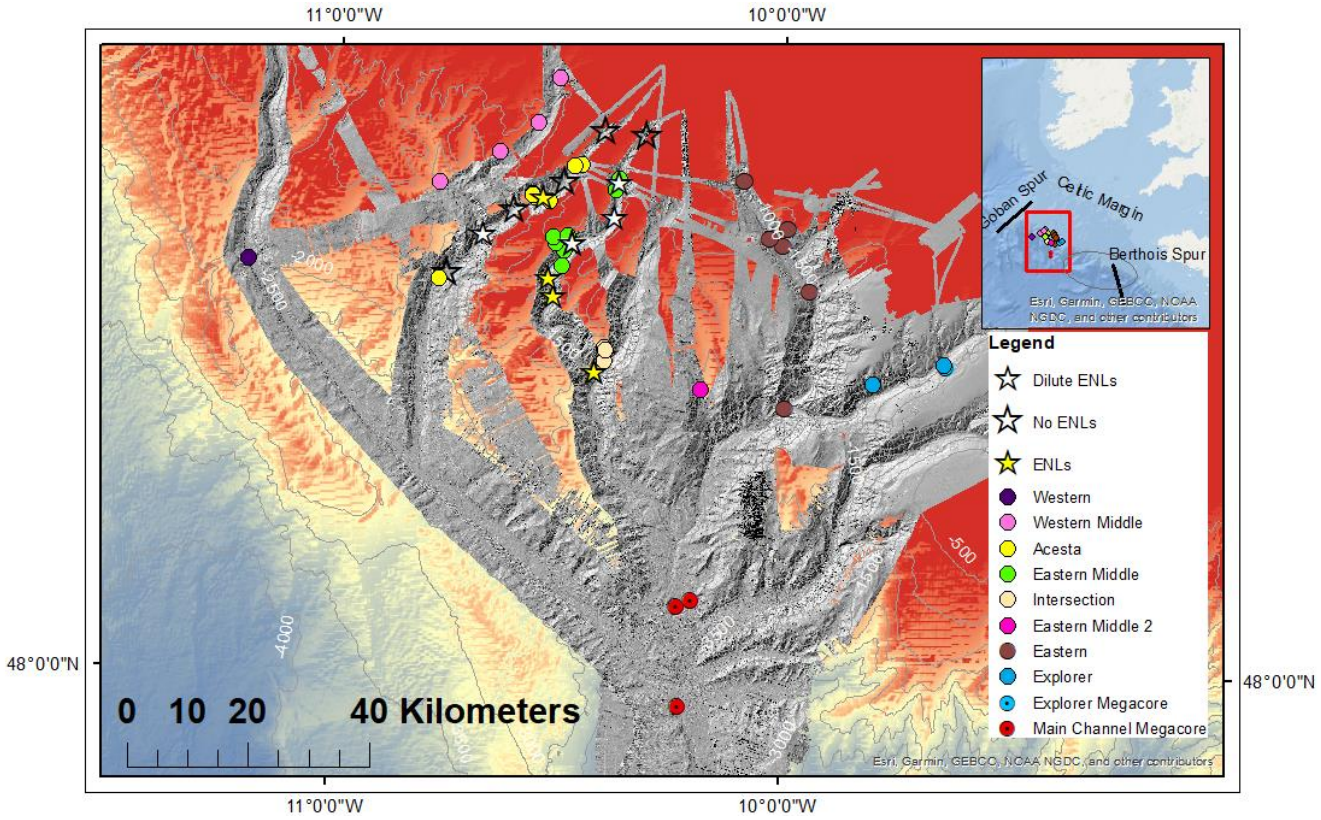

Figure 1:2 Targeted sites where known nepheloid layers have occurred (Wilson et al., 2015). Clear stars are where no enhanced nepheloid layers where found; White stars are where dilute nepheloid layers were found; Yellow stars are where enhanced nepheloid layers were found. Bathymetry data from Esri, Garmin, GEBCO, NOAA, NGDC and other contributors. (Inset map) Sidescan sonar map of the Whittard Canyon and proximal part of the Whittard Channel and adjacent slopes, showing all the stations used for this paper. Bathymetry courtesy of the RRS James Cook Cruise JC35, 7-19 Jun 2009 and RRS James Cook cruise JC125 13 Aug-09 Sept 2015. Projected coordinates (WGS84).

II. *Hydrological regime*

Lander records indicate that in the upper canyon reaches, from the shelf edge to ~2500m and the near-bed current regime is dominated by strong semi-diurnal tidal currents, flowing in both up and down canyon directions (van Weering et al., 2000; Amaro et al., 2016a). However, net suspended sediment transport, driven by tidal currents, generally appears to be in an up-canyon direction. Likewise, net water flow at deeper sites has been recorded as flowing in an up-canyon direction, indicating that tidal currents do not contribute to down-canyon sediment transport (Mulder et al., 2012).

Bottom water turbidity is often observed to rise during periods of increased current speed, indicating that bottom sediment is suspended and entrained by the tidal current. It has been noted that during current peaks, rapid horizontal particulate fluxes have reached values in the order of several grams m^{-2} s^{-1}. At increased depth, within the main Whittard channel (4166m), semi-diurnal currents are weak, not exceeding 0.1-0.15m s^{-1}, with no sign of resuspending bottom sediment (Amaro et al., 2015).

III. *Ecosystem threats*

Hydrological fluxes drive nutrient changes, fueling enhanced primary productivity in surface waters along the Bay of Biscay (100-250$gcm^{-2}yr^{-1}$) (Vlasenko et al., 2014). Furthermore, accelerated currents, due to topographic forcing, increase the organic matter flux to the benthos, therefore enhanced food availability is recorded at depth, compared to less active areas on the continental slope (Morris et al., 2013c). As a result, the canyon exhibits different faunal patterns from the wider NE Atlantic.

The Whittard Canyon is associated with Vulnerable Ecosystems (VMEs) and sites of novel

biodiversity. Coldwater corals (CWCs) have been reported at ~500 to ~2500m in the Whittard Canyon (Huvenne et al., 2011; Johnson et al., 2013a; Morris et al., 2013b; Amaro et al., 2016b). Unique and dense assemblages of the CWC scleractinian coral *Lophelia pertusa* and giant bivalves *Acesta excavata* have been associated with intermediate nepheloid layers, that likely provide a sufficiently organically enriched food-source. A vertical wall, spanning 1600m, at ~1350m, within the Eastern branch has found to be dominated by novel *L.pertusa.* At depths of ~700m, in the Acesta branch, *A.excavata* and giant oysters *Neopycnodonte zibrowii* have been recorded.

Due to the high primary productivity in this area, the Celtic Sea Shelf is heavily exploited for fishing using bottom trawls, pelagic trawls and longlines (Gerritsen and Lordan, 2014). Based on the last decade, the fishing intensity is variable across the Whittard Canyon (Daly et al., 2018). Fishing intensity has been associated with the possible smoothing of the seafloor, particularly over steeper sloping parts of canyon interfluves (Daly et al., 2018). Trawling along the continental margin, east of the Whittard Canyon is seasonal, with much of fishing occurring between July and March, peaking in August (Sharples et al., 2013). However, due to the scale and complexity of the canyon, the canyon is not exploited to the degree that other submarine canyons, closer to coastal regions, would endure (Palanques et al., 2006). Furthermore, due to the technical constraints of fishing gear, slopes >20° are rarely fished (Daly et al., 2018 estimated 90h in 10 years).

Nevertheless, recent work by Wilson et al. (2015) on one of the eastern branches suggests that human activity in the form of deep-sea trawling in the interfluves does affect material transport and input into the canyon. Both benthic nepheloid layers (BNL) and intermediate nepheloid layers (INL) line the branches of the Whittard Canyon (Huvenne et al., 2011;

Johnson et al., 2013b; Wilson et al., 2015c) (Figure 1:2). These cloudy layers, thick with suspended particulate material, are driven by energetic hydrodynamics and act to link the productive shallow environments with the nutrient-depleted deep waters (Puig and Palanques, 1998; Wilson et al., 2015c). In the upper region of the canyon (~700m) a dense assemblage or corals and large bivalves have been associated with a nepheloid layer. It is believed that the nepheloid layer, thick with sediment and organic matter, is transporting the necessary nutrients for these organisms to thrive (Johnson et al., 2013b). Figure 1:2 illustrates that these sites were targeted to reveal a sedimentary signature of these occurrences. While nepheloid layers are a natural phenomenon, formed by gravity flows and other disturbance events, there is evidence that anthropogenic activity, such as bottom trawling within the Whittard Canyon, act to enhance these layers beyond the concentration levels that are typically observed in the region9 (~1mgL(-1)) (Wilson et al., 2015b). This may lead to significant disturbance of little-known natural processes, possibly affecting local ecosystems and carbon export and remineralisation rates, thus affecting the supply of energy to the benthos and the potential of carbon storage by altering carbon burial. If confirmed, this would be one of the rare observed cases of large-scale human impacts in the deep-sea, rendering the study of this system significant.

1.4 Data collection

1.4.1 Cruise strategy

Owing to the high cost of research cruises and the number of scientists often involved, sampling is time-restricted, and it is necessary to be flexible when having a sampling strategy. Unlike most fieldwork on land, it is not always possible or cost-effective, for sampling to be undertaken at all sites each scientist requests. Rarely will a research cruise have one objective, but instead various, and numerous sample types will be taken at each location. The three voyages (CE13008, CE14009, CE16006), discussed in this paper, aim to answer a range of questions that include (but are not limited to) the canyon's biology, hydrology, chemistry and sedimentary characteristics. The benefit of taking discrete samples at the same sites is that it provides a more comprehensive understanding of each location. Using published papers to inform this research, principal branches and sites were identified, suggesting that interesting mechanisms and processes were taking place.

1.4.2 Sampling and data methods

I. *Core retrieval*

A total of forty-two push cores and four mega cores, taken during three surveys, have been analysed (Table 1:1). Core codes have been attributed to each sample, indicating the cruise name, event number, push-core tube (where available) and depth. Colours and numbers have been assigned to branches, where 1 and purple= Western, 2 and pink= Western Middle, 3 and yellow= Acesta, 4 and green= Eastern Middle, 5 and beige= Intersection, 6 and magenta= Eastern Middle 2, 7 and brown= Eastern, 8 and blue= Explorer and 9 and red= Main Channel. Thirty-three push cores were taken onboard the *Celtic Explorer* using the

mechanical arm of the remotely operated vehicle (ROV) *Holland I* (Figures 1:3 and 1:4). These short cores (10-25cm) were collected across four main branches along their axes and adjacent slopes of the Whittard Canyon (Northwest Atlantic Ocean) over spring and summer research cruises in 2014 and 2016 as part of the *Ecosystem Functioning and Biodiscovery at Whittard Canyon* program led by Dr. Martin White and Dr. Louise Allcock of the National University of Ireland, Galway. A further nine push cores and four mega cores were taken aboard the *RRS James Cook* vessel in 2015 as part of the *CODEMAP project (Complex Deep-sea Ecosystems: Mapping habitat heterogeneity as proxy for biodiversity)*, funded by the European Research Council and led by Dr. Veerle Huvenne of the National Oceanography Centre (Grant No 258482).

Table 1:1 Core sites targeted across 9 branches of the Whittard Canyon with longitude and latitude. Canyon branches are colour coded Purple (Western Branch), Pink (Western Middle Branch), Yellow (Acesta Branch), Green (Eastern Middle Branch), Cream (Intersection), Magenta (Eastern Mid 2), Brown (Eastern Branch), Blue (Explorer Canyon) and Red (Main Channel).

BRANCH No.	BRANCH	DEPTH (m)	CRUISE	YEAR	SAMPLE CORE CODE	LONGITUDE	LATITUDE
1	**Western**	2740	JC125	2015	JC125-083-PSH03-	48.6078	-11.198
2	**Western Middle**	440	CE14009	2014	CE14009-045-440m	48.8864	-10.5099
	Western Middle	719	CE14009	2014	CE14009-042-719m	48.77501	-10.6415
	Western Middle	781	CE16006	2016	CE16006-087-	48.81914	-10.556
	Western Middle	819	CE14009	2014	CE14009-042-819m	48.77501	-10.6415
	Western Middle	1601	CE16006	2016	CE16006-081-	48.72878	-10.7748
3	**Acesta**	499	JC125	2015	JC125-078-PSH02-	48.7582	-10.4558
	Acesta	640	JC125	2015	JC125-080-PSH04-	48.75588	-10.4733
	Acesta	780	CE16006	2016	CE16006-033-	48.70419	-10.5277
	Acesta	974	CE16006	2016	CE16006-084-	48.71236	-10.5648
	Acesta	974.2	CE16006	2016	CE16006-084-	48.71236	-10.5648
	Acesta	1130	CE14009	2014	CE14009-009-	48.7089	-10.5607
	Acesta	1487	CE14009	2014	CE14009-027-	48.58651	-10.7708
	Acesta	2816	CE14009	2014	CE14009-027-	48.58651	10.7708
4	**Eastern Middle**	501	CE14009	2014	CE14009-040-501m	48.7379	-10.3718
	Eastern Middle	511	CE16006	2016	CE16006-030-	48.64928	-10.519
	Eastern Middle	574	CE14009	2014	CE14009-012-574m	48.63147	-10.4937
	Eastern Middle	659	CE14009	2014	CE14009-030-659m	48.71344	-10.5658
	Eastern Middle	700	CE14009	2014	CE14009-030-700m	48.71344	-10.5658
	Eastern Middle	700	CE16006	2016	CE16006-030-	48.64183	-10.5113
	Eastern Middle	723	CE14009	2014	CE14009-033-723m	48.72148	-10.3787
	Eastern Middle	731	CE16006	2016	CE16006-022-	48.65172	-10.4869
	Eastern Middle	1095	CE14009	2014	CE14009-040-	48.7379	-10.3718
	Eastern Middle	1271	CE16006	2016	CE16006-062-	48.60796	-10.4993
	Eastern Middle	1323	CE14009	2014	CE14009-012-	48.63147	-10.4937
5	**Intersection**	1487	CE14009	2014	CE14009-031-	48.48728	-10.3999
	Intersection	1776	CE14009	2014	CE14009-031-	48.48728	-10.3999
	Intersection	1836	CE14009	2014	CE14009-025-	48.46718	-10.401
	Intersection	2086	CE14009	2014	CE14009-025-	48.46718	-10.401
	Intersection	2384	CE14009	2014	CE14009-025-	48.46718	-10.401
6	**Eastern Mid 2**	1845	CE16006	2016	CE16006-056-	48.42784	-10.1828
	Eastern Mid 2	1850	CE16006	2016	CE16006-056-	48.42784	-10.1828

7	**Eastern**	450	CE14009	2014	CE14009-005-450m	48.66627	-10.5607
	Eastern	571	JC125	2015	JC125-109-PSH03-	48.73715	-10.0931
	Eastern	571	JC125	2015	JC125-109-PSH05-	48.73715	-10.0931
	Eastern	681	CE14009	2014	CE14009-005-681m	48.7089	-10.5607
	Eastern	1233	JC125	2015	JC125-111-PSH05-	48.64067	-10.0047
	Eastern	1298	CE16006	2016	CE16006-002-	48.6524	-10.0359
	Eastern	1620	CE16006	2016	CE16006-042-	48.5746	-9.94462
	Eastern	2979	JC125	2015	JC125-091-PSH05-	48.4008	-9.9981
8	**Explorer**	664	JC125	2015	JC125-101-MC-	48.46327	-9.63735
	Explorer	764	JC125	2015	JC125-035-764.4m	48.4376	-9.7995
	Explorer	861	JC125	2015	JC125-076-PSH02-	48.46698	-9.64245
9	**Main Channel**	3723	JC125	2015	JC125-045-MC-	48.1149	-10.1994
	Main Channel	3759	JC125	2015	JC125-028-MC-	48.1054	-10.2306
	Main Channel	4010	JC125	2015	JC125-063-MC-	47.95632	-10.2239

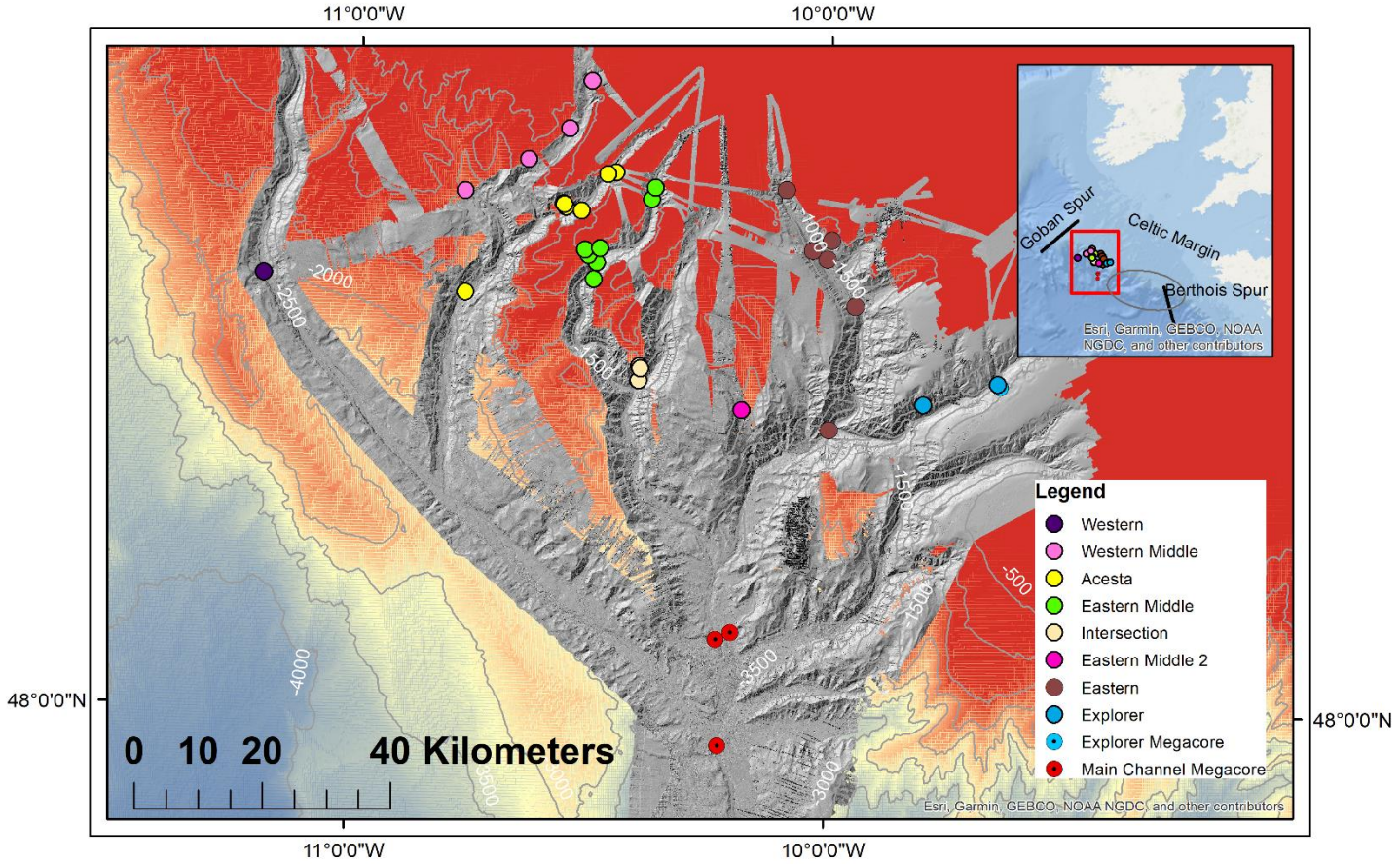

Figure 1:3 (Inset) Location map of the Whittard Canyon along the Celtic Margin, Bay of Biscay. Bathymetry data from Esri, Garmin, GEBCO, NOAA, NGDC and other contributors. (Main map) Sidescan sonar map of the Whittard Canyon and proximal part of the Whittard Channel and adjacent slopes, showing all the stations used for this paper. Bathymetry data courtesy of Esri, Garmin, GEBCO, NOAA, NGDC and RRS James Cook cruise JC35, 7-19 Jun 2009 and RRS James Cook cruise JC125 13 Aug-09 Sept 2015. Projected coordinates (WGS84).

Figure 1:4 ROV Holland deployed during CE16006 (Kershaw, 2016).

Once recovered, the *Celtic Explorer* samples were processed on deck, taking care to avoid contamination. From the sediment/water interface, the core was sliced using a sterile blade at 1cm intervals down to 10cm and then at 2cm intervals to the base of the core. The blade was washed in deionised water between slicing each section, to avoid cross-contamination of sediment. These sub-samples were stored in pre-combusted foil (400°C; 24h) before being stored in a freezer (-80°C). On return to shore, the samples were freeze-dried before being stored at -20°C.

The National Oceanographic Centre (NOC), Southampton, UK, undertook initial processing of the push core samples, taken aboard the *RRS James Cook*. The samples were stored, in their plastic tubing, in the vessel's onboard freezer (-80°C). Additionally, mega cores of 56mm diameter × 600mm long were taken using a multi-corer. These were not sliced onboard but instead stored in a freezer within their tubes at -80°C.

Upon returning to Southampton, all push cores and mega cores were transferred to pre-combusted foil (400°C; 24h) before being transferred, chilled by dry-ice, to Liverpool John

Moore's University where they were stored at (-80°C). The push core samples, partially thawed, every cm down to 10cm and subsequently every 2cm using the same protocol as described above. The mega core sampling was similar, but thaw time was generally longer due to the thickness of the core, and a larger knife was used to section the core every cm down to 10cm and subsequently every 2cm. Both push cores and mega cores were freeze-dried for 36 hours before being stored at -20°C.

II. *Methodological considerations*

When recovering sediment cores, it has been suggested that changes in temperature and pressure lead to alterations in carbon, nitrogen and oxygen compositions (Hall et al., 2007). While care was taken during sampling and undisturbed sediment at the seafloor was targeted, with minimal resuspension occurring, it is possible that the surficial sediment layers were disturbed during sampling. However, while this data set may contain some artefacts, it describes the relative differences of biochemical parameters across the Whittard Canyon.

III. *Cruise observations and photographs*

During the *Celtic Explorer* CE16006 2016 cruise, ROV observations and photographs were taken to provide a context of the sites.

IV. *Statistical analysis*

Bathymetric and sample location maps were created using ArcGIS Desktop 10.6. Base map general bathymetric ocean data is attributed to the General Bathymetric Chart of the Oceans (GEBCO).

The Shapiro-Wilk test was used to determine normality distributions within the software IBM SPSS Statistics 23. Non-parametric tests were used, as all data were either non-normally distributed ($p < 0.05$) or were of sample size less than 50.

As most of the results failed the assumption of homogeneity of variances under Levene's test, where results were significantly different ($p > 0.05$), the null hypothesis was retained. The significant differences between mean values across all branches were determined using the independent samples Kruskal-Wallis (one-way ANOVA on ranks) test, before the nature of differences was evaluated using Dunn-Bonferroni post-hoc pairwise comparison tests.

Non-parametric and Spearman's rank correlation tests were used to examine relationships between selected variables.

Sedimentological and biogeochemical values were plotted using Ocean Data View 4.7.4 (ODV) software, Matlab, Microsoft Excel and IBM IBM SPSS Statistics 23. Canyon branches are colour coded and abbreviated throughout the results as follows; Purple (Western Branch), Pink (Western Middle Branch), Yellow (Acesta Branch), Green (Eastern Middle Branch), Cream (Intersection), Magenta (Eastern Mid 2), Brown (Eastern Branch), Blue (Explorer Canyon) and Red (Main Channel).

Down core grain size composition was presented as sand–silt–clay percentages and end-member analyses were achieved using the AnalySize plugin Matlab, developed by Greig A. Paterson and David Heslop (2015).

Numerical unmixing of end-member data by end-member analysis (EMA) was undertaken to sort grain size data into its constituent components. EMA can provide valuable insight into the geological processes and palaeo-environmental changes within a sample. For in-depth

methods, please see Chapter 3. Methods.

Within Primer- E v7.0.13 software, principal coordinate analysis (PCoA), also known as multidimensional scaling, was undertaken to interpret the similarity, or dissimilarity of all geomorphological, sedimentological and biogeochemical parameters of mean samples down core. Each parameter was assigned a location on a graphical plot, in a low-dimensional Euclidian space. Also, relationships between these variables were examined using the non-parametric multivariate test PERMANOVA within Primer-E v7.0.13. PERMANOVA compares groups of variables and tests the hypothesis that the dispersion of the groups is equal for all groups. A rejection of the null hypothesis means that the spread of the variables is different (Anderson et al., 2008). For in-depth methods, please see Chapter 5. Methods.

Chapter 2: Geomorphology

2.1 Canyon morphology

The study of the deep-sea environment often requires the study of the processes that influence and shape the geomorphology of the seabed. This is because marine species are sensitive to their environments. For many marine organisms, depth, substrate type and seafloor shape dictate their presence and distribution (Harris and Baker, 2012; Di Stefano and Mayer, 2018; Novaczek et al., 2019).

The irregularity of canyon topography and its influence on the hydrodynamic regime that often results in nutrient supply to the surface is known to enhance primary productivity in places (Allen and Hickey, 2010; Ryan et al., 2005). Due to the incised morphology of submarine canyons organic matter, lithogenic and organic material may be transported to the deep-sea, resulting in increased biomass and regional species diversity and richness (DE Leo et al., 2010; Amaro et al., 2015).

The transportation of unconsolidated sediments both downslope and upslope, by local hydrodynamic regimes, has been widely observed within submarine canyons (Cunningham et al., 2005; Puig et al., 2014; Amaro et al., 2016a). While material found on the deep-sea floor is dominated by fine-grained sediment, suggestive of low energy depositional environments, canyon sediments have been found to have a greater range of grain sizes which indicates unique depositional regimes within them. Reid and Hamilton (1990) stressed that individual canyon morphology likely affects the hydrological regime of the environment, and therefore an increased/decreased potential to deposit coarser grains and organic matter (Amaro et al., 2016b). For example, a narrow canyon cross-section could

result in higher flow velocity within the channel, increasing energy and hence the ability to transport material. Gardner (1989) revealed that particle size in the Baltimore Canyon decreased along the canyon axis, with coarse and medium grain sands gradually fining out to silt and clays, as energy, in the form of local currents, decreased converting the regime from transport-dominated to depositional. However, work within the Nazaré, and Setúbal Canyons located at the west Iberian Margin (de Stigter et al., 2007; Arzola et al., 2008) revealed a more complex picture. Areas of intense deposition dominated by fine-grained (silt to clay grade) material, were found near areas dominated by coarser grain sediments indicating relatively complex depositional systems. This illustrated the small-scale complexity of such systems and suggested that different canyons (or parts thereof) may be affected by various combinations of hydro-sedimentological processes (Turnewitsch et al. 2008; Tyler et al. 2009). While the complex topography may well be the primary causal factor that leads to the observed variety of depositional/erosional regimes over relatively small spatial scales, the sediment source further complicates matters (Rajput et al., 2016). Sand particles at the seafloor, need comparatively lower energy to erode, transport and deposit than coarser-grained gravels. However, due to the mineralogy of silt and clay, regardless of their fine grain size, they require a higher energy environment to erode the particles at the seafloor but have a lower energy requirement for transportation and deposition (Hjulstrom, 1939; Sundborg and Sundborg, 1956).

As individual canyon morphology influences sedimentation in submarine canyons, recent studies have investigated the impact that sediment type has on canyon morphology and biodiversity. Carter et al. (2018) proposed that lithostratigraphic units with increased tensile strength, such as mud-rich carbonates, may form overhanging ledges that provide an ideal

environment for sessile species to inhabit. Conversely, where weaker "pure" carbonate units exist, undercutting and receding sections of rockwall may occur, preventing sessile organisms colonising.

2.1.1 Bathymetric mapping

Recent work in shallower water has signalled the importance of seafloor mapping and landform characterisation (Bekkby et al. 2002; Dartnell and Gardner 2004; Lundblad et al. 2006), but there has been little work in deeper waters beyond the continental shelf. While flat, abyssal plains occupy approximately 28% of the global seafloor (Voelker, 2016), the ocean is bordered by continental margins that host approximately 9,477 submarine canyons (Harris et al., 2014). These canyons are some of the most geomorphological complex features found within the oceanic environment, with consequences that extend beyond the canyon, making the mapping of them essential.

Geomorphometric digital terrain models (DTMs) are increasingly used to identify and quantify geomorphic features through manual expert interpretation or by way of semi-automated or automated tools (MacMillan and Shary, 2009; Lecours et al., 2016). Accurate bathymetric maps and DTMs of seafloor geomorphology are not only important as they provide a baseline characterisation of the seafloor, but they also form a critical component in informing ocean management decisions and understanding marine ecosystems (Mountjoy and Micallef, 2018; Wölfl et al., 2019). Land surface parameters such as slope, rugosity and ruggedness are useful in geomorphological interpretation. A land surface parameter is a continuous field of quantitative values, such as a raster image or a map, for the same digital elevation map extent (Pike et al., 2009). Where biological information is not

available, reliable geomorphometric data can be utilised by scientists to predict areas where organisms may or may not colonise. Slope and terrain variability are known to act as significant predictors in species distribution. Smoother, flatter areas may exhibit different seabed facies, supporting communities that differ to those on steeply sloping areas (Dartnell and Gardner, 2004; Lundblad et al., 2006; Wilson et al., 2007). Increasing slope angles are also known to have a limiting effect on fishing activity (Daly et al., 2018).

Furthermore, where there is a high slope angle, current flow is known to become accelerated (Mohn and Beckmann, 2002). Seafloor mapping forms an essential tool in marine geo-hazard assessments, and the study of mass transport processes as high slope value may indicate areas at risk of failure (Rovere et al., 2014) (Rovere, Gamberi et al., 2014). Submarine canyon landslides can trigger tsunamis and flood events, resulting in infrastructure damage and loss of life. Therefore it is crucial to identify the triggers and frequency of submarine slope failures (Deering et al., 2019; Novaczek et al., 2019).

2.2 Aims

Due to the complex nature of canyons, it is imperative to gain an improved understanding of the morphology of the individual core sites at a high resolution. Spatial analyses were performed on the high-resolution acoustic data sets acquired over past surveys

The geomorphology of the Whittard canyon system was explored using digital elevation models (DEMs) and generating quantitative terrain attributes, such as vector ruggedness measurements (VRM), rugosity and slope analysis. These geomorphometric measures of canyon topography may provide insight into slope stability, sediment and hydrodynamics. Furthermore, images taken at the sites, courtesy of the National University of Ireland

Galway (NUIG) CE16006 cruise CE16006, attempt to further aid the understanding of the morphology and sampling environment. The increased knowledge of canyon geomorphology aims to support sedimentological and biogeochemical techniques.

2.3 Methods

Bathymetric and sample location maps were created using ArcGIS Desktop 10.6. Base map general bathymetric ocean data is attributed to the General Bathymetric Chart of the Oceans (GEBCO 2019). Seabed topographic bathymetry within the Whittard Canyon was derived using digital elevation data provided by the NUIG, combined with high-resolution swath acoustic multi-beam and 30kHz TOBI (resolution 20m by 20m) side-scan sonar data from the National Oceanography Centre (NOCS) collected in 2009 (JC35). Hill shade was added to the bathymetry to present the data in a visually more effective manner.

Canyon topography derivatives were extracted from the bathymetry using geospatial analyst within the geographical information systems (GIS) ARC Map software. Using the Benthic Terrain 3.0 Modelling Plugin developed by (Walbridge et al., 2018) geomorphometry scripts were run to better examine the benthic landscape characteristics. Terrain slope, rugosity and ruggedness were determined using the spatial analyst tool within ARC Map (Burrough and McDonnell, 1998; Campanyà-Llovet et al., 2018; Walbridge et al., 2018). This can give an indication of what the environmental features are but is by no means diagnostic.

Terrain slope measurements were calculated within the Benthic Terrain Modeler application. The slope tool calculates the maximum difference of change in value from that cell to neighbouring cells of a raster in degree units. Theoretically, the tool fits a plane to the

z-value of a 3 x 3 (grid cell) neighbourhood around the centre cell to find the average gradient in the horizontal and vertical directions at each location in the surface raster. A single slope value of this plane is then calculated using the average maximum technique created by Burrough and McDonnell (1998). The direction the plane faces is the aspect of the central cell. Essentially, the lower the slope value, the flatter the terrain and the higher the slope value, the steeper the terrain.

A non-standardised, unitless descriptor for seafloor roughness was obtained using the high-resolution bathymetric data collected during the JC35 cruise. Within the benthic terrain modeller toolbox in ARC Map, rugosity values were derived using the Arc-Chord ratio (Du Preez, 2015). The benefits of using an ACR rugosity index is that it is simple, accurate and independent of data dimensionality (2-D, 3-D). Importantly, it decouples from background slope, using a plane of best fit, rather than a horizontal plane. Thus, it is well suited for use over highly complex topographical features within the Whittard Canyon.

Terrain attributes were generated based on recommendations from Lecours et al. (2017) and Novaczek et al. (2019) (slope, rugosity and VRM). Using the method created by Sappington et al. (2007), a further non-standardised measure was derived. This method accurately presents variability in aspect and slope in a single measure. Using the Vector Benthic Terrain Modeler 3.0 application within ARC GIS, ruggedness measure values were calculated for a 3-cell analysis window at 25m scale bathymetry (Hobson, 1972). Research has found that VRM decouples terrain ruggedness from slope better than indices such as land surface ruggedness index (LSRI) and terrain ruggedness index (TRI) (Sappington et al., 2007). Rugged terrain is defined at being topographically uneven, broken, rocky or steep. Sappington et al. (2007) developed a robust quantitative tool using a geographic

information system. Unlike previous measures, that heavily relied on slope measurements, Sappington et al. (2007) developed a 3-dimensional vector ruggedness measure (VRM) of terrain based on a geomorphometry method for measuring vector dispersion. The VRM method effectively represents the variability in slope and aspect into one measurement. Vector ruggedness measure values range from 0 (no terrain variation) to 1 (complete terrain variation). Typical natural terrains range between 0 and 0.4 (Sappington et al., 2007)(Sappington, Longshore and Thompson, 2007). While the vector ruggedness measurement proxy was initially created to predict areas well adapted for species to inhabit, its application is useful in better understand canyon morphology (Novaczek et al., 2019).

Cruise observations and photographs captured during the CE16006 cruise was used to support bathymetric data.

2.4 Results

Slope analyses of the canyon branches indicate that the thalwegs and the shallower shelf breaks are characterised by slope angles <20° (Figure 2:1), while higher slope angles are observed at canyon walls and cliffs reaching 80°.

Vector ruggedness measure highlights areas characterised by terrain variability across the canyon. With exception of the Intersection site (0.41 VRM), VRM at all sites are below 0.4 (Figures 2:2 and 2:3).

The Western Middle sites show variability in slope and ruggedness downslope. The uppermost site CE14009-045-440m presents the highest slope angle 40-80° and a VRM value of 0.12, compared to site CE16006-087-PSH02-781.13m, which is less than 10km away and is characteristically flat, with slope angles below 20° and a VRM value of 0.02. Cruise photography (Figure 2:4) and ROV observations depict a core site that is flat, sparse, with only a single *Pennatulacea* observed.

While the resolution of maps and photography differ, the bedforms observed indicate the erosional, transport and depositional action of the bottom currents. ROV photography reflects flat and sparse areas were ruggedness values <0.05 at sites CE16006-087-PSH02-781.13m (Western middle), CE16006-033-PSH08-780m (Acesta branch), CE16006-062-PSH07-1270.84m and (Eastern middle) (Figure 2:4). Where ruggedness values exceed 0.05, observations made during the dive reflect an environment that is characterised by ripples, stepped edges, steep cliffs and overhangs (CE16006-056-PSH05-1845m, CE16006-056-PS07-1845m, CE16006-002-PSH05-1297.81m and CE16006-042-PSH02-1620m). While no photography is available for site CE16006-084-PSH02-974.2m (Acesta branch), due to a

technical limitation, it was noted that this site was characterised by varying smooth and steep areas. A ruggedness value of 0.17 supports this. Furthermore, a large net was observed here along with coral and fish, indicating trawling activity in the surrounding areas, which has been previously noted to occur by Wilson et al. (2015).

The Western site JC125-083-PSH03-2740m is <0.01km from slope values of 60-80°, with ruggedness values reaching 0.60, suggesting steep and high terrain variability close by. Onboard footage confirmed a nearby canyon wall which may support this. Sappington et al. (2007) describe typical natural terrain being less than 0.4 VRM, supporting the knowledge that this is indeed a highly rugged site.

2.4.1 Slope angle

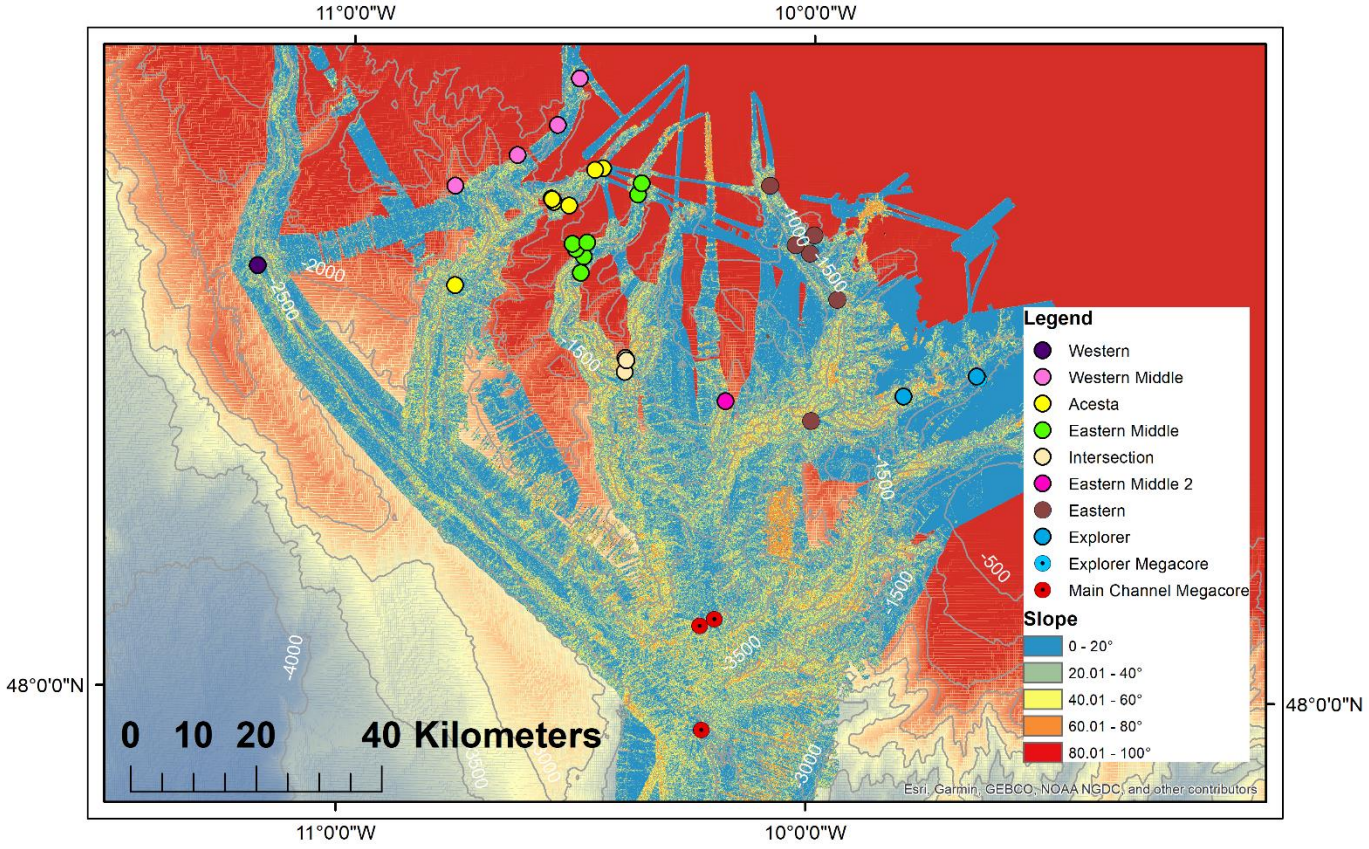

Figure 2:1 Map image of slope angle with areas in green greater than 20°. Slope angles of 0-20° characterise thalwegs and upper canyon reaches. Canyon walls are characterised by steeper slopes reaching 60-80°, calculated within ARCMAP using the Benthic Terrain Modeler 3.0 plugin.

2.4.2 Terrain ruggedness

I. *Vector ruggedness measure across the Whittard Canyon*

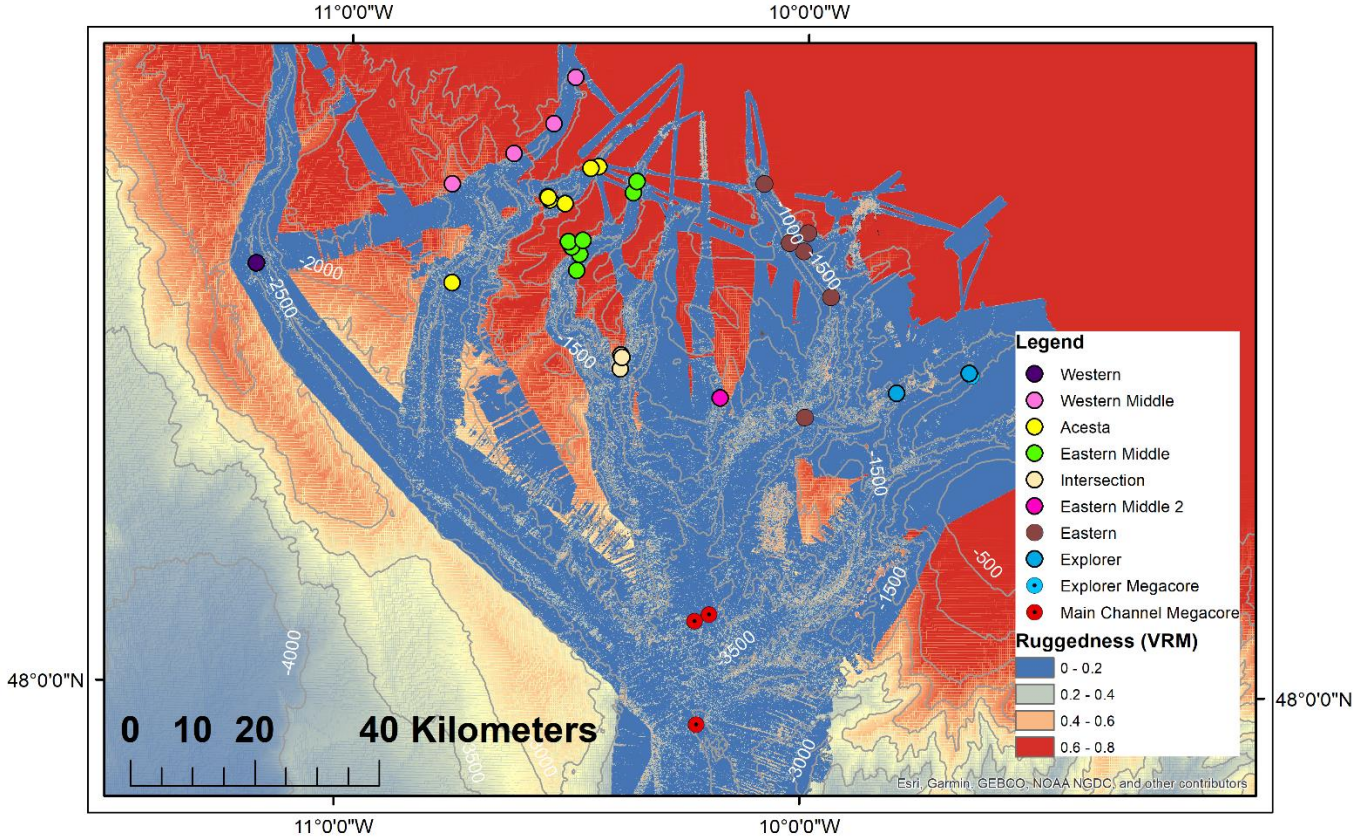

Figure 2:2 Vector ruggedness measure terrain attributes calculated within ARCMAP using the Benthic Terrain Modeler 3.0 plugin. VRM values recorded in the canyon reach >0.6.

II. *Vector ruggedness measure with depth*

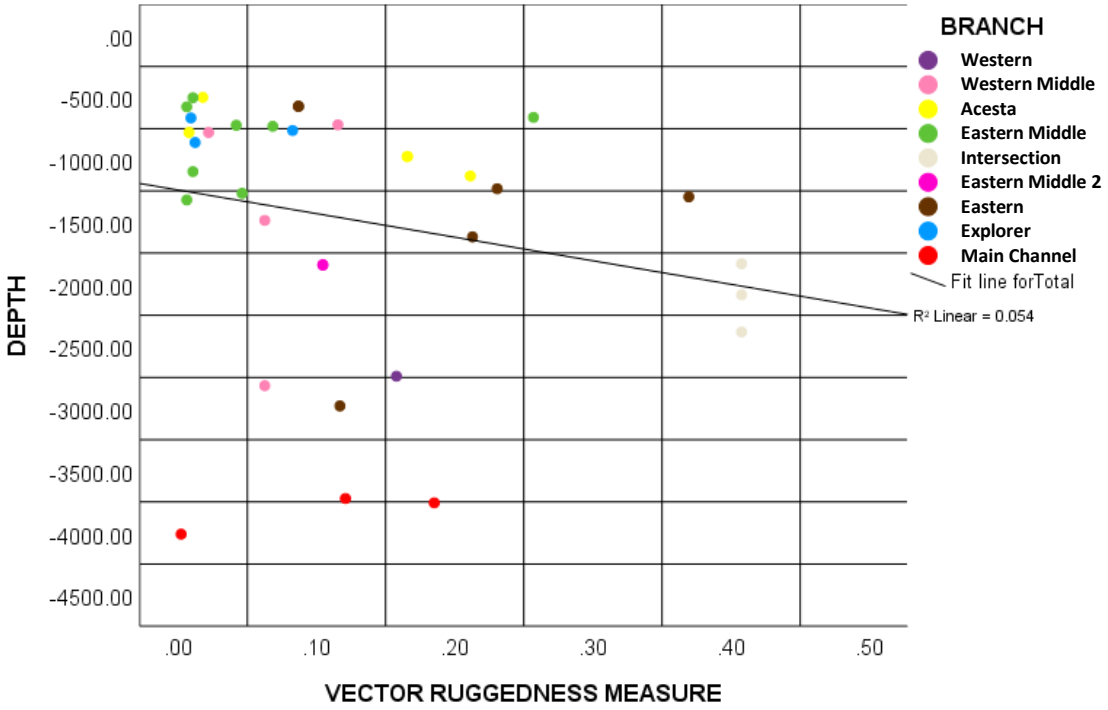

Figure 2:3 Vector ruggedness measure (VRM), as per Sappington's method (2007), for sites across all Whittard Canyon branches, where high-resolution bathymetry data was available. The graph highlights the variability of ruggedness across sites, with the highest ruggedness value observed at the Intersection (CE14009 event 25, all depths) and another large peak at the Eastern branch (CE16006-002-PSH05-1297.81). The lowest reading was recorded within the main channel at 4010m (JC126-063-MC-4010m) indicating lowest variability in terrain. R-squared linear correlation coefficient on analysis revealed no significant linear relationship between depth and vector ruggedness measure.

2.4.3 Cruise photography and observations

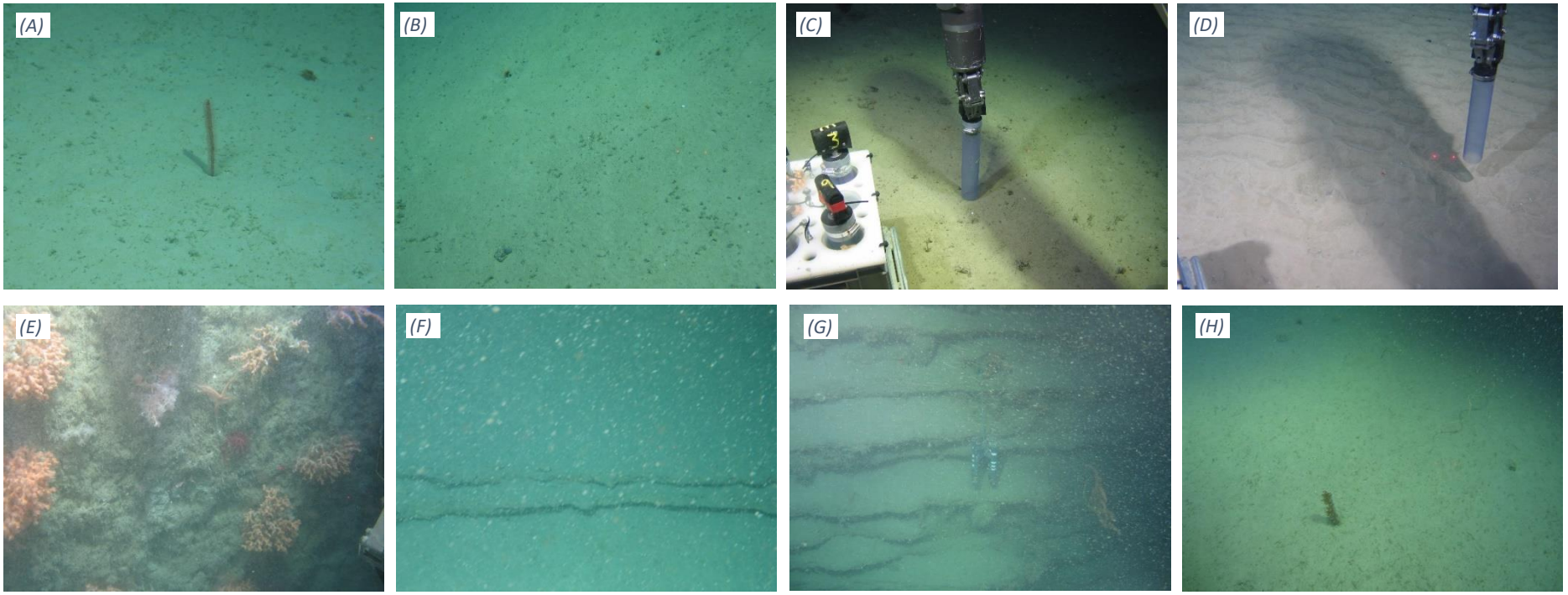

Figure 2:4 ROV photography and shipboard observations: (A) Western Middle Branch: CE16006-087-PSH02-781.13m. ROV observations: flat, sparse, sea pen Pennatulacea. (B) Acesta Branch: CE16006-033-PSHO8-780m. ROV observations: flat, sparse. (C) Eastern Middle Branch: CE16006-022-PSH06-731.38m. ROV observations: sandy ridge, Cladorhiza sponge and Brachyura crab. (D) Eastern Middle 2 Branch: CE16006-056-PSH05-1845m and CE16006-056-PSH07-1845m. ROV observations: Flat area with sandy ripples. (E) Eastern Branch: CE16006-002-PSH05-1297.81m. ROV observations: easy penetration, poor visibility. Nearby area (>0.1km) characterised by a steep bedded wall and dense coral. (F) (G) (H) Eastern Branch: CE16006-042-PSH02-1620m. ROV observations: vertical chalky cliff, with stepped edges and overhangs before sloping out to flatter sandier area, where the core was taken. Images courtesy of CE16006 cruise.

2.5 Discussion

While there is no clear trend in slope and ruggedness variability between the Western and the Eastern sides of the canyon, depth does appear to contribute to terrain ruggedness variability. In most deep-sea settings, below 1000m VRM rarely rises above 0.1. However, the results suggest it is more common to observe VRM values above 0.1 at this depth, which is expected as canyons are known to be highly topographically variable (Figure 2:3). Furthermore, slope analyses of the canyon branches indicate that the thalwegs and the shallower shelf breaks are characterised by slope angles <20° (Figure 2:1), while higher slope angles are observed at canyon walls and cliffs reaching 80° which may indicate areas of slope instability (Locat, 2001)

The Eastern branch displayed the most considerable variability in VRM of all branches. Aslam et al. (2018) indicated that this branch exhibits the largest energy fluxes of all branches. The steep and heterogenic topography may focus this. This is also reflected in the images taken along the branch where Figures 2:4 (E-H) present a branch with highly variable terrain, consisting of steep bedded wall, dense coral and vertical, chalky cliffs with stepped edges and overhangs that flatten out to sandy areas.

Chapter 3: Sedimentology

3.1 Deep-sea sediments

Deep-sea sediments, also referred to as deposits, were first systematically studied during the British Challenger Expedition (1872-1876). Scottish naturalist John Murray was responsible for the study of thousands of samples. Alongside his coworker, Alphonse-François Renard (1842-1903) he published a report on their findings, with much of their focus on sediments. Later, in the 1920s-1930s, William H. Twenhofel became one of the first scientists to catapult the study of sedimentation to worldwide attention (Twenhofel, 1933). Now recognised as Sedimentology, there is extensive knowledge of continental sediment and their importance in nutrient supply and carbon storage. However, due to the inaccessibility of the ocean, it has been problematic to study ocean sediments to the same degree. Though with improved technology, we now understand that deposits found on land and the seafloor differ significantly in their characteristics because they are exposed to different physical and chemical conditions.

Ocean sediments are important to us as they provide many of the resources we use, such as oil and gas. However, many of these products are not renewable and can have devastating impacts on natural ecosystems. With increasing pressure on Earth's resources and the threat of a rapidly deteriorating climate and environment, scientists are looking to oceanic sediments to increase understanding of their global significance. The study of these sediment characteristics is particularly valuable to Oceanographers, as such characteristics can act as extensive archives of information regarding the Earth's past and present processes. Allowing scientists to unravel the mystery of the origin of these sediments and the complex processes that have acted to form, transport and preserve them over many years (Rajput et al., 2016).

Marine sediments originate primarily from two sources, allochthonous and autochthonous. Allochthonous refers to deposits not indigenous of the deposition site; contrastingly autochthonous refers to deposits formed in situ (Rounick et al., 1982; Pedrosa-Pàmies et al., 2015). External allochthonous material can be in both particulate and dissolved form. It may be transported to the ocean as eroded terrigenous material, volcanic ash or cosmogenic matter before being deposited to the sea. Autochthonous sediments, found on the deep ocean floor, at depths that generally exceed 3km and often hundreds of kilometres from continental margins, cover 55 % of the earth's surface (Douglas, 1978).

Marine sediments can be further separated into two components: biogenic and lithogenic. The biogenic component primarily originates in productive surface waters, with a smaller contribution from the benthos (Dunlea et al., 2018). Further biogenic material may also be transported from the land. The biogenic segment can be divided into three main categories: organic material, calcium carbonate and opal-A (biogenic silica). Coccolithophores and foraminifera are the main contributors to calcium carbonate. Opal-A (biogenic silica) is comprised of siliicoflagellates, radiolarians, siliceous sponges, and occasionally includes terrestrially derived phytoliths and freshwater diatom inputs. The lithogenic fraction consists of pre-existing rock detritus (igneous, metamorphic, and sedimentary) which has been eroded on land before being deposited to the sea (Maslin and Swann, 2006). Organic matter may range from terrigenous pollen grains, wood plant fragments and marine macrophyte detritus, but it is not limited to this. Rowe and Staresinic (1979) estimated that terrestrial contribution to deep-sea sediments is low. Sediment trap data indicated that small planktonic particulate organic matter (POM) contributes to approximately 4g cm^{-2} to the deep-sea carbon pool annually.

While a range of factors influences the distribution of sediment including latitude dependence, the productivity of organic matter, nature of terrigenous inputs, the influence of large-scale eddies and climatic fluctuations, the distance from the continents is one of the most significant factors (Rajput et al., 2016). The contribution of external eroded continental landmass material contributes considerably to the sedimentation of continental margins, resulting in significantly higher allochthonous content in these shallow areas and proportionately higher pelagic autochthonous, with a lesser degree fine sand, volcanic and cosmogenic material accumulating at the ocean floor . Weathered continental mass and organic matter are transported to the oceans by fluvial, gravity, æolian or glacial movement. Here oceanic currents carry the eroded, fragmented rock particles and organic matter to different regions of the sea for deposition, depending on the particle size and strength of the current flow (Rajput et al., 2016).

One of the primary controls of the pattern and texture of sediments is the rate of sedimentation. During a low rate of deposition, the oceanic currents have enough time to sort the sediment grains, leading to a uniform distribution in the deposits. Contrastingly, a faster rate of sedimentation may result in poorly-sorted sediment grains, resulting in deposits with mixed grain size fractions, e.g. sand and mud (Pinet, 2009).

During transit, particles are subjected to varied physical (mechanical) and chemical alterations before deposition. There are three critical categories of load that may be transported; dissolved, suspended and bedload. The dissolved material is carried in solution throughout the water column and includes dissolved organic matter (DOM) and nutrients, such as nitrogen and phosphorus, all of which support biological activity in the sea. The suspended load is characterised as fine-grained particulate organic matter (POM), including

silt and clay that remains in the water during transportation and is defined as being less than <0.062mm. Sand is defined as material that is between 0.062 and 2mm and may be resuspended or saltated dependent on the current velocity. Coarser material, such as pebbles >4mm, travelling along the seafloor is described as bedload, rarely resuspending when a high-energy turbulent event, such as a deep-sea trawling and internal waves occur (Folk and Ward, 1957).

Aggregates of both biogenic and lithogenic material create ballasts commonly referred to as marine snow (particles >5mm). Marine snow is important in the transport of rich organic matter, their large particle size contributing to increased sinking velocities. However, fine material is also often observed in the deep-sea. Hemipelagic sediments, red clay, manganese nodules (Van Dongen et al., 2014) and biogenic ooze (such as *Globigerina)* are formed *in situ* conditions and are typically confined to the deep quiescent environment of the ocean (Douglas, 1978). Pelagic sediment is composed of very fine-grained particles that have less than a quarter of particles larger than >5 μm in size (Weissert, 2011). They are deposited from suspension to the ocean floor; however, they are not automatically found at depth but instead are usually located away from continental margins (Henrich and Hüneke, 2011; Weissert, 2011).

Previous observations have found that the sinking velocity of ocean particles is between 10 and 150m d^{-1} (McDonnell and Buesseler, 2010; McDonnell, 2011). However, Lampitt (1985) estimated that the deep Atlantic Ocean may have much higher velocities of ~3000 m d^{-1}, suggesting that processes are increasing vertical transport here, such as higher levels of production, high-velocity events or a combination of processes not yet fully understood. Previous research has found that the fluxes of ballast minerals (calcium carbonate, opal and

lithogenic material) and the organic carbon fluxes are correlated in the bathypelagic zones of the ocean, leading to the shared hypothesis that organic carbon export is directly controlled by the presence of ballast minerals within settling aggregates. Thus, it is proposed that where increased aggregate density exists and sinking velocity is higher, there is increased organic carbon preservation when ballast minerals are present or by the protection of the organic matter due to the quantitative association to ballast minerals (Armstrong et al., 2001; Francois et al., 2002; Klaas and Archer, 2002). Findings by Klaas and Archer (2002) observed that ~83% of the global particulate organic carbon fluxes were associated with carbonate, suggesting that carbonate is a more efficient ballast mineral compared to opal and terrigenous material. However, this was unsupported by a later study by De La Rocha et al. (2008) which found no positive correlation between calcium carbonate and organic matter, so doubts still exist.

Thus, while historically the deep-sea was believed to be spatially homogenous, often compared to a nutrient-deprived, flat, soft-sediment desert, unable to support rich and varied life forms, improved sampling over the last few decades has disregarded this theory. Instead, species richness and diversity have been linked to large-scale variation in sediment grain size diversity, nutrient and oxygen availability, hydrologic conditions and catastrophic events. Deep-sea sediments are now recognised as being highly dynamic and closely linked to the biosphere at global, regional and landscape scales (Levin et al., 2001).

3.2 Aims

This studies approach aims to characterise the Whittard canyon sediments down core and compare them with the adjacent slopes at different points along several canyon branches, to acquire a more representative spatial and temporal view of the processes that operate in

the system. Laser diffraction will be used to determine the particle size of sediment <2mm in diameter.

In addition, a robust statistical approach will be undertaken in an attempt to identify and quantify generic sediment transport processes and palaeo-environmental changes from grain size distributions of sedimentary core data (Weltje, 1997; Paterson and Heslop, 2015; Yu et al., 2016; Jiang et al., 2017). Within the software MATLAB, the Analysize plugin developed by Paterson and Heslop (2015), powerful unmixing techniques and several routine methods for quantifying grain size data, will be performed to understand better the extensive grain size data set. These include vector ruggedness measurements (VRM), End-member Analysis (EMA) and *C* (one percentile of the grain size) and *M* (the median) plots.

The combined analyses of the canyon sediments will be done to evaluate the role of the system in transporting material from the upper reaches of the ocean to the abyss and its potential for carbon burial.

3.3 Methods

3.3.1 Grain size distribution analysis

One of the most popular tests undertaken for the study of soil and sediments in geological investigations is that of particle, or grain size distribution (GSD) analysis (Folk and Ward, 1957; Passega and Byramjee, 1969; Martín et al., 2014). Particle size distribution is an essential aspect of the oceanic system and its study can create an understanding of the palaeoenvironmental environment, sedimentary processes and depositional conditions. The behaviour of particles is governed mainly by their size, density and shape and it is these physical characteristics that ultimately affect the erosion, transportation and deposition of

material (Passega, 2003; Blott et al., 2004; McCave and Syvitski, 2010).

I. Sediment sample preparation

As particles did not exceed 2mm, it was not necessary to sieve material prior to analysis. Due to the very low organic matter (>2%) (OM) contents of the samples, OM removal was not necessary prior to analysis. Using the laser diffraction method, a Beckman Coulter LS13320 Laser Diffraction Particle Size Analyser was used to determine the granulometric properties of particles ranging between 0.04µm to 2mm.

II. Instrument operation

Laser diffraction analysis technologies were developed in the 1970s (Agrawal et al., 2010). The technology is based on the principle that when a laser beam is passed through a sediment suspended in a fluid smaller particles scatter a parallel beam of monochromatic light at specific intensities and higher angles than larger particles (Cheetham et al., 2008). The method is fast, automated, reproducible and non-destructive, allowing for a large number of samples to be run and a statistically significant data spread to be achieved (Blott et al., 2004; Switzer and Pile, 2015).

Approximately 0.5g of each cm core section was run five times; this was done to ensure that aggregates were broken down and accurate particle size was measured. The data collected from the first four runs was discarded. No significant flocculation of particles was observed due to the low organic content. Flocculation is known to be one of the fundamental processes for determining the size, settling velocity, and deposition rate of fine-grained cohesive sediment particles in marine environments (Fettweis et al., 2012; Lee et al., 2014).

3.3.2 Statistical analysis

The raw data retrieved from the Beckman Coulter LS13320 Analyser was put into the GRADISTAT macro for Excel (Blott and Pye, 1986). Descriptive statistics such as mean, mode, sorting (σ_G), skewness (S_{KG}) and kurtosis (K_G) were calculated arithmetically and geometrically (metric units) and logarithmically (phi units) using moment and Folk and Ward graphical methods (Blott and Pye, 2001).

In the early 1900s, Chester Wentworth devised a solution to standardise the analysis of clastic sediments using the phi scale (Wentworth, 1922). Method evaluation by Blott and Pye (2001) identified that the Folk and Ward measures (in metric units) appeared to provide the most robust foundation for comparing variable sediments routinely, particularly where data is non-normally distributed and polymodal, as is the case in this study area. However, there are still limitations when interpreting multimodal distributions using descriptive moments (Folk and Ward, 1957; Blott and Pye, 2001).

All statistics were expressed with standard deviation to express value dispersion. Of the descriptive statistics recorded, sorting indicates the fluctuation in the amount of kinetic energy and the depositional regime on grain size characteristics. Skewness measures the degree of particle distribution asymmetry. The skewness for a normal distribution is zero, positive values (skewed left) indicate skewness towards finer grain sizes, while negative values (skewed right) indicate skewness towards coarser material (Pedrosa-Pàmies et al., 2015). Kurtosis measures the “peakedness” of grain size frequency curves and the degree of outliers from the normal distribution. General forms of kurtosis are as follows; leptokurtic (positive) mesokurtic (normal) and platykurtic (negative). The term leptokurtic refers to a statistical distribution where excess kurtosis values are positive, therefore resulting in a

higher probability of extreme positive or negative outliers. Mesokurtic refers to a distribution that is close to or the same as the normal distribution. Lastly, the term platykurtic refers to a statistical distribution where excess kurtosis values are negative, therefore resulting in fewer extreme positive or negative outliers (Folk and Ward, 1957; Blott and Pye, 2001; Rajganapathi et al., 2013).

Down core (0-10cm) descriptive statistics, including mean and standard deviation, were generated using IBM SPSS Statistics 23. Within this software, normality distributions were identified using the Shapiro-Wilk test. All granulometric data was either non-normally distributed ($p < 0.05$) or of small sample size, so nonparametric tests were used. Comparison of mean values were determined using IBM SPSS Statistics 23. For independent samples, the non-parametric Kruskal-Wallis (one-way ANOVA on ranks) test was used.

Where results failed the assumption of homogeneity of variances ($p > 0.05$), therefore retaining the null hypothesis, the nature of differences was evaluated using Dunn-Bonferroni post-hoc pairwise comparison tests.

Non-parametric Spearman's rank correlation test was used to examine relationships between the data sets for further information; please refer to Chapter 1: Methods.

Surficial and average down core sedimentary parameters plots (grain size, sorting, skewness and kurtosis) were created using Ocean Data View 4.7.4 software (ODV) © 2016 Reiner Schlitzer, for further information, please refer to Chapter 1: Methods.

Down core grain size composition was presented as sand–silt–clay percentages using the AnalySize plugin in Matlab.

CM patterns were explored to better understand the relationship between the depositional environment and the hydrodynamic conditions of the Whittard Canyon sediments (Passega, 1957, 1964). *C* (coarse one percentile in micron of the grain size) and *M* (the median value in micron) values were obtained from phi values of the *C* and *M* from cumulative frequency curves. These values were plotted on a lognormal probability plot with the help of the AnalySize package in Matlab. As per Passega's methodology, the *CM* pattern is divided into five segments to determine the depositional mechanisms – 1: rolling; 2: bottom suspension and rolling; 3: graded suspension no rolling; 4: uniform suspension and 5: pelagic suspension. Further to this, the *CM* pattern was used to establish the sedimentary sub-environment-1: pelagic; 2: tills; 3: river-terrace gravel; 4: tractive current and 5: beach.

Grain size data, composing of all core sections (320 samples), generated by the Beckman Coulter LS13320 Laser Diffraction Particle Size Analyser was reanalysed using the AnalySize plugin within software Matlab. Upon generating end-members, the linear correlation chart between multiple correlation coefficient (R^2) and end-member numbers was examined for the goodness of fit. A high R^2 value is required along with a low theta value, as this indicates that the model has not altered the particle size data to apply fit significantly. Further to this, a low-end-member similarity (*EM* R^2) is preferred as it suggests that the model is not overfitting the data.

Mean surficial and down core sedimentological values (μm, σ_G, S_{KG} and K_G) were plotted using ODV software, for more information refer to Chapter 1: Methods.

3.4 Results

3.4.1 Granulometric properties

The largest down core mean grain size, very fine sand, was observed at the Eastern site CE14009-005-450m (122.10 ± 11.45µm). The smallest deposits, very fine silt, were found at the Explorer site JC125-076-PSH02-861.2m (5.66 ± 1.07µm) (Table 3:1).

Surficial sediments mainly consisted of fine particles, with grain size generally less than 60 µm (Φ 4, silt) in the upper 1cm (Figure 3:1). Very fine sand and silt was observed at the Eastern branch CE14009-005-450 (Φ4 to Φ3, 111.56µm). Fine to medium sand was observed at the Eastern Middle 2 site CE16006-056-PSH05-1845m (Φ3 to Φ2, 187.67µm). This coarser sandy material is present down core to 2cm before it fines out to silts. However, at the same site, a mean GS reading of 19.9µm was also recorded, highlighting variability within sites. The largest range was observed at Eastern Middle 2 and Eastern branches.

One-way ANOVA on ranks analysis indicated that there was a significant spatial change in the surficial grain size distribution across branches (p = 0.038). The Dunn-Bonferonni post-hoc test revealed that there was a significant difference in mean grain size between most branches and the Eastern Middle 2 branch, excluding the Western and Eastern branches. Western Middle and Eastern Middle 2 branch (p =0.045), Acesta and Eastern Middle 2 branch (p = 0.026), Eastern Middle Branch and Eastern Middle 2 branch (p =0.036), Intersection and Eastern Middle 2 branch (p = 0.020), Explorer and Eastern Middle 2 branch (p =0.021), and Main Channel (p =0.010). One-way ANOVA on ranks analysis showed that there was no significant spatial change in the down core grain size distribution across

branches ($p < 0.05$).

Mean down core sorting values reveal that all samples range between very poorly sorted (2.00-4.00σ_G) and extremely poorly sorted (>4.00σ_G) (Figure 3:2). The Eastern Middle site CE16006-030-PSH07-700m is the most well-sorted (2.02σ_G). However, it is still considered very poorly sorted by Folk and Ward. The most poorly sorted site was the Explorer site JC125-076-PSH02-861.2m (5.66σ_G). One-way ANOVA on ranks analysis showed that there was a significant spatial change in the surficial sorting across branches ($p = 0.043$). As a result of a significant spatial change across branches being recognized further analysis was undertaken to explore this further. Dunn-Bonferroni Post-hoc analysis revealed that there was no significant difference in sorting at the Eastern Middle 2 branch compared to all branches ($p > 0.05$), the Eastern branch only differed significantly from the Main channel ($p > 0.24$). Significant difference in sorting were observed between the Western and Western Middle branches ($p = 0.007$), Western and Intersection ($p = 0.041$), Western and Main Channel ($p = 0.004$), Western Middle and Eastern Branch ($p = 0.043$), Western Middle and Explorer Branch ($p = 0.034$), Acesta and Main Channel ($p = 0.029$), and Explorer and Main Channel ($p = 0.017$).

Most sites, except for two (Eastern CE14009-005-681m and Explorer JC125-076-PSH02-861.2m), were negatively and very negatively skewed (-0.3 to-1S_{KG}) (Figure 3:3). The Eastern CE14009-005-681m and Explorer site JC125-076-PSH02-861.2m site recorded down core skewness measures that were nearly symmetrical (-0.01 ± 0.03 and -0.08 ± 0.02 S_{KG}). One-way ANOVA on ranks analysis showed that there was no significant spatial change in surficial sorting across branches ($p < 0.05$).

Mean down core kurtosis values recorded at most sites were mesokurtic and not especially

peaked (Figure 3:4). However, some sites displayed large kurtosis values and were very highly peaked. These sites include sites: Western JC125-083-PSH03-2740m (1.88 ± 0.15K_G), Western Middle CE16006-081-PSH03-1601m (1.64 ± 0.83K_G), Eastern Middle 2 CE16006-056-PSH05-1845m (1.91 ± 1.12K_G) and the Eastern branch site CE14009-005-450m (1.88 ± 0.15K_G). One-way ANOVA on ranks analysis showed that there was no significant spatial change in the surficial kurtosis across branches ($p < 0.05$).

Grain size revealed both positive and negative correlations when compared to other variables. A high negative correlation with skewness (rs [48] = -0.651, $p = 0.000$), moderate positive correlation with kurtosis (rs [48] = 0.320, $p = 0.030$). Mean down core grain size was found to be negatively correlated with sorting (rs [48] =-0.404, $p = 0.005$) and negatively correlated with skewness (rs [48] = -0.732, $p = 0.000$). Mean down core grain size was positively correlated with kurtosis (rs [48] = 0.439, $p = 0.002$).

Skewness was negatively correlated with kurtosis (rs [48] = -0.362, $p = 0.013$). Kurtosis negatively correlated with sorting (rs [48] = -0.651, $p = 0.000$). Sorting positively correlated with skewness (rs [48] = -.424, $p = 0.003$).

Relationships between sedimentological characteristics and depth were also explored. A minor positive correlation between kurtosis and depth was recorded (rs [48] = 0.296, $p = 0.046$). Furthermore, surficial grain size negatively correlated with depth (rs [48] = -0.322, p = 0.029).

Table 3:1 Down core mean values with standard deviations of granulometric properties of particles from 9 branches of the Whittard Canyon. Canyon branches are colour coded Purple (Western Branch), Pink (Western Middle Branch), Yellow (Acesta Branch), Green (Eastern Middle Branch), Cream (Intersection), Magenta (Eastern Mid 2), Brown (Eastern Branch), Blue (Explorer Canyon) and Red (Main Channel). N = number of sections, where 10 where not met.

BRANCH	DEPTH (m)	CORE	SURFICIAL GRAIN SIZE (µm)	DOWN CORE MEAN GRAIN SIZE (µm)	DOWN CORE SORTING ($б_G$)	DOWN CORE SKEWNESS (S_{KG})	DOWN CORE KURTOSIS (K_G)
Western	2740	JC125-083-PSH03-	52.72	35.40 ± 18.91	4.35 ± 0.42	-0.46 ± 0.25	1.88 ± 0.15
Western Middle	440	CE14009-045-440m	44.48	53.23 ± 6.93	3.41 ± 0.21	-0.52 ± 0.05 N9	1.12 ± 0.11 N9
Western Middle	719	CE14009-042-719m	18.95	20.43 ± 1.11	3.38 ± 0.08	-0.33 ± 0.03	1.06 ± 0.03
Western Middle	781	CE16006-087-PSH02-	26.38	26.21 ± 1.58	3.60 ± 0.07	-0.38 ± 0.33	1.00 ± 0.02
Western Middle	819	CE14009-042-819m	35.02	35.39 ± 6.32	3.88 ± 0.15	-0.34 ± 0.09	0.97 ± 0.03
Western Middle	1601	CE16006-081-PSH03-	49.23	67.02 ± 41.13	3.11 ± 1.02	-0.52 ± 0.17	1.64 ± 0.83
Acesta	499	JC125-078-PSH02-	46.27	24.739 ± 14.35	4.65 ± 0.45	-0.39 ± 0.26	0.83 ± 0.07
Acesta	640	JC125-080-PSH04-	34.62	28.68 ± 4.12	3.90 ± 0.11	-0.47 ± 0.10 N7	0.83 ± 0.03 N7
Acesta	780	CE16006-033-PSH08-	19.42	17.37 ± 2.16 N5	4.12 ± 0.34 N5	-0.21 ± 0.03 N5	1.06 ± 0.03
Acesta	974	CE16006-084-PSH05-	21.56	59.91 ± 68.88 N9	3.41 ± 0.40	-0.36 ± 0.18 N7	1.00 ± 0.09 n7
Acesta	974.2	CE16006-084-PSH02-	24.69	27.27 ± 4.07 N7	3.73 ± 0.11	-0.36 ± 0.10	1.03 ± 0.03 N10
Acesta	1130	CE14009-009-1130m	29.06	31.87 ± 3.79	3.38 ± 0.07	-0.44 ± 0.44	1.03 ± 0.04
Acesta	1487	CE14009-027-1487m	21.57	18.63 ± 1.39	3.43 ± 0.07	-0.32 ± 0.12	1.12 ± 0.03
Acesta	2816	CE14009-027-2816m	38.29	47.88 ± 28.15	3.45 ± 0.63	-0.44 ± 0.15	1.18 ± 0.53 n9
Eastern Middle	501	CE14009-040-501m	41.91	45.16 ± 1.70	3.24 ± 0.06	-0.41± 0.02	1.17 ± 0.03
Eastern Middle	511	CE16006-030-PSH12-	47.44	37.11± 17.26	4.05 ± 0.47	-0.41 ± 0.18	1.01 ± 0.15
Eastern Middle	574	CE14009-012-574m	30.25	44.73 ± 18.79	3.19 ± 0.46	-0.40 ± 0.08	1.29 ± 0.34
Eastern Middle	659	CE14009-030-659m	24.34	21.85 ± 1.64	3.67 ± 0.11	-0.30 ± 0.01	1.00 ± 0.03
Eastern Middle	700	CE14009-030-700m	34.58	27.77 ± 2.52	3.73 ± 0.12	-0.25 ± 0.04	1.00 ± 0.08
Eastern Middle	700	CE16006-030-PSH07-	31.62	23.22 ± 5.10	2.02 ± 0.32	-0.35 ± 0.02	1.01 ± 0.03
Eastern Middle	723	CE14009-033-723m	30.19	48.93 ± 23.76	3.16 ± 0.58	-0.36 ± 0.05	1.26 ± 0.31
Eastern Middle	731	CE16006-022-PSH06-	21.49	21.20 ± 1.68	3.84 ± 0.12	-0.27 ± 0.02	1.06 ± 0.04
Eastern Middle	1095	CE14009-040-1095m	48.69	27.86 ± 15.89	3.67 ± 0.50	-0.30 ± 0.13	1.09 ± 0.12
Eastern Middle	1271	CE16006-062-PSH07-	23.51	22.68 ± 1.55	3.99 ± 0.17	-0.23 ± 0.01	1.03 ± 0.05
Eastern Middle	1323	CE14009-012-PSH09-	60.25	64.68 ± 13.20	4.20 ± 0.40	-0.31 ± 0.08	1.14 ± 0.08
Intersection	1487	CE14009-031-1487m	21.75	21.42 ± 1.50	3.64 ± 0.11	-0.28 ± 0.02	1.01 ± 0.06
Intersection	1776	CE14009-031-1776m	20.43	20.01 ± 1.36	3.53 ± 0.12	-0.29 ± 0.03	1.09 ± .003
Intersection	1836	CE14009-025-PSH12-	24.73	22.91 ± 3.78	3.50 ± 0.16	-0.33 ± 0.04	1.06 ± 0.04
Intersection	2086	CE14009-025-2086m	24.48	26.70 ± 5.40	3.61 ± 0.19	-0.30 ± 0.18	1.06 ± .0.03
Intersection	2384	CE14009-025-2384m	36.95	48.02 ± 8.63	3.54 ± 0.19	-0.51 ± 0.06	1.10 ± .0.07
Eastern Mid 2	1845	CE16006-056-PSH05-	187.67	57.11 ± 72.08	3.43 ± 0.85	-0.38 ± 0.17	1.91 ± 1.12

Eastern Mid 2	1850	CE16006-056-PSH07-	19.91	20.10 ± 3.97	3.83 ± 0.20	-0.27 ± 0.07	1.02 ± 0.09
Eastern	450	CE14009-005-450m	111.56	122.10 ± 11.45	2.61 ± 0.21	-0.48 ± 0.03	1.88 ± 0.15
Eastern	571	JC125-109-PSH03-	33.68	43.02 ± 7.87	3.79 ± 0.18	-0.60 ± 0.08	1.07 ± 0.19
Eastern	571	JC125-109-PSH05-	27.89	36.08 ± 6.83	3.71 ± 0.17	-0.60 ± 0.08	1.07 ± 0.19
Eastern	681	CE14009-005-681m	25.04	19.18 ± 4.99	5.64 ± 0.21	-0.01 ± 0.03	0.90 ± 0.09
Eastern	1233	JC125-111-PSH05-	21.05	18.52 ± 3.51	4.25 ± 0.19	-0.20 ± 0.07	0.85 ± 0.02
Eastern	1298	CE16006-002-PSH05-	22.75	47.93 ± 64.10	3.56 ± 0.17	-0.32 ± 0.13	0.98 ± 0.03
Eastern	1620	CE16006-042-PSH02-	31.97	ABSENT	ABSENT	ABSENT	ABSENT
Eastern	2979	JC125-091-PSH05-	20.55	36.68 ± 45.29	3.87 ± 0.91	-0.25 ± 0.20	1.17 ± 0.57
Explorer	664	JC125-101-MC-664m	22.75	11.03 ± 4.52	3.52 ± 0.21	-0.21 ± 0.02	1.18 ± 0.07
Explorer	764	JC125-035-764.4m	26.41	23.10 ± 4.54	4.24 ± 0.15	-0.41 ± 0.11	0.79 ± 0.02
Explorer	861	JC125-076-PSH02-	7.35	5.66 ± 1.07	5.66 ± 1.07	-0.08 ± 0.02	0.88 ± 0.01
Main Channel	3723	JC125-045-MC-3723m	11.63	12.78 ± 2.61	3.25 ± 0.18	-0.28 ± 0.06	1.13 ± 0.08
Main Channel	3759	JC125-028-MC-3758m	18.79	28.65 ± 11.84	3.20 ± 0.18	-0.37 ± 0.11	1.14 ± 0.06
Main Channel	4010	JC125-063-MC-4010m	10.07	17.22 ± 15.43	3.30 ± 0.24	-0.35 ± 0.10	1.21 ± 0.15

I. *Surficial and down core mean grain size*

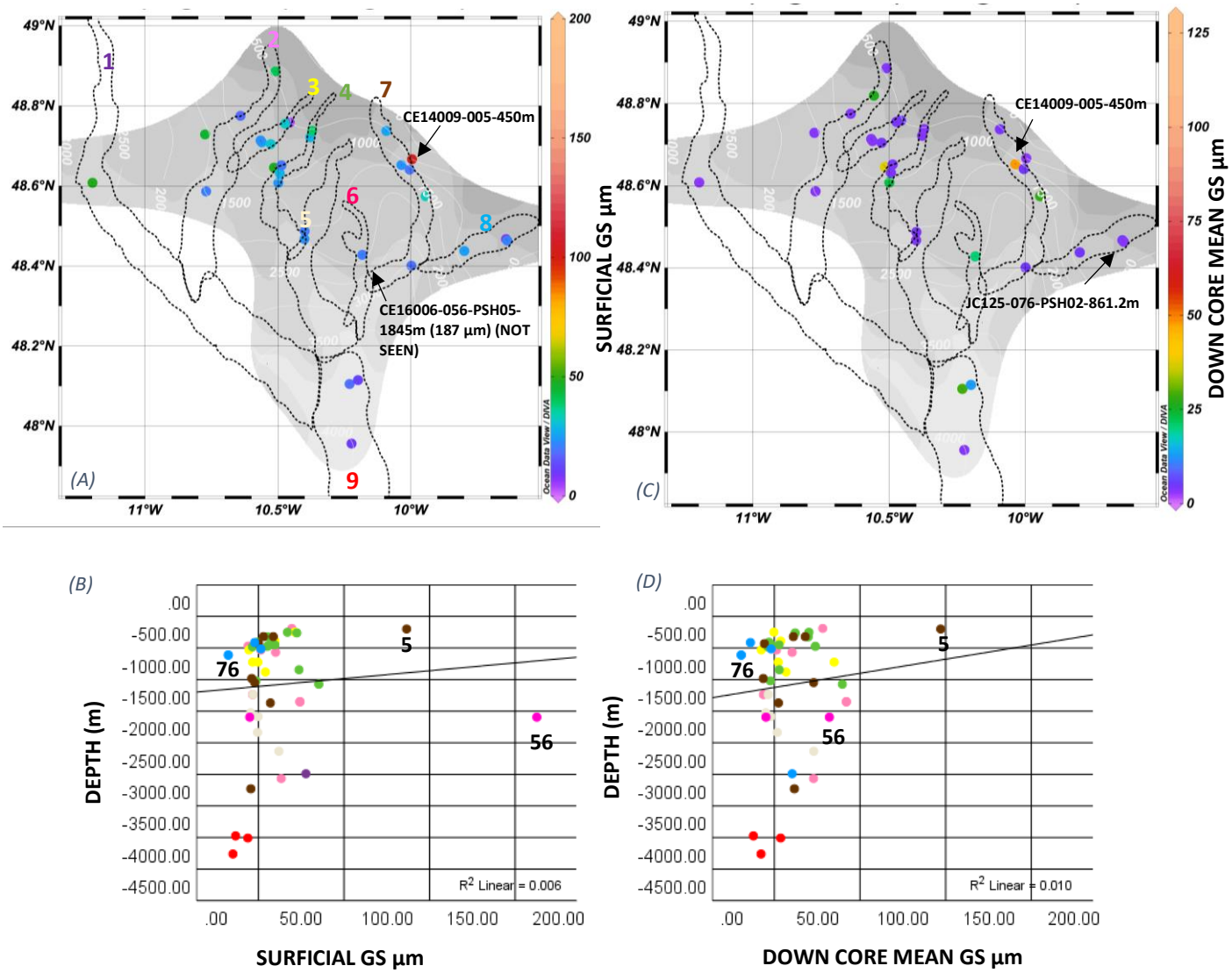

Figure 3:1 (A, B) Surface plot and scatter diagram of the grain size of the first-centimetre section across sites. Sediments mainly consist of fine particles, with grain size generally less than 60 µm (Φ 4, silt). Very fine sand observed at the Eastern branch CE14009-005-450 (Folk and Ward Method mean M_G 111.56µm (Φ 4 to 3, silt and very fine sand). Fine sand to medium sand observed at the Eastern Middle 2 site CE16006-056-PSH05-1845m (Φ 3 to 2, 187.67µm) However, an additional core was taken at the same site, recorded a surficial mean GS reading of 19.9µm. One-way ANOVA on ranks analysis revealed a significant spatial change in the surficial grain size distribution across the branches (p= 0.038). Most sites, excluding the Western and Eastern branches, significantly deviated from the mean grain size of the Eastern Middle 2 branch. Surficial grain size negatively correlated with depth (rs [48] = -0.322, p = 0.029). (C, D) Surface plot and scatter diagram of mean grain size down core across sites. Sediments mainly consist of fine particles, with the grain size generally less than 60 µm (Φ 4, silt). However, at the Eastern branch CE14009-005-450, an average down core particle size of 112.11µm was recorded. Numbers are events.

II. *Down core mean sorting*

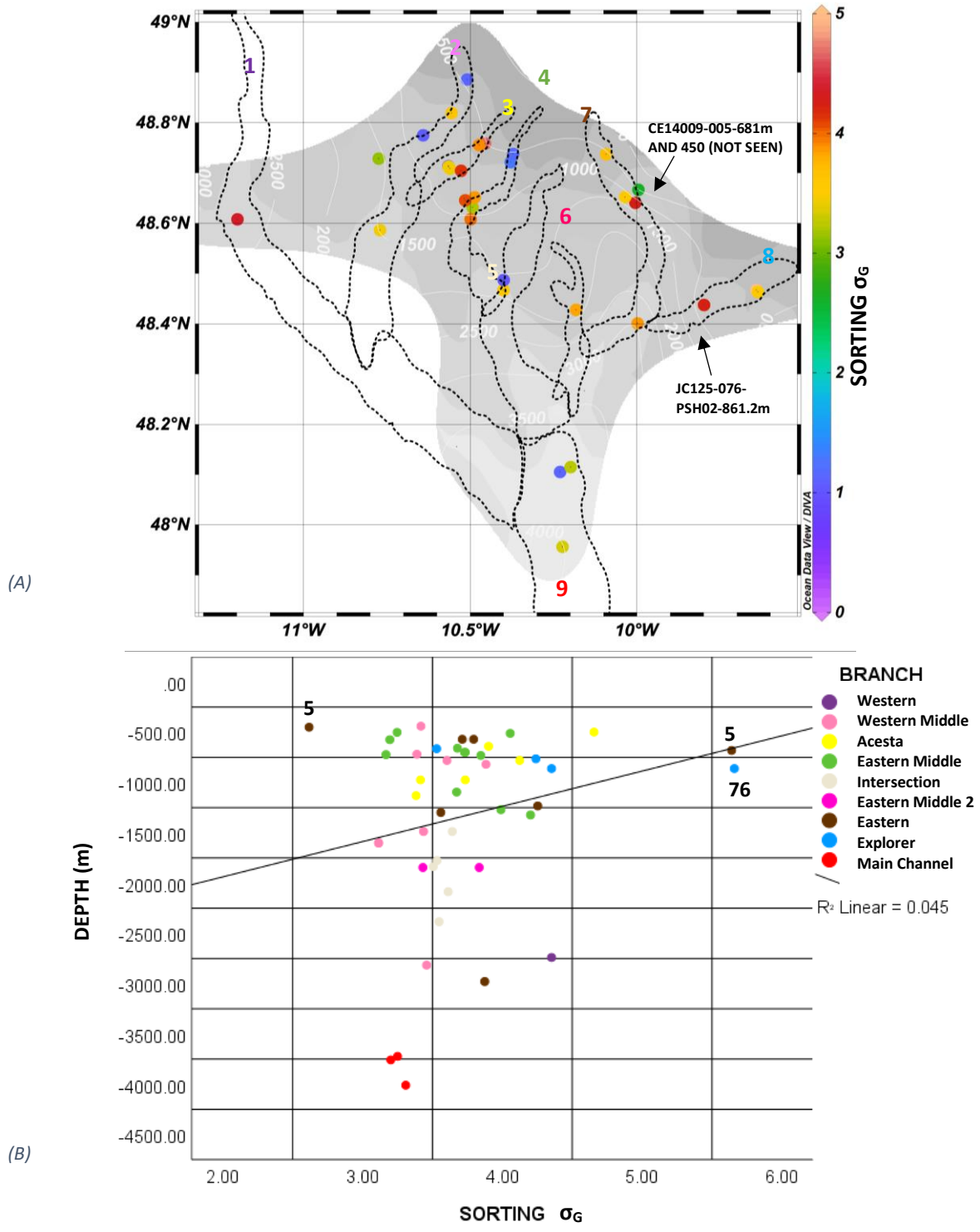

Figure 3:2 (A) Surface plot of down core mean sorting across sites. Sediments consist of very poorly and extremely poorly sorted sediments, within the range of 2-6 σ_G*. (B) Scatter diagram of the range of mean down core sorting across all branches with depth. The largest ranges observed at the Acesta and Eastern branches. The most poorly sorted site was within the Explorer branch. The most sorted, yet still classified as poorly sorted was within the Eastern branch. R-squared linear correlation coefficient revealed no significant linear relationship between depth and sorting. One-way ANOVA on ranks analysis showed that there was a significant difference in sorting across the branches (p = 0.43). Dunn-Bonferroni post-hoc analysis revealed that there was a significant difference in sorting between some branches. Numbers are events.*

III. *Down core mean skewness*

(A)

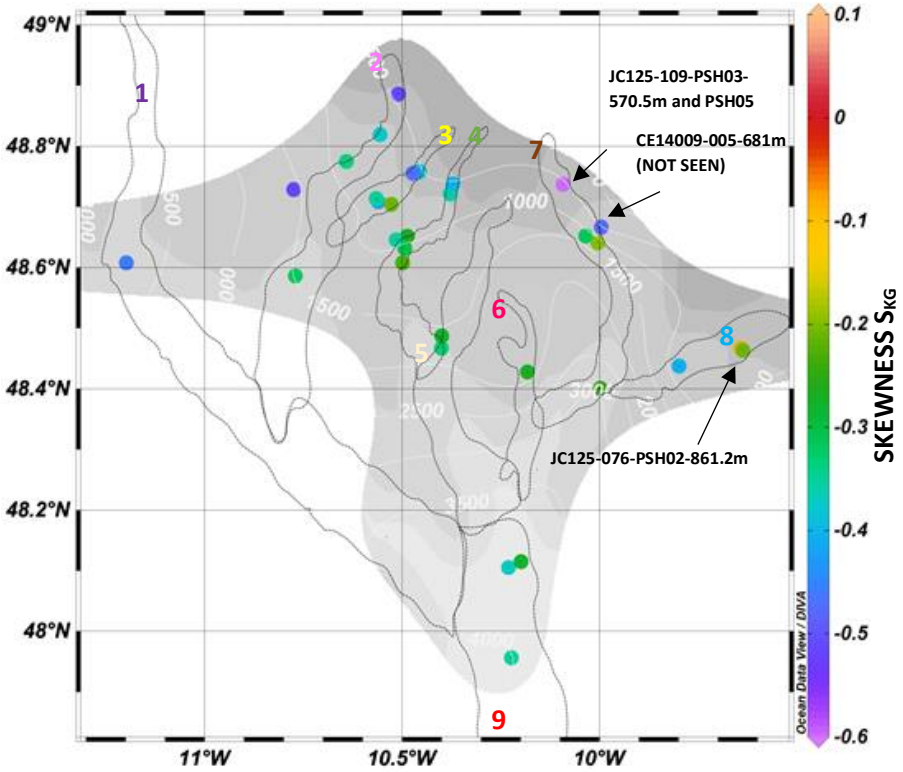

(B)

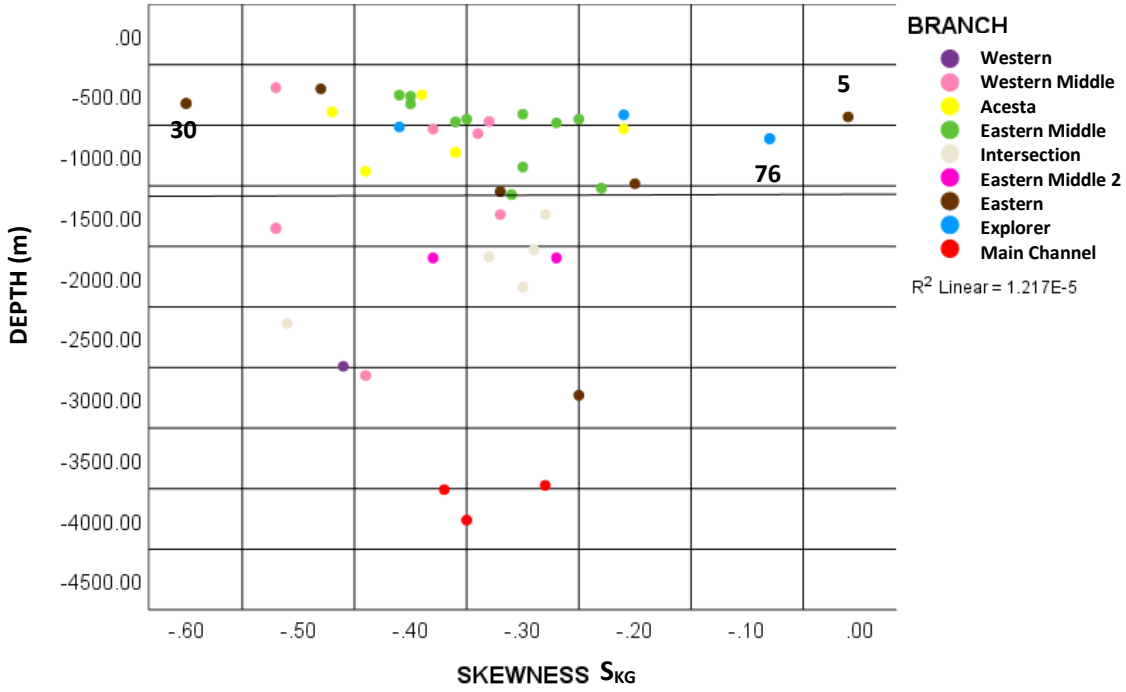

Figure 3:3 (A) Surface plot of down core mean skewness across sites. Sediments mainly consist of negatively skewed sediments. (B) The most positively skewed site was in the Eastern sites JC125-109-PSH03-570.5m and PSH05 (-0.6 S_{KG}). However, at the Eastern branch CE14009-005-681, an average down core of near-symmetrical skewness of -0.01 S_{KG} was also recorded. Scatter chart of the range of mean down core skewness across all branches. Largest range observed at the Eastern branch. R-squared linear correlation coefficient analysis revealed no significant linear relationship between depth and skewness. One-way ANOVA on ranks analysis showed that there was no significant difference in sorting across the branches ($p > 0.05$). Numbers are events.

IV. *Down core mean kurtosis*

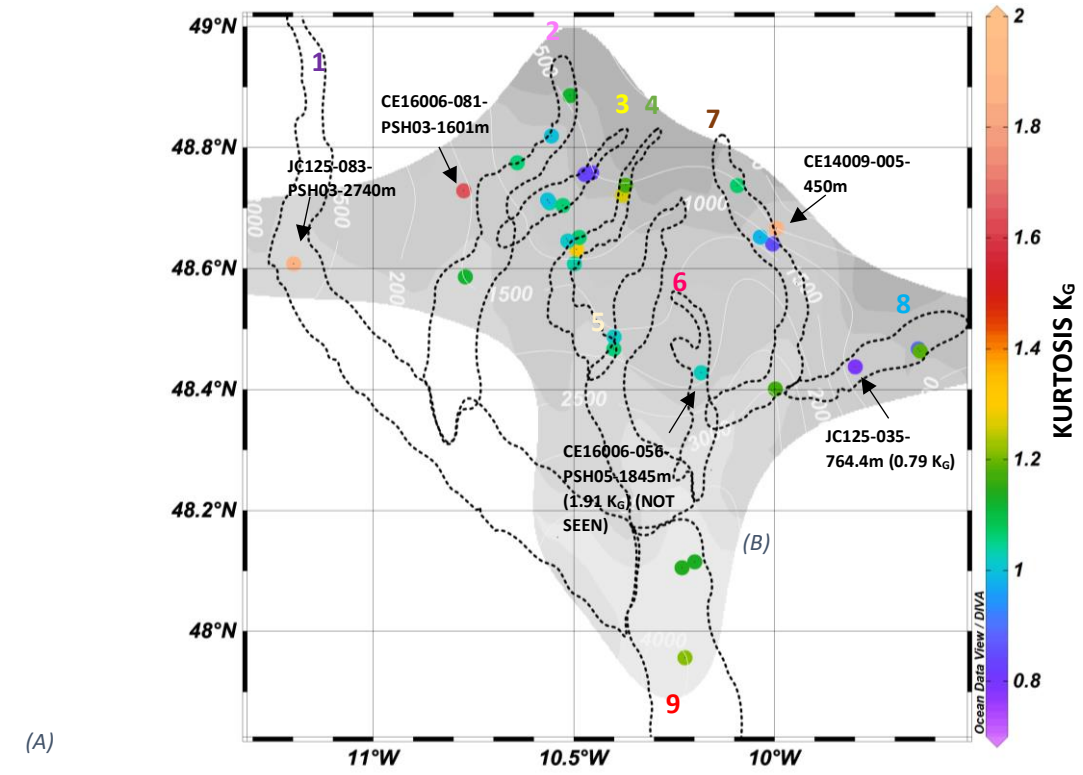

(A)

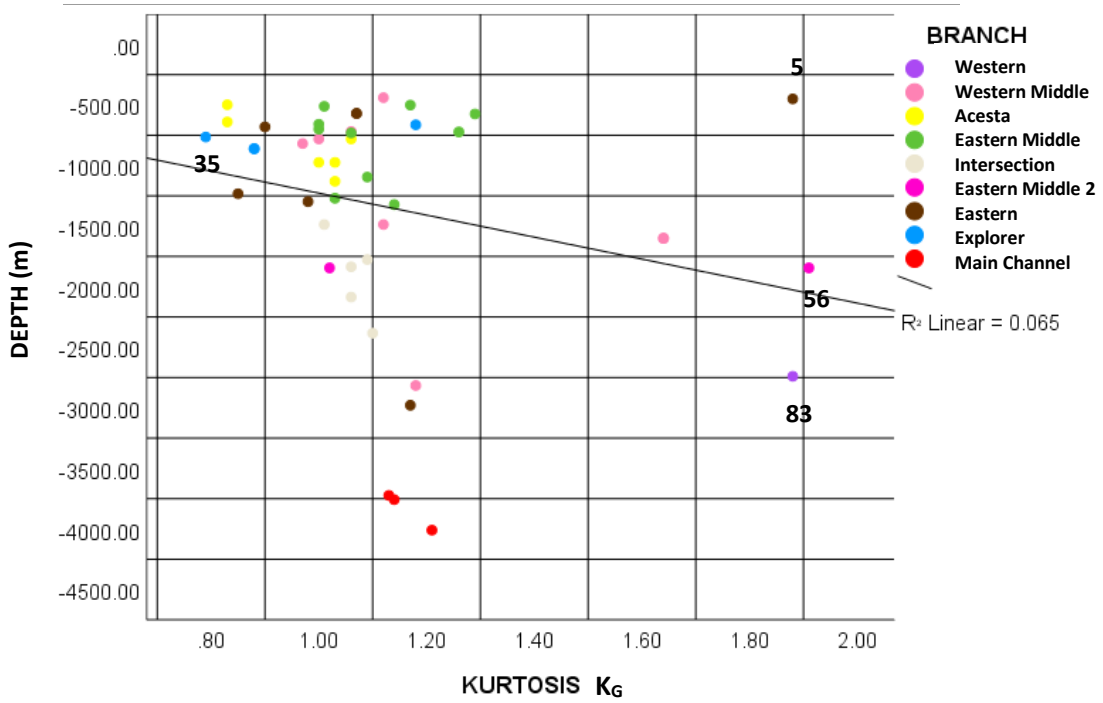

(B)

Figure 3:4 (A) Surface plot of down core mean kurtosis across sites. Mesokurtic sediments, not especially peaked or "normal" (0.9-0.11K_G) and leptokurtic and very leptokurtic, highly peaked, sediments (1.11->1.50) were observed across most sites. However, some platykurtic, flat peaked, values were observed within the Explorer, Acesta and Eastern branches. (B) Scatter diagram of the range of mean down core kurtosis across all branches. Largest range observed at the Eastern branch. R-squared linear correlation coefficient on analysis revealed no significant linear relationship between depth and kurtosis, however Spearman's rank analysis did reveal a minor positive relationship (rs [48] = 0.296, p = 0.046). One-way ANOVA on ranks analysis showed that there was no significant difference in sorting across the branches (p > 0.05). Numbers are events.

V. *Clast percentages*

The down core grain size variation is presented in Figure 3:5 as sand–silt–clay percentages. All cores displayed a minimum of three grain-size modes (e.g. Western branch JC125-083-PSH03-2740m) however, within some sections bi-modal distributions were observed (e.g. Main Channel JC125-045-MC-3723m 2-3cm). The presence of these distinctive polymodal grain-size modes in the samples is consistent with changing modes of deposition and the contribution of different material over time. The populations are partitioned as follows, fine sand (A), silt (B) and clay (C). Sediments from the upper reaches, down to 500m, were dominated by silty sand (>50%). Beyond this, excluding the Explorer canyon and the Main Channel, fine sand and silt continue to dominate the sites to depths of 2816m. The Explorer branch of the canyon had the most considerable clay fraction of the sites analysed (~ 40%). Within the Explorer site JC125-076-PSH02-861.2m, the sand fraction was observed in the first three-centimetre sections, before a bimodal signature was observed. While sand depletes beyond 2816m, silt continues to dominate to the lower reaches of the canyon. However, within the main channel, at depths exceeding 3500m coarse sand punctuates the core profile.

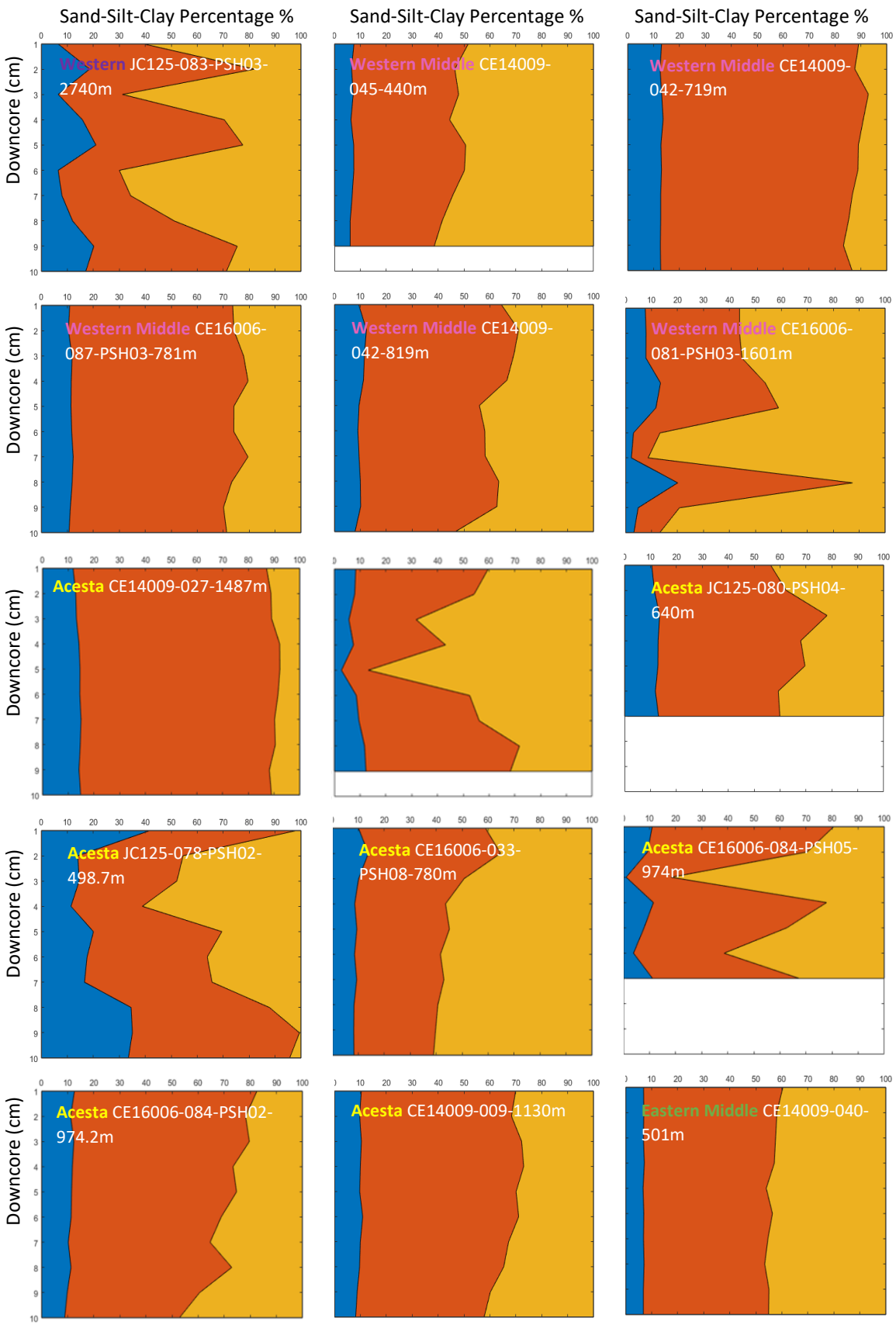
Sand-Silt-Clay Percentage %
Sand-Silt-Clay Percentage %
Sand-Silt-Clay Percentage %
Downcore (cm)
Western JC125-083-PSH03-2740m
Western Middle CE14009-045-440m
Western Middle CE14009-042-719m
Western Middle CE16006-087-PSH03-781m
Western Middle CE14009-042-819m
Western Middle CE16006-081-PSH03-1601m
Acesta CE14009-027-1487m
Acesta JC125-080-PSH04-640m
Acesta JC125-078-PSH02-498.7m
Acesta CE16006-033-PSH08-780m
Acesta CE16006-084-PSH05-974m
Acesta CE16006-084-PSH02-974.2m
Acesta CE14009-009-1130m
Eastern Middle CE14009-040-501m

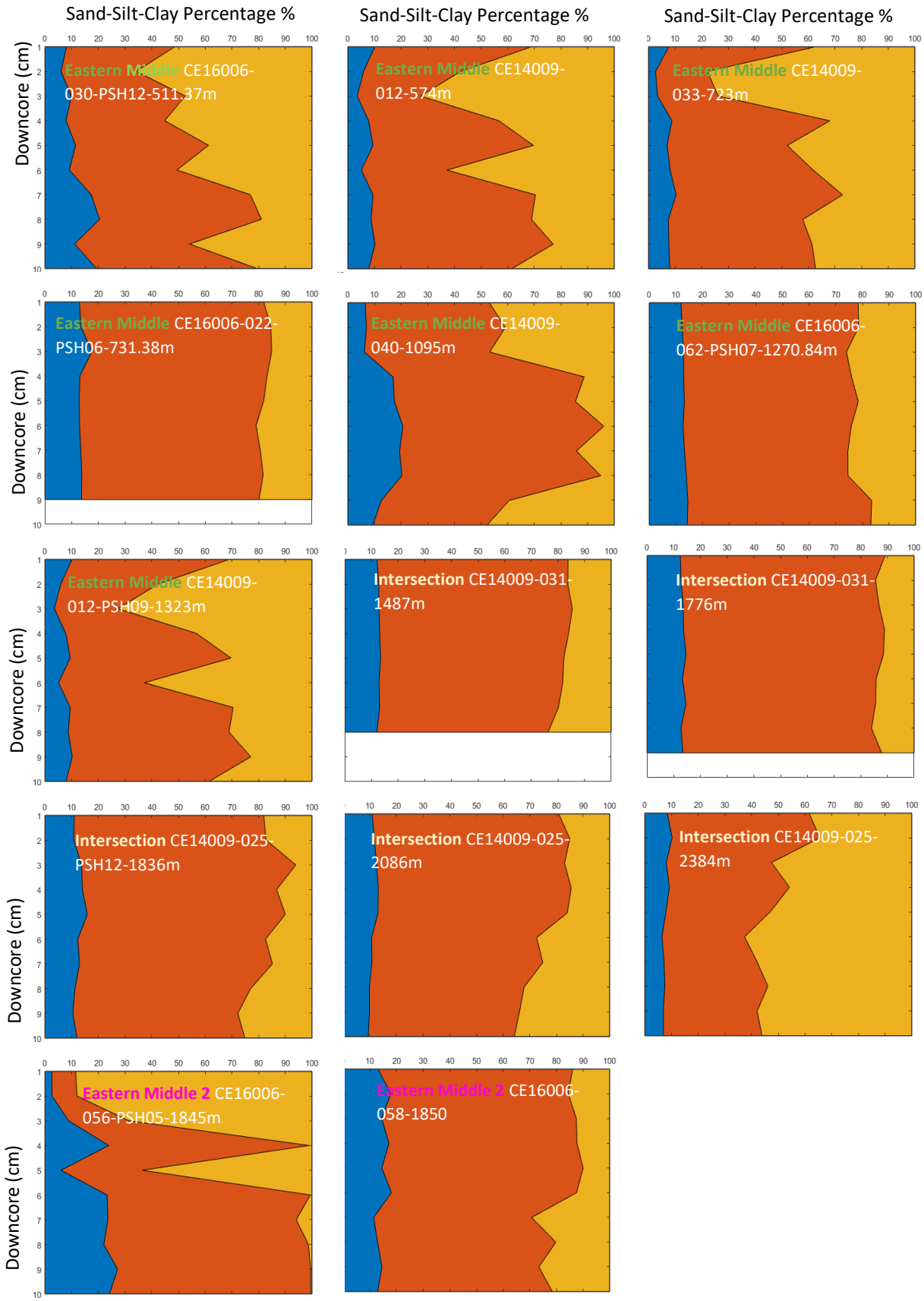
Sand-Silt-Clay Percentage %
Sand-Silt-Clay Percentage %
Sand-Silt-Clay Percentage %
Downcore (cm)
Eastern Middle CE16006-030-PSH12-511.37m
Eastern Middle CE14009-012-574m
Eastern Middle CE14009-033-723m
Eastern Middle CE16006-022-PSH06-731.38m
Eastern Middle CE14009-040-1095m
Eastern Middle CE16006-062-PSH07-1270.84m
Eastern Middle CE14009-012-PSH09-1323m
Intersection CE14009-031-1487m
Intersection CE14009-031-1776m
Intersection CE14009-025-PSH12-1836m
Intersection CE14009-025-2086m
Intersection CE14009-025-2384m
Eastern Middle 2 CE16006-056-PSH05-1845m
Eastern Middle 2 CE16006-058-1850

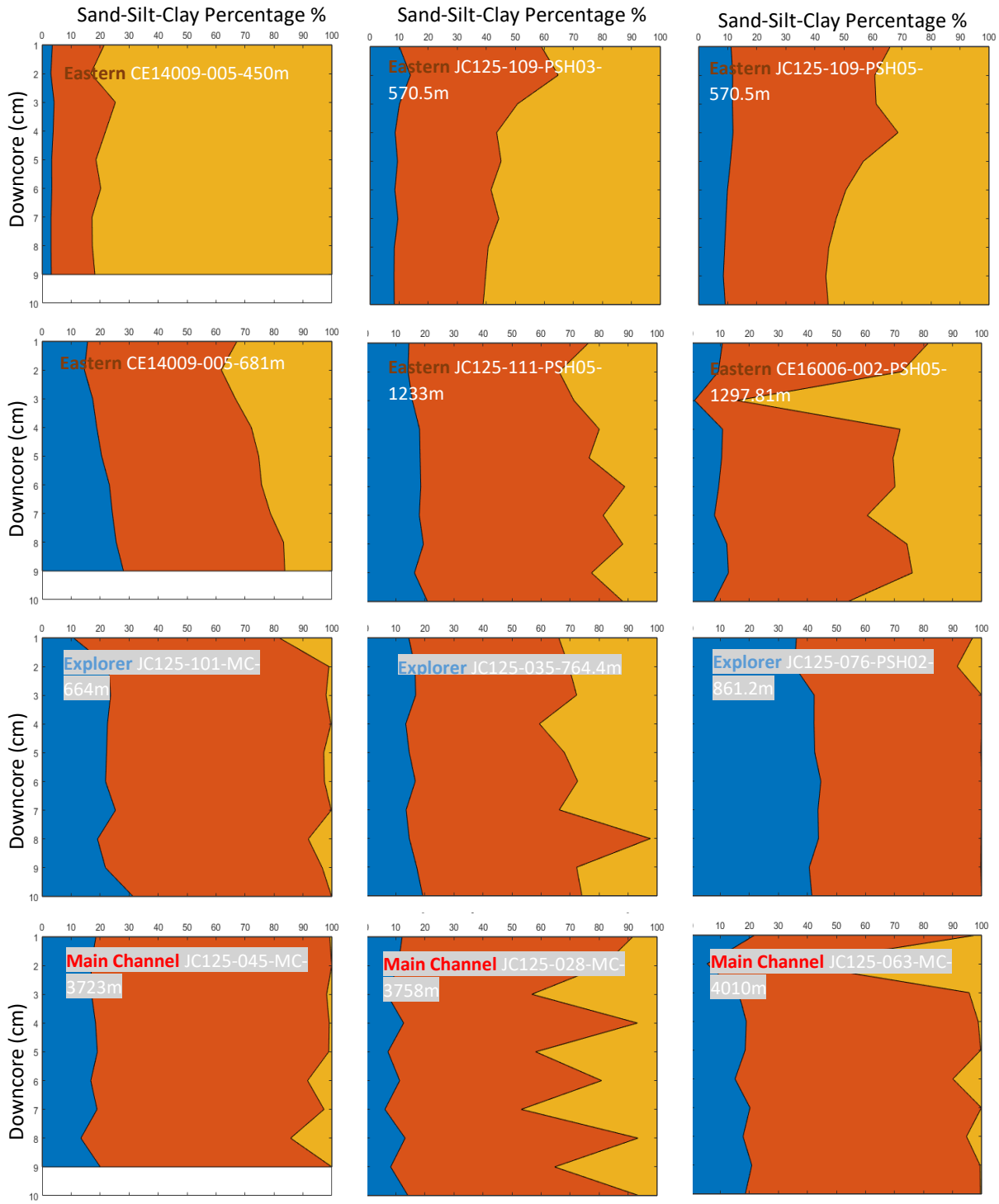

Figure 3:5 Mean down core total sand–silt–clay percentages of sites across nine branches of the Whittard Canyon. Where blue is clay, red is silt and yellow is sand.

VI. *Passega diagram*

Plots between *C* (coarse one percentile in microns) and *M* (median value in microns) obtained from phi values of the *C* and *M* from the cumulative frequency curves, are plotted on the lognormal probability plots. The Whittard Canyon samples fall within graded suspension no rolling to uniform and pelagic suspension in the pelagic and tractive current sub environments (Figure 3:6).

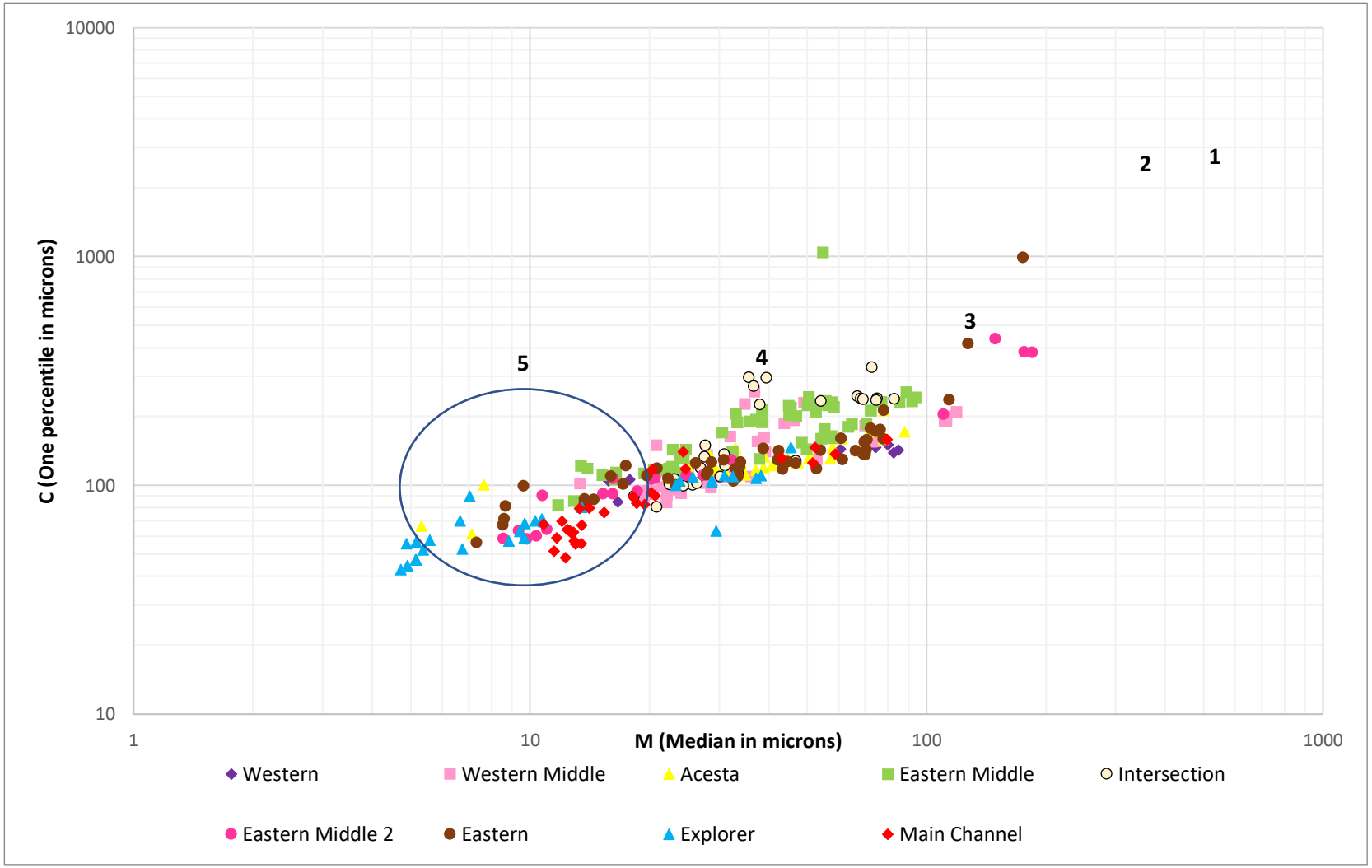

Figure 3:6 CM plot indicating depositional mechanisms and sedimentary sub environments. Numbers indicate mechanisms and sub environments 1= rolling and beach deposits 2= bottom suspension and rolling tractive current deposits 3= graded suspension, no rolling, river-terrace gravel 4= uniform suspension of tills 5= pelagic suspension and pelagic. All sediments fall within graded, uniform suspension of tills and pelagic suspension hydrological conditions (Passega, 1957, 1964).

3.4.2 End-member analysis

The linear correlation chart between multiple correlation coefficient (R^2) and end-member numbers (Figure 3:7A), end-member (EM) modelling improved greatly from three to four end-members but changed less between four to five end-members. A high R^2 value of 0.9443 suggested that four end-members explain the particle size distribution well. A low theta value (11.4102), indicates that the model has not altered the particle size data to apply fit significantly and there is a low-end-member similarity (0.0135 EM R^2) suggesting that the model is not overfitting the data. This combined information suggests that four end-members may explain the data set well. EM 1 (blue) peaked between 1-3 (phi units), EM 2 (orange) peaked between 3 and 4 (phi units), EM 3 (yellow) peaked between 4 and 5(phi units), and EM 4 (purple) peaked between 5 and 6 (phi units) (Figure 3:7B).

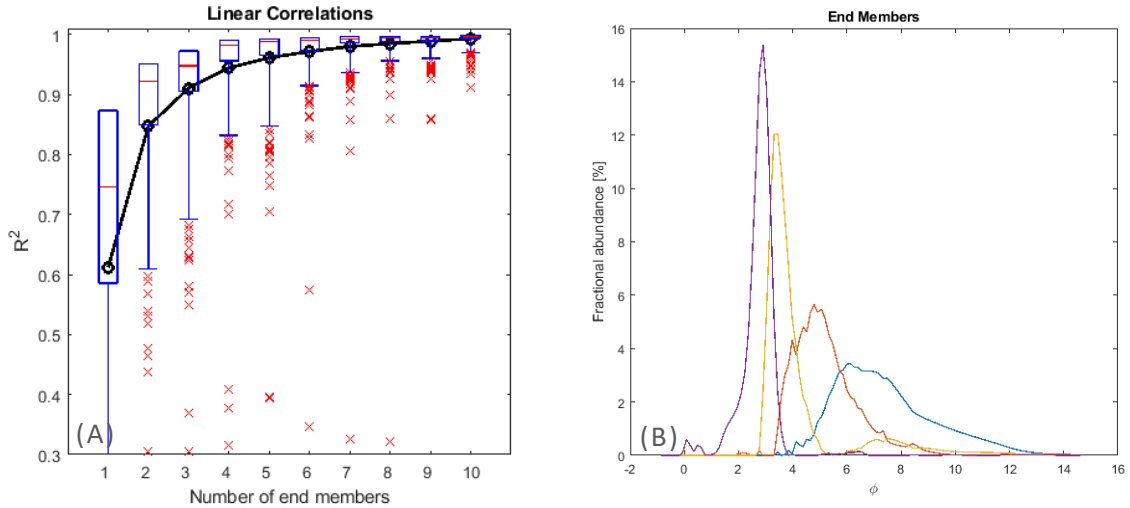

Figure 3:7 (A) Linear correlation map between the multiple correlation coefficient (R^2) of end-members (B) Four selected end-members.

The end-members were superimposed over multi-specimen plots for all samples, and each branch (Figure 3:8). End-members 1 (blue) and 3 (yellow) appear to fit the Western branch best indicating that there are two main processes or sources occurring within this branch (Figure 3:8B). End-member three accounts for the largest fractional abundance at the Western site and EM 4 appears absent. While all end-members fit the Western Middle branch, it appears to be influenced less from EM 1 (blue) and EM 3 (yellow) and instead EM 2 (orange) and EM 4 (purple) appear to explain the majority of variability observed here (Figure 3:8C). The Acesta branch reflects a broader spread of end-member data, with end-members 3 and 4 accounting for the largest abundance (Figure 3:8D). The Eastern Middle branch has the first noticeable pulse of coarser material observed from West to East; this is associated with EM 4 (purple). EM 3 (yellow) accounts for the largest fractional abundance at the Intersection site. End-member 1 (blue) represents the lowest fractional abundance (Figure 3:8E). The Eastern Middle 2 and Eastern branch sites reflect all end-members. However, a sizeable fractional abundance of coarser material between 0-2Φ is seen, attributed to EM 4 (purple) (Figures 3:8F and 3:8G). The Explorer branch is unlike all sites, EM 1 (blue) and EM 2 (orange) appear to be responsible for the large fraction of smaller grain sizes observed. EM 2 reflects grain sizes of fractional abundances exceeding 14%. There is an absence of EM 4 at the Explorer branch and main channel (Figures 3:8H and 3:8I).

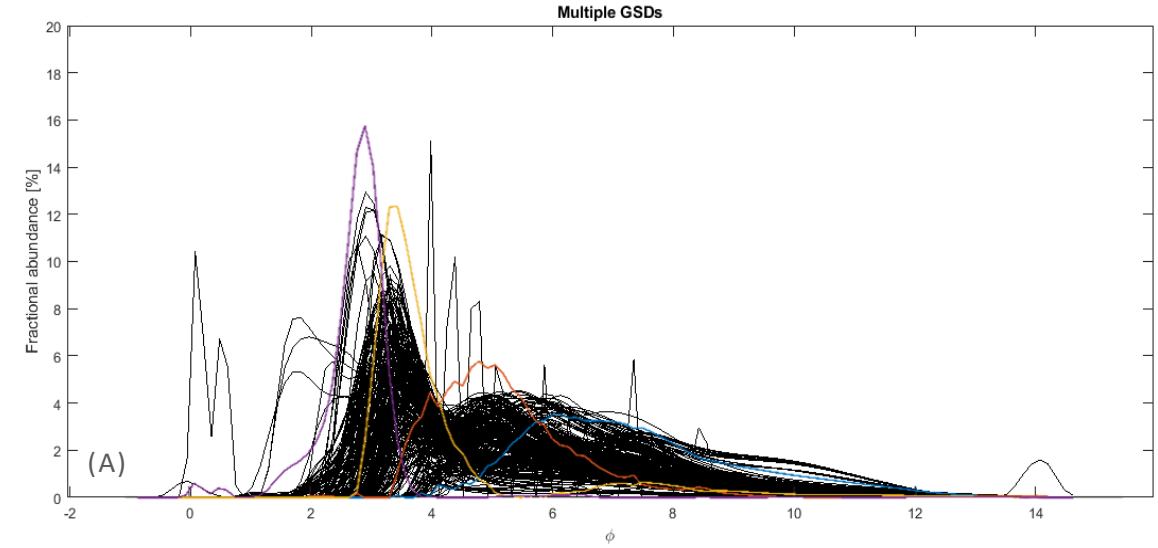
Multiple GSDs
Fractional abundance [%]
(A)
ϕ

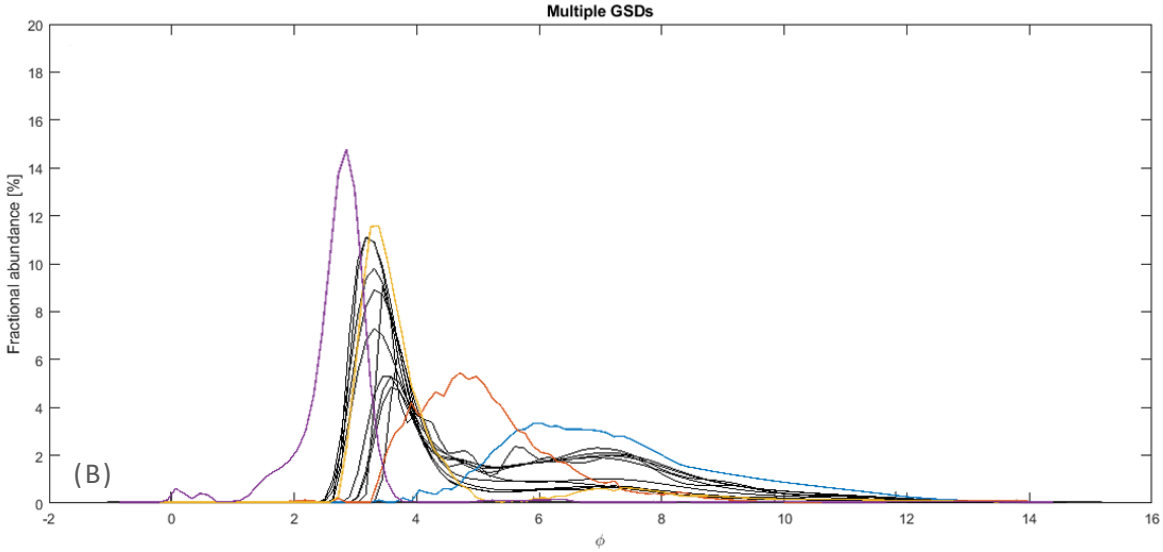
Multiple GSDs
Fractional abundance [%]
(B)
ϕ

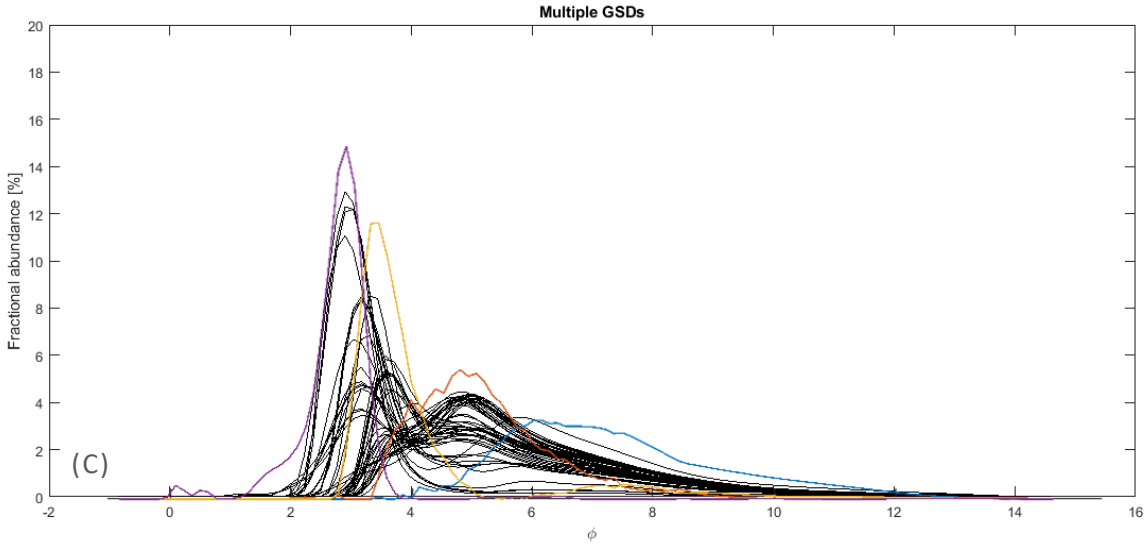
Multiple GSDs
Fractional abundance [%]
(C)
ϕ

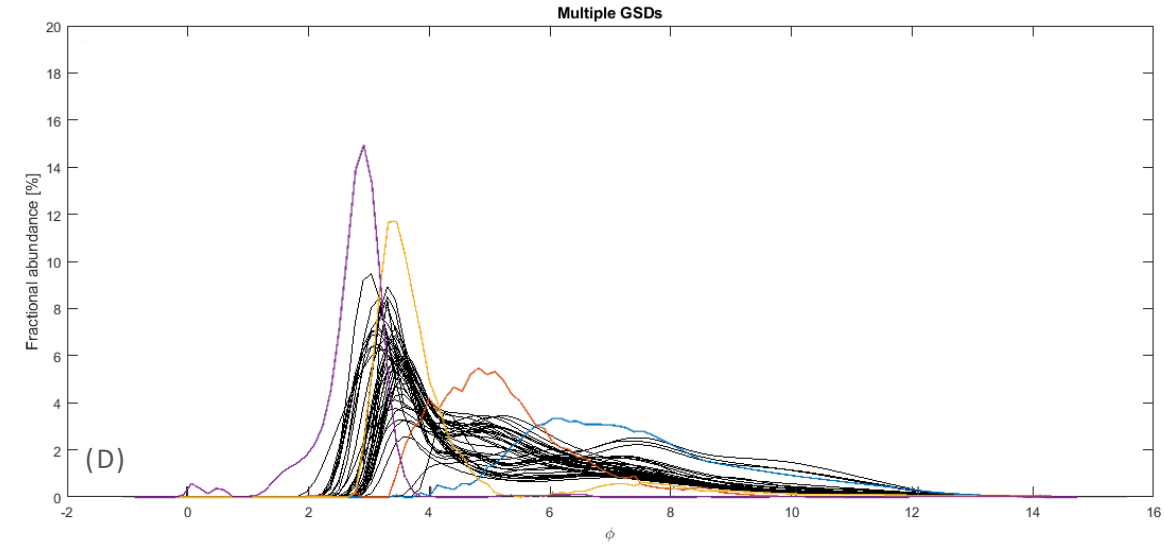
Multiple GSDs
Fractional abundance [%]
(D)
ϕ

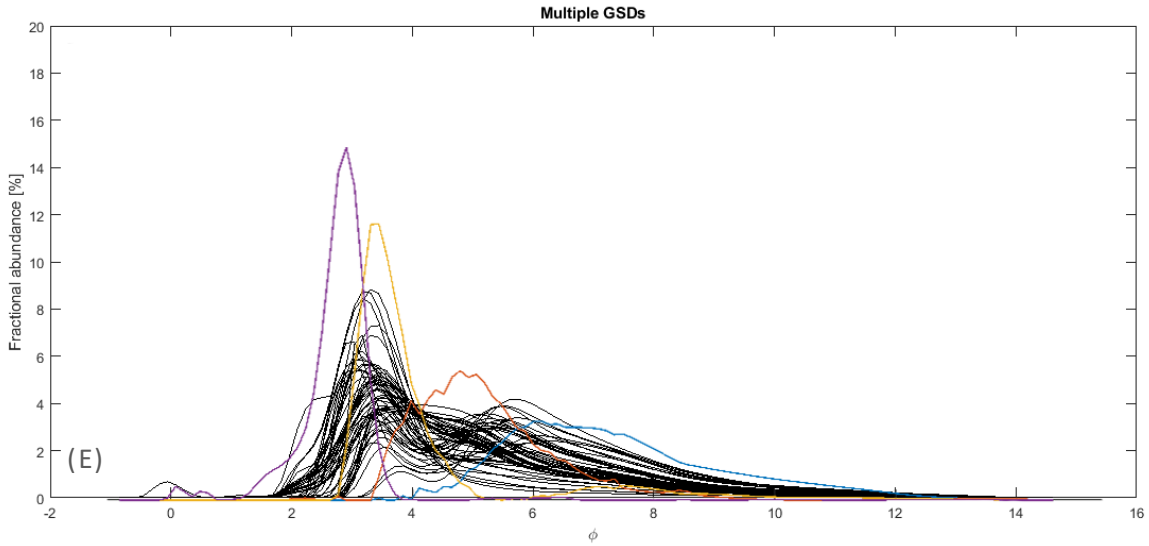
Multiple GSDs
Fractional abundance [%]
(E)
ϕ

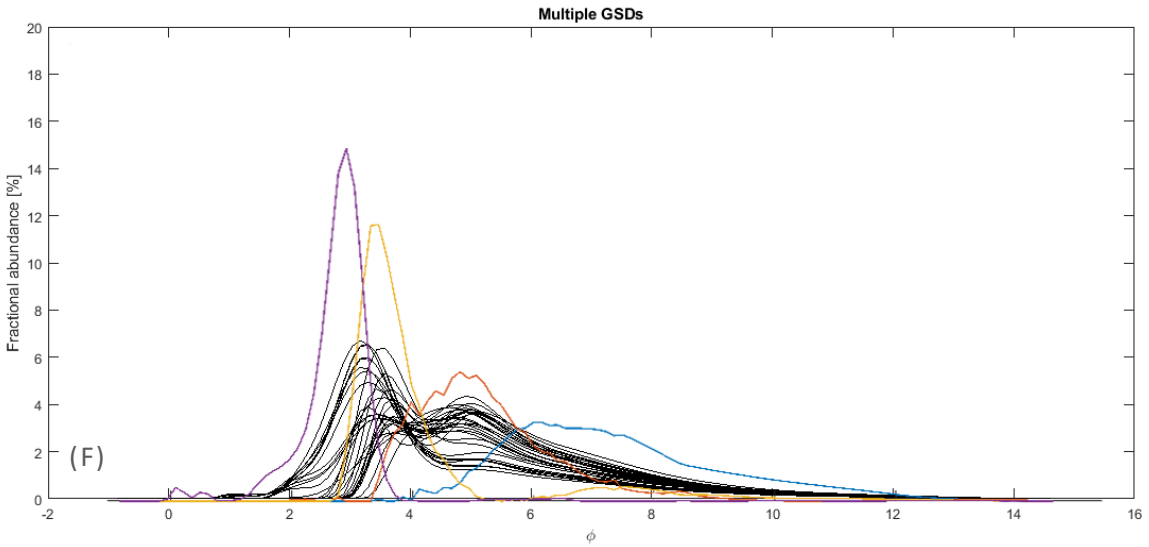
Multiple GSDs
Fractional abundance [%]
(F)
ϕ

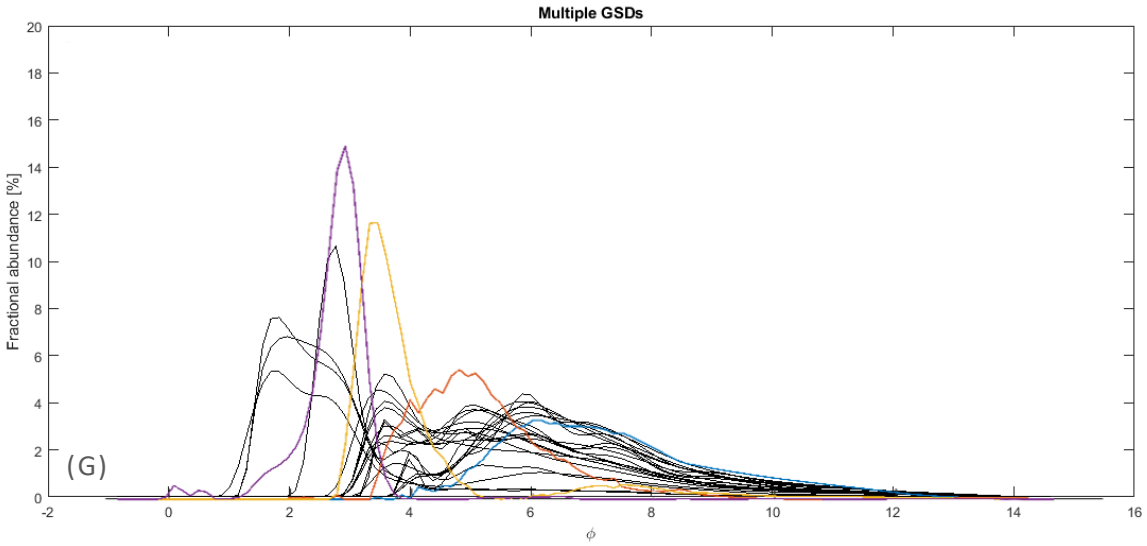
Multiple GSDs
Fractional abundance [%]
(G)
ϕ

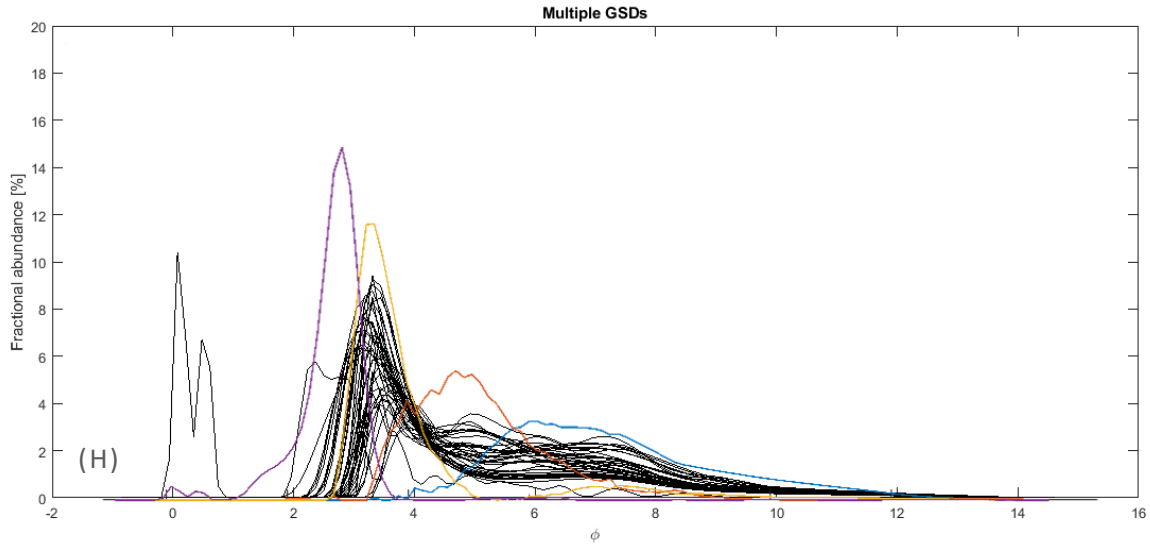
Multiple GSDs
Fractional abundance [%]
(H)
ϕ

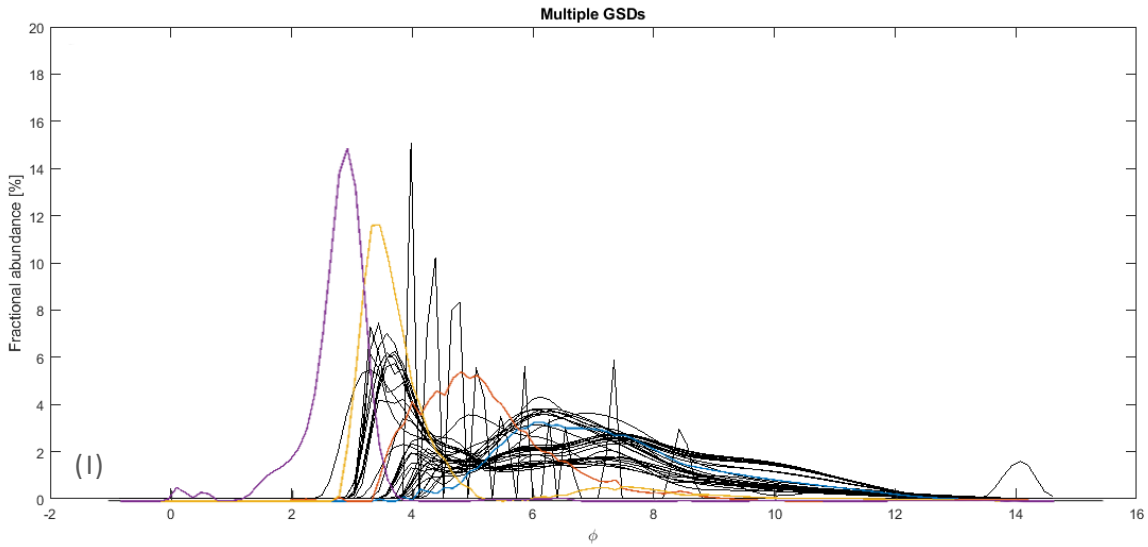
Multiple GSDs
Fractional abundance [%]
(I)
ϕ

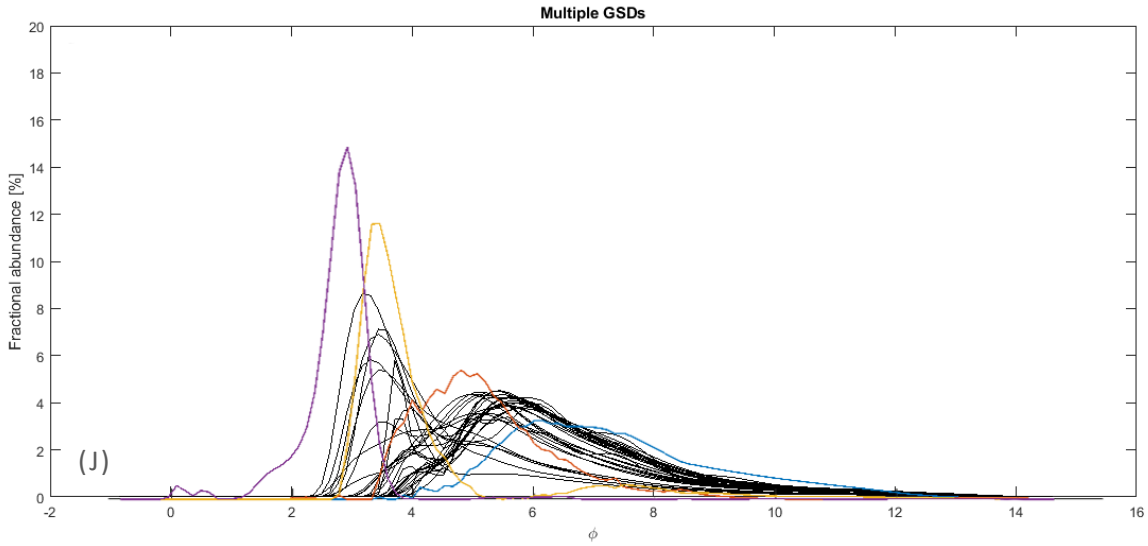

Figure 3:8 (A-J) Four end-members superimposed over multi-specimen grain size distribution plots across all branches. An R^2 value of 0.9443, Theta value of 11.4102, and EM R^2 0.0135 indicates goodness of fit and reduced likeliness of overfitting data. EM 1 (blue) signifies pelagic deposition, EM 2 (orange) is indicative of the silt population, EM 3 (yellow) is indicative of the coarser, sand population and EM 4 (blue), seen at some branches, indicates extreme events, such as gravity flows, responsible for distributing coarse material like turbiditic sediments as discussed by Amaro et al. 2015. A= All branches, B= Western, C= Western Middle, D= Acesta, E= Eastern Middle, F= Intersection, G= Eastern Middle 2, H= Eastern, I= Explorer, J= Main Channel.

3.5 Discussion

Within the upper reaches of the canyon, to depths of ~500m, structureless alternating patterns composed of silt and very fine sand dominate the core profiles. Very fine sand, the largest fraction mean down core, was observed at the Eastern site (CE14009-005-450m) indicating spillover of shelf-derived material. Variability in grain sizes was observed well at the Eastern Middle 2 branch, both fine and coarse sediment was recorded in surficial sediment of two cores. Sandy coarse material is present down core to 2 cm within core CE16006-056-PSH05-1845m, indicating another event where shelf-derived material may have been deposited.

While, surficial sediments mainly consist of fine silty particles, indicating that coarse material is not transported due to reduced hydrological energy, the finest material, very fine clay, was observed at the Explorer site JC125-076-PSH02-861.2m indicating quiescent conditions (Deacon, 1964). Furthermore, where the Western branch is characterised by smooth sloping topography, lower velocity bottom currents and increased microphagous feeders typical of quiescent environments (Amaro et al., 2016b; Aslam et al., 2018). Coarse material is notably absent from the Western sample site, indicating insufficient energy levels to transport larger particle sizes.

One-way ANOVA on ranks analysis did not have enough evidence to reject the null hypothesis that the grain size means significantly differ across sites. However, while this may be the case, increasing the power of the test by increasing the sample size or improving the process may improve testing in the future (Holcomb et al., 2018). Surficial grain size negatively correlated with depth, indicating that with increasing depth, grain size becomes smaller. This is in agreement with an early model of ocean sedimentology, where the energy

of the ocean currents decrease with depth and therefore smaller particles may settle to the less energetic seafloor (Johnson et al., 1977; Karl, 2006).

All sites targeted displayed, on average, poorly sorted sediments down core, signifying a large variance in grain size. Thus, indicating that the energy, rate or sediment source responsible for the deposition of sediment differs over time. It also suggests that the sediment has been deposited close to the source area, i.e. it has not undergone sorting during a long period of transportation (Middleton, 1962; Blott and Pye, 2001). A Spearman's rank test found that as grain size increased, sorting values decreased. This may support the idea that coarser material has been transported quickly, resulting in poorly sorted material.

While, all sites are poorly sorted, hotspots of poor sorting appear on the outer flanks of the canyon system. This indicates that the energy regime and sources at these locations are variable. A hotspot of very poorly sorted material is indicated within the Explorer canyon, indicating varying particle sizes. While the particle size is the smallest recorded (5.66 ± 1.07µm), the mixture of both biogenic gravel, comprised of coral and shell fragment debris, and lithogenic material has been observed within this branch (Cunningham et al., 2005; Stewart et al., 2014).

Variations of skewness and kurtosis in these sediments may be related to the mixing of two or more grain size populations, in varying proportions. By applying Folk and Wards geometric graphical measures (1957), skewness is pronounced when one population is dominant. Most sites were negatively and very negatively skewed. Only two sites Eastern CE14009-005-681m and Explorer JC125-076-PSH02-861.2m presented near symmetrical down core mean skewness measures. The dominance of mesokurtic and leptokurtic nature of sediments indicates compositionally and mineralogically mature sands (Martins and

Hope, 2020). Most sands are leptokurtic in nature and are either positively or negatively skewed; this may be explained by the fact that most sand consists of two populations, one dominant population and other subordinate population. If the dominant population is finer, it will lead to negative skewness; if the dominant population is coarse, it will lead to a positive skewness (Friedman, 1967). The trend towards positive skewness measures within the surficial section of the main branches of the canyon and the westerly slope may be due to a more significant percentage of coarse material and less fine material (McLaren, 1981). This indicates the winnowing out of fine sediment, through constant wave and current action (Nicholas, 2003). Down core trends of negative skewness across the canyon suggest that the dominant fraction of material is finer, indicating reduced lithogenic input and coarse grain deposition.

Mean down core kurtosis values at most sites were mesokurtic, suggesting that extreme outliers in much of the sites were rare. However, there is a trend towards leptokurtic sediments to the flanks and within the lower center of the canyon (Blott and Pye, 2001). Large leptokurtic kurtosis values are observed at the following sites; Western JC125-083-PSH03-2740m, Western Middle CE16006-081-PSH03-1601m, Eastern Middle 2 CE16006-056-PSH05-1845m, and the Eastern branch site CE14009-005-450m. This indicates that high energy events may have occurred, resulting in the large values observed. Mean down core grain size was positively correlated with kurtosis (r_s [48] = .432, p = .002), supporting this hypothesis as extreme events may transport larger grain sizes. Some flat peaked, platykurtic values are observed within the Explorer, Eastern and Acesta branches, indicating that at these sites a normal distribution and contribution of grain sizes is present and there are less frequent extreme outliers.

Skewness was negatively correlated with kurtosis (rs [48] = -.372, *p* = .009). In other words, as a sample is closer to 0 (normally distributed), there are fewer samples with extreme outliers. Kurtosis was negatively correlated with sorting (rs [48] = -.546, p = .000), suggesting that extreme outliers resulted in poorly sorted material as one might expect.

Most sections displayed distinct polymodal populations down core, indicating three distinctive sources. These populations consist of fine sands (population A), silt (population B) and clay (population C). The coarser fraction, population A, with a mean of 0-4Φ, population B represents samples with a mean of 4-8Φ, and the finer clay population is represented by >8 Φ. According to the CM diagram, samples fall within graded suspension no rolling to uniform and pelagic suspension in the Pelagic and tractive current sub environments. Essentially, the largest grain size may be transported through graded suspension and that the finer material through uniform suspension (Passega, 1957). Furthermore, according to Passega (1957), graded suspension deposits of tractive current sub environments have characteristics of turbidity current deposits. Amaro et al. (2015) describe the alternating patterns of finer carbonate-rich hemipelagic ooze and thin turbiditic layers. The layers represent events in time, with the coarse turbiditic layers attributed to intermittent sedimentary gravity flows.

Sediments from the upper reaches, down to 500m, were dominated by silty sand. This suggests ongoing transport of lithogenic shelf-derived material. At increasing depth lithogenic fine sands and silt alternate with finer, hemipelagic clays. While sand depletes beyond 2816m, lithogenic silt continues to dominate to the lower reaches of the canyon. However, within the main channel, at depths exceeding 3500m lithogenic coarse sand continues to punctuate the core profile, demonstrating gravity-driven flows and turbidite

sediments from the upper canyon reach. The Explorer branch of the canyon had the most considerable clay fraction of the sites analysed. Within the Explorer site JC125-076-PSH02-861.2m, the sand fraction was observed in the first three-centimetre sections, before a bimodal signature was seen, indicating that the low energy environment allowed for fine particles to settle out of suspension.

End-member analysis (EMA) identified four sedimentary end-members that attempt to explain the particle size distribution population and processes. A low theta value (11.4102), indicated that the model did not alter the particle size data to apply fit significantly, and a low-end-member similarity (0.0135 EM R^2) suggesting that the model is not overfitting the data. The data indicate that EM 1 (blue) signifies pelagic deposition, EM 2 (orange) is indicative of the silt population, EM 3 (yellow) is indicative of the coarser, sand population and EM 4 (purple), seen at some branches, indicates extreme events, such as gravity flows, responsible for distributing coarse material like turbiditic sediments as discussed by Amaro et al. 2015. Grain size descriptive results support this, for example, an absence of EM 4 within the Explorer branch, is supported by the noticeable lack of coarse material observed at this site. Additionally, it must also be noted that the coarsest fraction was observed (0 Φ) at CE14009-005-450m, which may be explained by EM 4 (purple).

Chapter 4: Marine biogeochemistry

4.1 Marine carbon

With rapidly increasing temperatures observed over the 20th century, anthropogenic activity is recognised as a significant driver in climate change, relative to natural changes. The Intergovernmental Panel on Climate Change (IPCC) concluded that "It is extremely likely that human influence is the dominant cause of the observed warming since the mid-20th century" (IPCC, 2012). The emission of greenhouse gases such as carbon dioxide, methane and nitrous oxide, by anthropogenic activity, is mainly responsible for the observed surface temperature increase. Temperatures are predicted to rise a further 0.3-1.7°C in a moderate scenario, dependent on future greenhouse gas emissions and climate feedback effects (Fleitmann et al., 2013) Of the greenhouse gases, carbon dioxide ($C0_2$) is one of the main contributors to global warming (Weart, 2003). Therefore, it is critical to understand how the Earth system interacts with carbon in its different forms.

The organic carbon content in marine sediments depends on a series of factors such as sedimentary characteristics, terrestrial input, the rate of microbial degradation and primary productivity (Burone et al., 2003). Organic matter (OM) in sediments is an important sink of total organic carbon (TOC) and total nitrogen (TN) representing an important reservoir for the carbon cycle (Escobar-Briones et al., 2009). Organic carbon content is primarily affected by several factors;

- The amount of primary productivity in overlying waters may determine how much organic material is produced.

- The sedimentation rate, where fast rates of sedimentation may promote the

preservation of organic carbon and low rates which may promote decomposition of organic carbon.

- The distance with depth from the sources, where increased time during the descent of material may lead accelerated break down of organic material in the water column.

- Oxygen availability, where more oxygen may lead to the efficient breakdown of organic matter. However, anoxic/suboxic conditions may break down organic matter too, only slower so it is time restrained.

- Type of organic matter, e.g., marine vs terrestrial or degraded marine vs fresh marine. The association with minerals and surface area. Generally, organic carbon content is higher in finer-grained material due to the higher surface areas of the clay minerals that tend to 'trap' more organic matter (Mayer, 1994; Hedges and Keil, 1995).

I. *Carbon composition*

Carbon can take two forms - total inorganic carbon (TIC) and total organic carbon (TOC). Organic carbon is continually being produced and destroyed and, as a result, is the most dynamic form of carbon. It drives four major reservoirs, interconnected by pathways of exchange through physical, geological, biological and chemical processes. These reservoirs are the atmosphere, the terrestrial biosphere and biota (including land water masses), the oceans (dissolved inorganic carbon, and living and non-living biota) and carbon-rich sediments.

Two main types of inorganic carbon are found in the ocean - dissolved inorganic carbon (DIC) and total inorganic carbon. Dissolved inorganic carbon is made up of bicarbonate (HCO_{3-}), carbonate (CO^{2-}_3) and carbon dioxide (including both dissolved CO_2 and carbonic acid H_2CO_3). Photosynthesis acts as the primary process for inorganic carbon fixation in sediments (Lee, 1994). Furthermore, calcifying organisms, such as foraminifera, coccolithophores, crustaceans, echinoderms and mollusks utilize dissolved inorganic carbon to produce the total inorganic carbon, calcium carbonate ($CaC0_3$), for their shells and skeletons. On a global scale, the storage of organic matter, in terms of TOC, broadly reflects the distribution pattern of phytoplankton biomass in the overlying waters (Seiter et al., 2004).

Inorganic and organic carbon can be found in the ocean in both dissolved (DIC, DOC) and particulate (PIC, POC) form. Dissolved organic carbon is defined operationally as an organic molecule that can pass through a 0.2µm filter (Wagner et al., 2020). Dissolved organic carbon can be transformed into particulate organic carbon by heterotrophy, and it can also be converted to dissolved inorganic carbon through respiration. Particulate organic carbon consists of living and dead organisms and detritus. POC can be converted to DOC through the breakdown of molecules and by phytoplankton exudation. Lastly, POC is commonly transformed to DIC through heterotrophy and respiration (Ridgwell and Arndt, 2015).

II. *Carbon burial*

While organic carbon will likely be recycled within the water column by organisms, when calcifying organisms die, their calcium carbonate tests or shells may sink to the seafloor. However, as a result of respiration, increasing pressure and decreasing temperature, the water column can become increasingly undersaturated in calcium carbonate with depth,

resulting in the dissolution of calcium-rich tests and shells. The depth where the rate of calcium carbonate supply equals the rate of dissolution is referred to as the calcium carbonate depth (CCD). If the seafloor exists below this depth, calcium carbonate will be absent from sediments. Likewise, if the seafloor exists above the CCD depth, sediments can become enriched with calcium carbonate (Woosley, 2018). Present estimations of global carbonate burial rates in deep-sea environments are thought to be between 100 and 130PgC kyr^{-1} (Catubig et al., 1998; Sarmiento et al., 2002; Cartapanis et al., 2018). Calcium carbonate burial is of high importance too. While $CaCO_3$ burial removes carbon, it also reduces alkalinity (ALK) within the system. Therefore, the higher the alkalinity of seawater, the higher the solubility of CO_2, thus the reduced transfer of carbon from the atmosphere.

While the shallow ocean contains the largest active pool of organic carbon, the deep ocean is recognised for its slower rate of exchange with the atmosphere, by organic carbon burial within marine sediments (Broecker, 1982; Opdyke and Walker, 1992; Sigman and Boyle, 2000; Wallmann et al., 2016; Cartapanis et al., 2018). With increased exploration, the rates of organic matter oxidation and hence carbon burial has been found to vary across different environments. Past research has generally indicated that TOC burial is highly focused in nearshore environments and over continental shelves owing to several reasons (Dunne et al., 2007). Primary productivity is often enhanced over continental shelves, there are often higher rates of sedimentation and, due to the shorter vertical transects to the sediments, there is lower decomposition during sinking. In addition, there is a larger flux of terrestrial OM due to the proximity to land (Van Dongen et al., 2000). Thus, the burial of organic carbon is not uniformly distributed within the ocean. The ocean is not as homogenous as once thought. At smaller scales, diverse morphological, hydrological, biogeochemical and

sediment processes may alter patterns of TOC burial due to differing sediment types and organic matter production rates (Stein, 1990), TOC export flux rates (Suess, 1980; Tyler et al., 2009b; Amaro et al., 2016b), its origin (Mackin and Aller, 1984) and the amount of dissolved oxygen in the water (Canfield, 1994).

The flux of organic carbon delivery to sediments is poorly quantified, with estimates ranging by orders of magnitude (Petsch, 2013). While most TOC is recycled through grazing in the upper water column, some may sink to abyssal depths, effectively pumping $C0_2$ out of the atmosphere and helping to regulate the Earth's temperature (Boyd et al., 2019). Dunne (2007) estimated the burial rates of nearshore (<50m) and deep-sea sediments. He suggested that despite the deep-sea accounting for ~90% of the ocean area, nearshore deposits could potentially bury 480PgC kyr^{-1}, 190PgC kyr^{-1} on shelves (50-200m), 100PgC kyr^{-1} on slopes (200- 2000m) whereas the burial rate in the deep-sea abyssal plains (>2000m) to be a fraction of this at only 12PgC kyr^{-1}. Therefore, a small fraction (typically <2%) of the total biosynthesized organic carbon is buried at the seafloor, in coastal and pelagic environments (Escobar-briones et al., 2009; Kiriakoulakis et al., 2011; Sigman and Hain, 2012).

III. *Carbon burial in submarine canyons*

Recent work suggests that canyons may act to quickly transport organic matter to the deep-sea (Vetter and Dayton, 1999; Garcia et al., 2007). However, very little work exists on the ability to store carbon. Due to the accelerated rate of transportation (relative to other deep-sea environments) it is possible that localized primary production could be transported to deeper sections of the canyons by strong coastal, tidal and/or gravity currents. This would elevate the organic inputs into the sediments and could also lead to

enhanced burial rates (Vetter and Dayton, 1999). In other cases, the enrichment of carbon in canyon sediments may be a result of elevated terrestrial inputs (e.g. Lacaze-Duthier Canyon in the Gulf of Lions (Schmiedl et al. 2004)). Likewise, bioturbation and high respiration rates by benthic organisms that live in submarine canyons may promote recycling of carbon rather than burial. For example, cold-water corals found in canyon systems (e.g. Morris et al., 2013) are known to be hotspots of carbon recycling (Van Oevelen et al., 2011; White et al., 2012). However, the exchange of oceanic $C0_2$, through coral respiration, has been recognised as a source of CO_2 to the atmosphere (Chisholm and Barnes, 1998).

Low rates of OM oxidation and hence higher rates of burial are usually associated with high rates of sediment accumulation or organic matter influx. Such conditions have been observed in Nazaré Canyon, which acts as a depocentre of TOC in the west Iberian Margin (Masson et al., 2010; Kiriakoulakis et al., 2011). Ingels et al. (2011) suggested that at places in the Nazaré Canyon, high organic loads caused the depletion of oxygen in the sediments, leading to lowered infauna abundance or increased opportunistic species (Amaro et al., 2016b; Gambi and Danovaro, 2016). This could lead to lower OM recycling and consequently, higher TOC burial efficiency. Therefore, different processes may be operating in different canyons or even different parts of the same canyon at various spatial and temporal scales and questions remain regarding the controls of these processes.

4.1.1 Molar C/N ratio

As organic matter sinks through the water column it is transformed through zooplankton and microbial activity. Further transformations occur upon arrival to the deep-sea floor by the benthic fauna and sedimentary microorganisms (Wakeham and Lee 1989; Kiriakoulakis

et al., 2001). In areas of topographic complexity, such as continental margins, marine OM transformations may be impacted by physical processes, such as gravity flows, internal tides, Ekman drainage and cascading (Reid and Hamilton 1990). These processes can ultimately lead to alterations in the freshness and lability of the OM, carbon (C) and nitrogen (N) which contributes to its burial efficiency and its ecological potential (Berner, 1982; Wakeham and Lee, 1989; Walsh, 1991; Smith et al., 2009).

While carbon content can tell us something about the paleoenvironment and paleoclimate, only a small fraction of the initial organic matter survives degradation and alteration during sinking. Therefore, other analyses are required to understand canyon processes better. Past studies have highlighted the usefulness of molecular, elemental and isotopic analysis of sediments in understanding the origin and environmental history (Stoffers et al., 1984; Meyers, 1994). C/N elemental ratios and isotopic signatures may retain records up to millions of years and can provide information about the origin and processes occurring. In 1934 Redfield found that the global elemental composition of marine OM (dead and living) was remarkably consistent across all ocean regions with a stoichiometric ratio of C:N:phosphorous (P) of 106:16:1 (Redfield, 1958). He hypothesized that the elemental requirements of surface plankton controlled deep ocean nutrient concentrations. This concept was extended to include elements such as carbon, becoming fundamental in our understanding of ocean biogeochemistry.

Molar ratios of elemental C/N can be used as an indicator of the origin, lability and freshness of marine organic matter. C/N ratios in the range of 4-10 are usually from marine sources, whereas ratios for vascular terrestrial plants are often above 20 (Ishiwatari and Uzaki, 1987). This is because phytoplankton is rich in nitrogen, resulting in low C/N ratios,

indicating the dominance of marine organic matter (Carpenter and Capone, 2008). Higher terrestrial plant organic matter has a lower nitrogen content, thus a greater C/N ratio (Hunter et al., 2013). High C/N ratios of organic matter may also indicate the preferential scavenging of nitrogen-rich compounds by bacteria, indicating older, reworked material (Kiriakoulakis et al., 2001, 2006). However, lower ratios have also occasionally been observed in fine-grained sediments. C/N ratios below 6.6 may indicate the adsorption of dissolved inorganic nitrogen or nitrogen-rich compounds, such as those from phytoplankton blooms. As nitrogenous compounds break down, they produce ammonia (which may be retained by clay minerals) and the CO_2 released by the oxidation of organic carbon escapes (Libes, 1992; Müller, 1977).

4.1.2 Bulk stable isotopes

Stable carbon and nitrogen isotopic signals ($\delta^{13}C$, $\delta^{15}N$) preserved in carbonate rocks, and organic carbon are useful tracers for further determining organic matter origin and transformation processes (Middelburg, 2014). Hayes (1993) states that the carbon isotopic composition of any natural organic compound is dependent on the carbon source and on the isotopic fractionation associated with assimilation, metabolism and biosynthesis of carbon by the producing organism. Bulk stable isotopes of carbon and nitrogen are commonly used in trophic studies, where variations delineate biological, chemical and physical variability. $\delta^{13}C$ is often used as an indicator of carbon origin, while $\delta^{15}N$ values can be used to aid the interpretation of trophic relationships and improve the understanding of resource partitioning (Kiriakoulakis et al., 2005; Duineveld et al., 2012; Layman et al., 2012). Organic matter produced by terrestrial plants has a comparatively lighter average $\delta^{13}C$ isotopic signature value of ~-27‰ to -29‰ compared to the heavier isotopic value of

marine organic matter (~-22‰ to -15‰). Applying this theory, the analysis of the stable carbon isotopes ($\delta^{13}C$) and stable nitrogen isotope ($\delta^{15}N$)can be undertaken in order to differentiate between terrestrial and marine sources of organic matter (Calvert and Fontugne, 1987; Hayes, 1993).

I. $\delta^{13}C$

The ratio of ^{13}C and ^{12}C (expressed relative to a standard, $\delta^{13}C$) has been routinely used in biogeochemical analyses to evaluate the structure and dynamics of marine communities. It is useful where multiple sources of organic matter may be contributing to the marine ecosystem, for example, where a mangrove river may be depositing terrestrial material into a marine system (Rodelli et al., 1984; Alfaro et al., 2006). $\delta^{13}C$ may vary significantly depending on the source of primary production; however, the ratio of $\delta^{13}C$ changes are minor as carbon moves through the food-web (~1‰ per trophic level) (Rounick et al., 1982; Peterson and Fry, 1987; Gearing, 1991). Isotopic fractionation occurs during the autotrophic assimilation of carbon by an organism. Primary producers, such as plants contain less ^{13}C than the atmospheric CO_2 on which they rely for photosynthesis. Thus, they are relatively "depleted" of ^{13}C compared to the atmosphere. The variability is attributed to the preferential loss of ^{12}C during respiration and the preferential uptake of ^{13}C during assimilation, digestion or through metabolic fractionation during tissue synthesis (Michener and Kaufman, 2008). These processes vary among plants using different photosynthetic pathways. This depletion is caused by enzymatic and physical processes that discriminate against ^{13}C in favour of ^{12}C. Discrimination varies among plants using different photosynthetic pathways; the Calvin cycle (C3), Hatch–Slack (C4), Crassulacean acid metabolism (CAM) or from chemosynthetic processes (Levin and Michener, 2002; Layman et

al., 2012). The discovery of chemosynthetically supported deep-sea communities (such as those found around hydrothermal vents, methane and hydrocarbon seeps, sewage leaks, whale falls and seagrass beds) has increased knowledge of carbon origin and cycling in the marine environment (Rodelli et al., 1984; Levin and Michener, 2002; Kang et al., 2007; Selvaraj et al., 2015). Diagnostic indices of $\delta^{13}C$ signatures are shown in Table 4:1.

Table 4:1 Diagnostic indices $\delta^{13}C$ ‰ for primary organic matter sources in the marine environment.

$\delta^{13}C$	SOURCE INDICATOR
-16‰ to -9‰	Sulfide-oxidized derived carbon that involves form II Rubisco pathway (Levin and Michener, 2002)
-18‰ to -15‰	Methane released through basalt degassing (serpentinization) (Keir et al., 2005)
-22‰ to -15‰	Marine phytoplankton and zooplankton derived organic matter (Fry and Sherr, 1984; Levin and Michener, 2002)
-29‰ to -27‰	Terrestrial derived organic matter (Hayes, 1993)
-37‰ to -27‰	Sulfide-oxidized derived carbon that involves form I Rubisco pathway (Levin and Michener, 2002)
>-55‰ to -40‰	Methane-derived carbon via hydrothermal processes (the thermal breakdown of buried organic matter, bacterial fermentation or deep-water formation (Welhan, 1988; Levin and Michener, 2002; Keir et al., 2005)

II. $\delta^{15}N$

Nitrogen has two stable isotopes ^{14}N and ^{15}N. ^{14}N is the more abundant of the two, accounting for 99.63% of the nitrogen found in nature. Biological, physical and chemical processes discriminate between the two isotopes, resulting in quantifiable differences in the ratio of ^{14}N and ^{15}N (expressed relative to a standard, $\delta^{15}N$) thus enabling trophic position estimation (Sigman et al., 2010). Nitrogen is critical to marine biomass and one of the primary nutrients required by all phytoplankton (Gruber and Galloway, 2008). While nitrogen is an essential element for all life forms, it mostly occurs as dissolved N_2 gas (> 95%) that is unavailable to most species. The rest is reactive nitrogen (N_r), such as nitrate, ammonia and dissolved organic compounds. Therefore, the biological fixing of nitrogen is

crucial. Biological fixation of dinitrogen (N_2) by marine prokaryotic species is the main source of nitrogen to the ocean, estimated at 106–120Tg N y^{-1}. Nitrogen fixation is significant in tropical surface waters, some benthic systems as well as anoxic waters at the seafloor where diatom-diazotroph symbiosis exists (Dekas et al., 2009; Foster et al., 2011; Voss et al., 2013). The process of nitrification relies on oxygen availability, where autotrophic nitrifiers convert ammonia to nitrites NO_{2^-} and nitrates NO_{3^-}. Likewise, denitrification in the ocean is also controlled by oxygen availability; however, denitrification takes place under low oxygen conditions. Denitrification by eukaryotic species, such as foraminifera, is the microbial process of reducing nitrate and nitrite to gaseous forms of nitrogen, such as nitrous oxide (N_20) and nitrogen (N_2) (Voss et al., 2013). As sources and sinks are dominantly internal and biological, with marine N_2 fixation supplying most of the fixed nitrogen in the ocean, and the process of denitrification removing it. The study of nitrogen provides a way of exploring the cycle (input/output budget) of oceanic fixed N within the ocean (Sigman et al., 2010)

Typically, an organism is enriched in $\delta^{15}N$ by 3-4‰ relative to its diet and displays stepwise enrichment with trophic transfers (Minagawa and Wada, 1984; Peterson and Fry, 1987). However, deep-sea values may be less due to poor food availability. Iken et al. (2001) revealed that within the Porcupine Abyssal Plain (NE Atlantic), an overlap in nitrogen isotopic values between trophic levels, reducing the “typical” 3‰ stepwise enrichment was recorded, indicating an overlap in food sources. Iken et al. (2001) showed that suspension feeders exhibited a broad trophic spectrum as they fed on both particulate material and live prey, altering the nitrogen signature.

Field studies of the best-known genus of open ocean N_2 fixer *Trichodesmium*, have yielded

$\delta^{15}N$ values of ~ -2‰ to 0.5‰. Taking into consideration the $\delta^{15}N$ of dissolved N_2 (~0.6‰ in the surface mixed layer) this value is consistent, but less variable, than culture studies of *Trichodesmium* where values range between ~0‰ and 4‰.

The bacterial reduction of nitrate to nitrogen is the largest mechanism of fixed nitrogen loss from the ocean, occurring in both the water column and sediments, where oxygen levels fall below 5µmol/kg. Denitrification studies suggest that the isotope effect of denitrification is in between 5‰ to 30‰ (Sigman and Casciotti, 2001; Sigman et al., 2010). However, the observed isotopic effect of denitrification is believed to be limited by the rate of nitrate supply to the denitrifying bacteria. In some ocean margin sediments, denitrification completely consumes the nitrate that is supplied by diffusion through sediment pore waters, resulting in an 'effective' isotope close to 0‰ (Sigman and Casciotti, 2001). Studies of internal cycling and the assimilation by phytoplankton, of nitrate (NO_3^-), has resulted in isotopic signatures of 4-6‰. Where ammonium (NH_4^+) assimilation occurs, isotopic signatures of 6.5-20‰ have been recorded (Sigman and Casciotti, 2001). The return of organic nitrogen to the marine system as NO_3^-, by remineralization, occurs in two steps: the degradation of organic nitrogen to ammonium and the bacterial oxidation of ammonium to nitrate. Limited data suggest that the net effect on $\delta^{15}N$ is less than 5‰ in most cases, however where the nitrification of ammonium to nitrate occurs values as high as 35‰ have been recorded (Sigman and Casciotti, 2001).

While the complexity of the processes occurring can prove challenging to comprehend, the understanding of nitrogen cycling is crucial. The nitrogen cycle is closely related to that of carbon, phosphorous and other essential biological elements. The implication of this is that any human alterations to nitrogen cycling are likely to have large impacts for other

biogeochemical processes and ecosystem functioning (Voss et al., 2013).

4.2 Aims

This chapter aims to investigate the biogeochemical composition of sediment samples matter through a multi-proxy approach, which may improve the understanding of transport mechanisms and organic matter preservations within the morphologically complex Whittard Canyon.

4.3 Methods

Organic geochemical analysis was carried out across two laboratories. Elemental (isotopic carbon and nitrogen) analysis was undertaken at the Oceanographic Laboratories, Department of Earth, Ocean, and Ecological Sciences, University of Liverpool. Further elemental (carbon and nitrogen) analysis was undertaken at the Geography Laboratories, School of Biological and Environmental Sciences, Faculty of Science, Liverpool John Moores University.

4.3.1 Elemental carbon and nitrogen analysis

Carbon and nitrogen content were analysed using the Skalar Primacs $^{SNC-100}$ TN/TC Analyser within the solid sample module. High-temperature combustion, with non-dispersive infrared detection (NDIR), is used to analyse total carbon (TC), total inorganic carbon (TIC) and total nitrogen (TN). Calibration curve for quantification of total carbon and total nitrogen was achieved using glycine (5-30-60-90-120-150mg). Calibration curve for quantification of inorganic carbon was achieved using 1.00% $NaCO_3$ (100-200-400-600-800-1000-1200mg).

I. *Elemental carbon and nitrogen sample preparation*

Prior to analysis, sub-core samples were sectioned every cm down to 10 cm; samples were subsequently sectioned at 2cm intervals before being freeze-dried. Total carbon was determined by placing ~0.05mg of sediment into a weighed ceramic crucible. Alongside the TC run, total nitrogen results were also acquired using the Skalar Primacs $^{SNC-100}$ TN/TC Analyser. Due to the low concentrations of nitrogen within the samples, the sample weight was increased to ~ 2mg to ensure accurate nitrogen readings.

II. *Instrument operation*

The Dumas method was used to achieve total organic carbon and total nitrogen values. This was undertaken with the following instrument settings. High purity oxygen was passed through the injection system to remove any atmospheric gasses before the sample was heated to 1100^{o}C. Oxygen was added to the combustion crucible to increase the oxidation rate. The acid vapours and H_2O were removed by passing through the following: steel wool scrubber, Peltier cooler and a brass/cellulose scrubber. The sample gas stream was split with 79/80 of the sample forwarded to the IR detector for $C0_2$ quantification. Under a pure helium stream for N_2 measurement, the remaining 1/80 of the sample gas stream was collected within a copper collection vessel and passed to the reduction oven (750^{o}C) for detection by a Thermal Conductivity Detector.

The total inorganic carbon measurement was acquired by acidifying the sample using 20% phosphoric acid, heating to 110^{o}C and passed directly to the IR detection via the Peltier cooler and brass/cellulose scrubbers.

III. *Calculation of total inorganic, organic carbon and nitrogen*

The percentage of total carbon, total inorganic carbon and total nitrogen in each sample

were calculated by comparing the peak area of the sample components to those in the standards. The total organic carbon fraction could then be inferred by subtracting total inorganic from total carbon readings as per the method by Brian Schumacher (Schumacher, 2002). The following equation was used:

TOC (%) was calculated by subtracting TIC (%) from TC (%):

$$TOC(\%) = TC(\%) - TIC(\%)$$

Inorganic carbon is likely to be calcium carbonate. Inorganic carbon may be transformed into carbonate using the following equation:

$$TIC \times Y$$

Where $CaCO_3$ molecular weight is 100 and C is 12. Therefore 100 divided by 12 = 8.33 = Y

IV. *Calculation of C/N ratios*

Molar C/N was calculated by (TOC (%) divided by 12) divided by (TN (%) divided by 14):

$$Molar\ C/N = \frac{(\%\ weight\ TOC/12)}{(\%\ weight\ TN/14)}$$

4.3.2 Stable isotope analysis

The isotopic ($^{13}C/^{12}C$ and $^{15}N/^{14}N$) signatures of organic matter within sediment samples were derived using a Costech 4010 Elemental Analyser, connected to a Thermo Scientific Delta V Advantage mass spectrometer. Nitrogen and carbon were analysed with and without de-carbonation, respectively, at the School of Earth, Ocean, and Ecological Sciences,

University of Liverpool.

I. *Decarbonation of $\delta^{13}C$ samples and preparation of $\delta^{15}N$ samples*

The removal of carbonate was undertaken using an acidification method. Two aliquots of each sample containing 80-100µg of carbon were weighed into silver capsules (8 x 5mm, elemental microanalysis). Decarbonation was undertaken by placing the sample into silver capsules (Elemental Microanalysis Cat No: D2006; 6X4mm) within a cell well (Elemental Microanalysis Cat No: E2044 Cell Well 96 Flat Bottom). The silver capsules were left open and two drops of Ultrapure MiliQ water was added to moisten the sample before the cell well was then placed into a desiccator containing Hydrochloric acid (HCl) and left to decarbonate overnight (12-16 hours). The cell well was removed and placed in a drying oven at 50°C to ensure the samples were dry. The silver capsules were carefully sealed by twisting the top prior to analysis.

Two aliquots of each freeze-dried and ground sample, containing 80 –160µg nitrogen, were weighed into tin capsules (8 x 5mm, elemental microanalysis).

II. *Instrument operation*

In a pure 0_2 atmosphere, combustion took place at 980°C in a prepacked Costech NCH/NC/N combustion tube. The reduction column (Costech prepacked, heavy-walled, NCH/NC/N reduction tube) temperature was set to 700°C, packed with high purity Cu. H_2O was removed using a scrubbing tube (GL14 thread, 110mm, EOA Labs) filled with anhydrous magnesium perchlorate ($Mg(ClO_4)_2$). Gaseous products (N_2 and CO_2) were eluted and separated using a separation column (NC separation column, 3m, 6 x 5mm stainless, PQS, 2mm 6 MB ports, OEA Labs) in the order of N_2, CO_2. Compositional analysis of the eluted

gasses was determined using Isodat 2.5 software, Thermo Fisher Scientific.

III. *Calculation of $\delta^{13}C$ ‰ and $\delta^{15}N$ ‰*

The variation of bulk stable isotopes was calculated using the following equation:

$$Ratio\ (R) = \frac{abundance\ of\ heavy\ isotope}{abundance\ of\ light\ isotope}$$

$$\delta = \frac{Rsamp}{Rstd} - 1 * 1000$$

Rsamp is the ratio of the sample and *Rstd* is the ratio of the internal standard (as defined by the IAEA). δ values are multiplied by 1000 and reported as parts per thousand ‰. Variations in the isotope ratios of samples were measured against known standards USGS-41 ($\delta^{13}C$‰ 37.626; $\delta^{15}N$‰ 47.6) and USGS-40 ($\delta^{13}C$‰ -26.389; $\delta^{15}N$‰ -4.5).

IV. *Instrumentation drift correction*

The correction of isotopic values for analytical drift during isotopic analysis was undertaken by performing regression analysis on the known standards USGS-41 and USGS-40. These known standards were interspersed evenly, in duplicate, throughout the sample run. Where linear regression revealed a similar direction and slope strength, the correction for any deviation or "drift" was achieved using an average slope strength. The following formula was used:

$$DC\delta^{13}C‰ = Raw\delta^{13}C‰ - (SG \times (x - 1))$$

DC $\delta^{13}C$ ‰ is the drift corrected isotope value, Raw $\delta^{13}C$ ‰ is the raw isotope value, SG is the average slope gradient of USGS-41 and USGS-42 and x is the sequential run number.

V. *Scaling of isotope values to Vienna Pee Dee Belemnite (VPDB) and Atmospheric Nitrogen Drift*

Drift corrected (DC) isotope values were scaled to USGS standard values through regression analysis of the IAEA USGS standard values versus measured values. Gradient and *y*-intercept of regression were used with the following formula:

$$VPDB\delta^{13}C = DC\delta^{13}C \times SG + y - intercept$$

VPDB $\delta^{13}C$ ‰ is the Vienna Pee Dee Belemnite scaled carbon isotope value, *DC* $\delta^{13}C$ ‰ is the drift corrected isotope value and *SG* is the slope gradient of USGS standard values vs measured values.

$$AN\delta^{15}N = DC\delta^{15}N \times SG + y - intercept$$

AN$\delta^{15}N$ ‰ is the Atmospheric Nitrogen scaled nitrogen isotope value, *DC* $\delta^{15}N$ ‰ is the drift corrected isotope value, and *SG* is the slope gradient of USGS standard values vs measured values.

4.3.3 Statistical analysis

Mean surficial and down core biogeochemical values (IC%, OC%, C/N, $\delta^{13}C$ ‰ and $\delta^{15}N$ ‰) were plotted using ODV software, for more information refer to Chapter 1: Methods.

Biogeochemical values (IC%, OC%, C/N, $\delta^{13}C$ ‰ and $\delta^{15}N$ ‰) were plotted as scatter charts with linear fit lines within IBM SPSS Statistics 23 software.

Within IBM SPSS Statistics 23 software, normality distributions were identified using the Shapiro-Wilk test. All biogeochemical data was either non-normally distributed ($p < 0.05$) or

of small sample size, so nonparametric tests were used. Comparison of mean values were determined using IBM SPSS Statistics 23. For independent samples, the non-parametric Kruskal-Wallis (one-way ANOVA on ranks) test was used.

Where the results failed the assumption of homogeneity of variances ($p < 0.05$), therefore retaining the null hypothesis, the nature of differences was evaluated using Dunn-Bonferroni post-hoc pairwise comparison tests.

Spearman's rank correlation tests were used to examine relationships between the data sets.

4.4 Results

4.4.1 Elemental carbon and nitrogen

Surficial and down core mean elemental concentrations of TIC%, $CaCO_3$%, TOC%, TN % and C/N ratio with standard deviations, across nine branches of the Whittard Canyon, are shown in Tables 4:1 and 4:2 Surficial and down core values are shown in Figures 4:1-4:7.

I. *Total inorganic carbon*

Surficial mean percentages of TIC across all branches of the canyon ranged between 1.62% at the Explorer canyon to 3.65% at the Western Middle branch (*n* = 33). Surficial mean percentages of TIC in the Upper canyon (0-1000 m) ranged from 1.44% at the Explorer canyon to 3.65% at the Western Middle branch (*n* = 37). Within the mid canyon (1000-2000m) TIC ranged between 1.93% at the Eastern Middle branch to 3.03% at the Eastern Middle branch. Lower canyon >2000m TIC ranged between 1.62% at the Explorer canyon to 3.13% at the Main Channel. One-way ANOVA on ranks analysis showed that there was no significant difference in surficial TIC% across branches ($p > 0.05$). Likewise, no significant difference when compared across depth intervals (0-1000, 1000-2000 and >2000m) was recorded ($p > 0.05$). R-squared linear correlation coefficient analysis revealed no significant linear relationship between depth and surficial mean TIC%.

Down core mean percentages of TIC across all branches of the canyon ranged between 1.32% at the Western Middle branch to 3.76% at the Western Middle branch (*n* = 37). Down core mean percentages of TIC in the Upper canyon (0-1000m) ranged from 1.97% at the Explorer canyon to 3.76% at the Western Middle branch. Within the mid canyon (1000-2000m) TIC ranged between 1.32% at the Western Middle branch to 3.40% at the Eastern

Middle branch. Lower canyon >2000m TIC ranged between 2.02% at the Western Middle branch to 3.13% at the Main Channel. One-way ANOVA on ranks analysis showed that there was no significant difference in down core TIC% across branches ($p > 0.05$). Likewise, no significant difference when compared across depth intervals (0-1000, 1000-2000 and >2000m) was recorded ($p > 0.05$). R-squared linear correlation coefficient analysis revealed no significant linear relationship between depth and down core mean TIC%.

A moderate correlation was noted between surficial IC% and TN% ($rs [30] = - .446$, $p = 0.014$), however this was not observed down core ($p > 0.05$). Likewise, when IC is converted to carbonate, a moderate positive correlation was observed between surficial CaCO3 % and TN% ($rs [35] = - .496$, $p = 0.005$).

II. *Total organic carbon*

Surficial (first 1cm section) percentages of TOC across all branches of the canyon ranged between 0.33% at the Eastern branch to 2.32% at the Main Channel ($n = 33$). Surficial percentages of TOC in the Upper canyon (0-1000m) ranged from 0.33% at the Eastern branch to 2.26% at the Western Middle branch. Within the mid canyon (1000-2000m) TOC ranged between 1.06% at the Acesta branch to 3.03% at the Eastern Middle branch. Lower canyon >2000 m TOC ranged between 1.10% at the Western branch to 2.32% at the Main Channel. Despite an order of magnitude difference observed, One-way ANOVA on ranks analysis showed that there was no significant difference in down core TOC% across branches ($p > 0.05$). Likewise, no significant difference when compared across depth intervals (0-1000, 1000-2000 and >2000m) was recorded ($p > 0.05$). Depth intervals aim to separate the upper productive waters >1000 m, the areas in which cold-water corals, such as *L.pertusa,* may continue to persist >2000 m where nepheloid layers continue to occur but

are a great distance from overlying productive waters. R-squared linear correlation coefficient analysis revealed no significant linear relationship between depth and down core mean TOC%. Frequency distribution of TOC% in surface sediments shows organic enrichment (>2%) is observed at all depths; however, the upper slopes down to 500m presents the lowest TOC% observed (0- 0.5%). At depths between 3000 and 4000m, TOC contents higher than 2% were recorded.

Down core mean percentages of TOC across all branches of the canyon ranged between 0.71% ± 0.30 at the Western branch to 2.38% ± 0.51 at the Eastern Middle branch. Down core mean percentages of TOC in the Upper canyon (0- 1000m) ranged from 0.71%± 0.30 at the Eastern branch to 2.38% ± 0.51 at the Eastern Middle branch. Within the mid canyon (1000- 2000m) TOC ranged between 1.15% at the Eastern Middle branch to 2.31% at the Eastern branch. Lower canyon >2000m TOC ranged between 0.95% at the Western branch to 2.08% at the Main Channel. One-way ANOVA on ranks analysis showed that there was no significant difference in down core TOC% across branches ($p > 0.05$). Likewise, no significant difference when compared across depth intervals (0-1000, 1000- 2000 and >2000m) was recorded ($p > 0.05$). R-squared linear correlation coefficient analysis revealed no significant linear relationship between depth and down core mean TOC%.

III. *Total nitrogen*

Surficial total nitrogen ranged between 0.01% and 0.39% at the Eastern Middle branch CE16006-030-PSH07-700m and the Explorer Canyon branch JC125-076-PSH02-861.2m, respectively. One-way ANOVA on ranks analysis showed that there was no significant difference in surficial TN% across branches or by water depth interval ($p > 0.05$). A moderate negative correlation was observed between surficial TN% and surficial C/N (r_s [33] =-.859, p

= 0.000).

A moderate correlation was noted between surficial IC% and TN% (rs [30] = - .446, *p* = 0.014). Likewise, when IC is converted to carbonate, a moderate positive correlation was observed between surficial CaCO3 % and TN% (rs [35] = - .496, *p* = 0.005).

Down core total nitrogen ranged between 0.03% and 0.23% at the Eastern Middle branch CE16006-030-PSH12-511.37m and CE14009-042-719m, respectively. One-way ANOVA on ranks analysis showed that there was no significant difference in down core TN% across branches or by water depth interval (*p* > 0.05). A moderate negative correlation was observed between down core TN% and down core C/N (rs [33] =-.589, *p* = 0.000).

IV. *C/N ratio*

Surficial molar C/N ratio across all branches ranged between 3.47 at the Eastern branch and 79.46 at the Eastern Middle branch (*n* = 33). However, a stem and leaf analysis plot indicated that values > 58 are likely to be outliers. C/N ratio in the Upper canyon (0-1000m) ranged between 3.47 at the Eastern branch to 79.46 at the Eastern Middle branch. Within the mid canyon (1000-2000m) C/N ranged between 9.17 at the Eastern Middle branch 57.99 at the Eastern Middle 2 branch. Lower canyon >2000m C/N ranged between 6.99 to 22.75 at the Main Channel. One-way ANOVA on ranks analysis showed that there was no significant difference in surficial C/N across branches (*p* > 0.05). Likewise, no significant difference when compared across depth intervals (0-1000, 1000-2000 and >2000m) was recorded (*p* > 0.05). R-squared linear correlation coefficient analysis revealed no significant linear relationship between depth and surficial mean C/N.

Down core mean molar C/N ratio across all branches ranged between 5.43 at the Western

Middle branch and 64.47 at the Eastern Middle 2 branch. No trend with depth was observed. C/N ratio in the Upper canyon (0-1000m) ranged between 5.43 at the Western Middle branch to 64.47 at the Eastern Middle branch. Within the mid canyon (1000-2000m) C/N ranged between 10.22 at the Eastern Middle branch to 51.51 at the Eastern Middle 2 branch. Lower canyon >2000m C/N ranged between 14.28 to 27.52 at the Main Channel. One-way ANOVA on ranks analysis showed that there was no significant difference in down core C/N across branches ($p > 0.05$) R-squared linear correlation coefficient analysis revealed no significant linear relationship between depth and down core mean C/N.

Negative correlations were observed between surficial TN% and surficial C/N ($rs [33] = -.859$, $p = 0.000$) and down core values ($rs [33] = -.589$, $p = 0.000$).

Table 4:2 Surficial values for elemental properties of particles from 9 branches of the Whittard Canyon. Canyon branches are colour coded Purple (Western Branch), Pink (Western Middle Branch) Yellow (Acesta Branch), Green (Eastern Middle Branch), Cream (Intersection), Magenta (Eastern Mid 2), Brown (Eastern Branch), Blue (Explorer Canyon) and Red (Main).

BRANCH	DEPTH (m)	CORE	TIC%	$CaCO_3$%	TOC%	TN%	C/N RATIO
Western	2740	JC125-083-PSH03-2740m	1.62	13.49	1.10	0.17	7.71
Western Middle	440	CE14009-045-440m	2.64	21.99	1.85	0.07	30.01
Western Middle	719	CE14009-042-719m	3.65	30.40	1.94	0.26	5.62
Western Middle	819	CE14009-042-819m	3.08	25.65	2.26	0.13	20.28
Western Middle	2816	CE14009-027-2816m	2.30	19.15	1.53	0.12	14.88
Acesta	780	CE16006-033-PSH08-780m	2.43	20.24	1.65	0.08	23.22
Acesta	974	CE16006-084-PSH05-974m	2.20	18.40	ABSENT	ABSENT	ABSENT
Acesta	974.2	CE16006-084-PSH02-974.2m	2.95	24.57	ABSENT	ABSENT	ABSENT
Acesta	1130	CE14009-009-1130m	2.71	22.57	1.06	0.05	23.27
Eastern Middle	501	CE14009-040-501m	2.97	24.74	1.13	0.08	16.29
Eastern Middle	511	CE16006-030-PSH12-511.37m	2.19	18.24	.99	0.03	32.12
Eastern Middle	574	CE14009-012-574m	2.41	20.07	1.79	0.08	19.89
Eastern Middle	700	CE14009-030-700m	2.77	23.07	1.41	0.06	24.13
Eastern Middle	700	CE16006-030-PSH07-700m	3.27	27.23	1.23	0.01	79.46
Eastern Middle	723	CE14009-033-723m	3.19	26.57	1.65	0.17	10.86
Eastern Middle	731	CE16006-022-PSH06-731.38m	2.45	20.40	2.20	0.08	29.79
Eastern Middle	1095	CE14009-040-1095m	3.03	25.23	1.15	0.14	9.17
Eastern Middle	1271	CE16006-062-PSH07-1270.84m	2.65	22.07	1.53	0.08	21.81
Eastern Middle	1323	CE14009-012-PSH09-1323m	1.93	16.07	1.82	0.10	24.62
Intersection	1776	CE14009-031-1776m	2.85	23.74	1.73	0.08	24.08
Intersection	1836	CE14009-025-PSH12-1836m	2.79	23,24	1.91	0.20	10.89
Intersection	2086	CE14009-025-2086m	2.93	24.40	1.13	0.08	14.77
Intersection	2384	CE14009-025-2384m	2.44	20.32	1.21	0.08	17.43
Eastern Middle Two	1845	CE16006-056-PSH05-1845m	2.05	17.07	2.04	0.05	43.72
Eastern Middle Two	1850	CE16006-056-PSH07-1850	2.38	17.07	2.14	0.04	57.99
Eastern	450	CE14009-005-450m	3.55	29.57	.33	0.11	3.47
Eastern	681	CE14009-005-681m	2.44	20.32	1.33	0.04	36.81
Eastern	571	JC125-109-PSH05-570.5m	2.22	18.49	1.99	0.22	10.78
Eastern	1620	CE16006-042-PSH02-1620m	2.65	22.07	1.19	0.05	24.71
Eastern	1298	CE16006-002-PSH05-1297.81m	2.37	19.74	2.20	0.07	32.45
Explorer	664	JC125-101-MC-664m	1.80	14.99	1.60	0.10	18.12
Explorer	861	JC125-076-PSH02-861.2m	1.44	11.99	1.33	0.39	3.95
Main Channel	3723	JC125-045-MC-3723m	3.13	26.07	2.29	0.18	14.34
Main Channel	3759	JC125-028-MC-3758m	2.90	24.15	2.32	0.11	22.75
Main Channel	4010	JC125-063-MC-4010m	3.02	25.15	1.26	0.21	6.99

Table 4:3 Down core mean values with standard deviations for elemental properties of particles from 9 branches of the Whittard Canyon. Canyon branches are colour coded Purple (Western Branch), Pink (Western Middle Branch) Yellow (Acesta Branch), Green (Eastern Middle Branch), Cream (Intersection), Magenta (Eastern Mid 2), Brown (Eastern Branch), Blue (Explorer Canyon) and Red (Main). N =10 samples unless otherwise stated.

BRANCH	DEPTH (m)	CORE	TIC%	$CaCO_3$%	TOC%	TN%	C/N RATIO
Western	2740	JC125-083-PSH03-2740m	1.72 ± 0.34	17.96 ± 2.63	0.95 ± 0.36 N9	0.10 ± 0.06	18.34 ± 19.08 N9
Western Middle	440	CE14009-045-440m	2.58 ± 0.08	21.53 ± 0.71	1.70 ± 0.15 N8	0.05 ± 0.00	31.48 ± 3.10 N8
Western Middle	719	CE14009-042-719m	3.76 ± 0.07	31.29 ± 0.60	1.10 ± 0.20	0.23 ± 0.02	5.43 ± 0.93
Western Middle	819	CE14009-042-819m	2.99 ± 0.13	24.99 ± 1.15	1.17 ± 0.38	0.10 ± 0.01	12.23 ± 3.49
Western Middle	1601	CE16006-081-PSH03-1601m	1.32 ± 0.05	ABSENT	ABSENT	ABSENT	
Western Middle	2816	CE14009-027-2816m	2.02 ± 0.25 N9	16.82 ± 2.12 N9	1.50 ± 0.37 N8	0.10 ± 0.01	17.09 ± 3.82 N8
Acesta	700	CE14009-030-700m	2.96 ± 0.27	24.71 ± 2.29	1.47 ± 0.42	0.13 ± 0.07	15.13 ± 7.00
Acesta	780	CE16006-033-PSH08-780m	3.63 ± 1.14 N8	16.97 ± 3.29 N8	1.59 ± 0.91 N8	0.06 ± 0.02	27.95 ± 7.95 N8
Acesta	974	CE16006-084-PSH05-974m	2.03 ± 0.35	16.98 ± 2.98	ABSENT	ABSENT	ABSENT
Acesta	974.2	CE16006-084-PSH02-974.2m	2.09 ± 0.14	17.41 ± 1.20	ABSENT	ABSENT	ABSENT
Acesta	1130	CE14009-009-1130m	2.81 ± 0.33	23.44 ± 2.79	1.12 ± 0.30	0.05 ± 0.00	23.76 ± 6.67
Eastern Middle	501	CE14009-040-501m	2.90 ± 0.09	24.20 ± 0.79	1.23± 0.17	0.08 ± 0.00	16.38 ± 2.01
Eastern Middle	511	CE16006-030-PSH12-511.37m	2.14 ± 0.17	17.85 ± 1.43	1.74 ± 0.39	0.03 ± 0.00	64.47 ± 17.48
Eastern Middle	574	CE14009-012-574m	2.34 ± 0.18	19.55 ± 1.51	1.62 ± 0.14	0.08 ± 0.00	22.99 ± 2.41
Eastern Middle	700	CE14009-030-700m	2.96 ± 0.27	24.71 ± 2.29	1.47 ± 0.42	0.13 ± 0.07	15.13 ± 7.00
Eastern Middle	700	CE16006-030-PSH07-700m	3.45 ± 0.17	28.80 ± 1.44	1.39 ± 0.13	0.06 ± 0.03	50.43 ± 65.64
Eastern Middle	723	CE14009-033-723m	2.85 ± 0.24	23.77 ± 2.07	1.31 ± 0.29	0.10 ± 0.09	22.05 ± 11.72
Eastern Middle	731	CE16006-022-PSH06-731.38m	2.42 ± 0.13	20.22 ± 1.15	2.38 ± 0.51	0.10 ± 0.03	29.58 ± 10.11
Eastern Middle	1095	CE14009-040-1095m	2.42 ± 0.59	20.19 ± 4.99	0.81 ± 0.29	0.10 ± 0.01	10.22 ± 3.36
Eastern Middle	1271	CE16006-062-PSH07-	2.60 ± 0.11	21.71 ± 0.99	1.60 ± 0.13	0.08 ± 0.00	23.04 ± 3.24
Eastern Middle	1323	CE14009-012-PSH09-1323m	3.39 ± 0.69	28.30 ± 5.81	1.15 ± 0.32	0.08 ± 0.01	15.50 ± 4.05
Intersection	1487	CE14009-031-1487m	2.81 ± 0.05 N7	23.40 ± 0.44 N7	ABSENT	ABSENT	ABSENT
Intersection	1776	CE14009-031-1776m	3.07 ± 0.11	25.59 ± 0.93	1.72 ± 0.14	0.08 ± 0.00	23.98 ± 2.59
Intersection	1836	CE14009-025-PSH12-1836m	2.84 ± 0.07 N7	23.66 ± 0.64 N7	1.97 ± 0.08 N7	0.18 ± 0.01	12.79 ± 1.28 N7
Intersection	2086	CE14009-025-2086m	2.97 ± 0.11 N9	24.78 ± 0.98 N9	1.24 ± 0.25 N9	0.09 ± 0.01	14.81 ± 2.23 N9
Intersection	2384	CE14009-025-2384m	2.24 ± 0.10 N8	18.73 ± 0.88 N8	0.95 ± 0.14 N8	0.07 ± 0.00	29.35 ± 6.40 N8
Eastern Middle Two	1845	CE16006-056-PSH05-1845m	2.19 ± 0.09 N9	18.29 ± 0.75 N9	1.83 ± 0.11 N9	0.06 ± 0.01	34.88 ± 17.04 N9
Eastern Middle Two	1850	CE16006-056-PSH07-1850	1.95 ± 0.15	16.24 ± 1.30	2.10 ± 0.18	0.05 ± 0.01	36.07 ± 9.17
Eastern	450	CE14009-005-450m	2.78 ± 0.34 N9	23.19 ± 2.89 N9	0.71 ± 0.30 N7	0.10 ± 0.01	8.48 ± 4.42 N7
Eastern	571	JC125-109-PSH05-570.5m	2.38 ± 0.34	22.21 ± 0.55	1.46 ± 0.33	0.09 ± 0.07	39.23 ± 43.91
Eastern	681	CE14009-005-681m	2.39 ± 0.16 N9	19.91 ± 1.26	1.13 ± 0.19 N 9	0.07 ± 0.01	17.29 ± 9.62 N9
Eastern	1620	CE16006-042-PSH02-1620m	2.79 ± 0.09	23.09 ± 0.82	1.44 ± 0.13	0.06 ± 0.00	26.54 ± 1.59
Eastern	1298	CE16006-002-PSH05-	2.46 ± 0.15	20.55 ± 1.27	2.31 ± 0.25 N3	0.09 ± 0.02	29.81 ± 4.24 N3
Explorer	664	JC125-101-MC-664m	1.96 ± 0.07	16.39 ± 0.62	1.43 ± 0.09	0.09 ± 0.01	15.76 ± 6.58
Explorer	861	JC125-076-PSH02-861.2m	1.76 ± 0.49	18.52 ± 1.56	1.41 ± 0.25 N4	0.10 ± 0.12	42.63 ± 31.78 N4
Main Channel	3723	JC125-045-MC-3723m	2.70 ± 0.35	22.50 ± 2.96	2.08 ± 0.31	0.14 ± 0.03	18.45 ± 8.95
Main Channel	3759	JC125-028-MC-3758m	2.45 ± 0.88	20.44 ± 7.36	1.96 ± 0.29	0.07 ± 0.02	27.52 ± 12.71
Main Channel	4010	JC125-063-MC-4010m	2.87 ± 0.12 N8	23.96 ± 1.01 N8	1.93 ± 0.32 N8	0.17 ± 004	14.28 ± 5.28 N8

V. *Spatial pattern of surficial TIC*

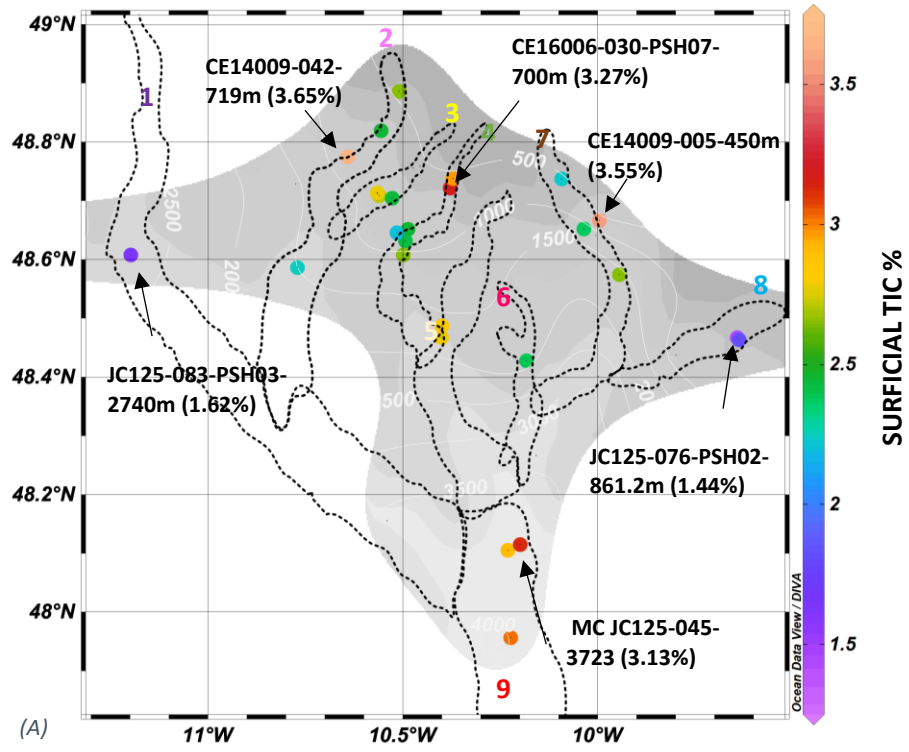

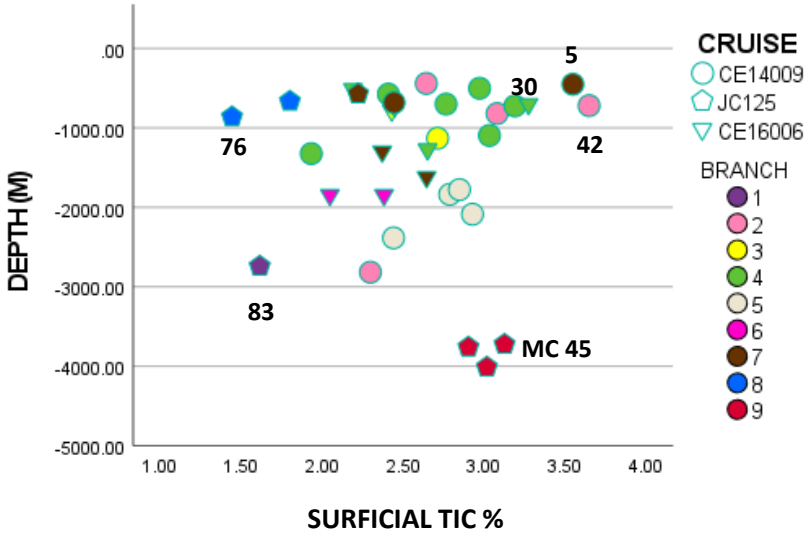

Figure 4:1 (A, B) Surface plot and scatter diagram of mean TIC% of the first-centimetre section across sites. Upper canyon 0-1000m ranges from 1.44% at the Explorer canyon to 3.65% at the Western Middle branch. Mid canyon 1000-2000m ranges from 1.93% at the Eastern Middle branch to 3.03 % at the Eastern Middle branch. Lower canyon >200m ranges from 1.62% at the Explorer canyon (JC125-076-PSH02-861.2m) to 3.13% at the Main Channel (JC125-045-MC-3723m). One-way ANOVA on ranks analyses revealed no significant difference in surficial mean TIC% across branches or with depth ($p > 0.05$).

VI. *Spatial pattern of down core TIC*

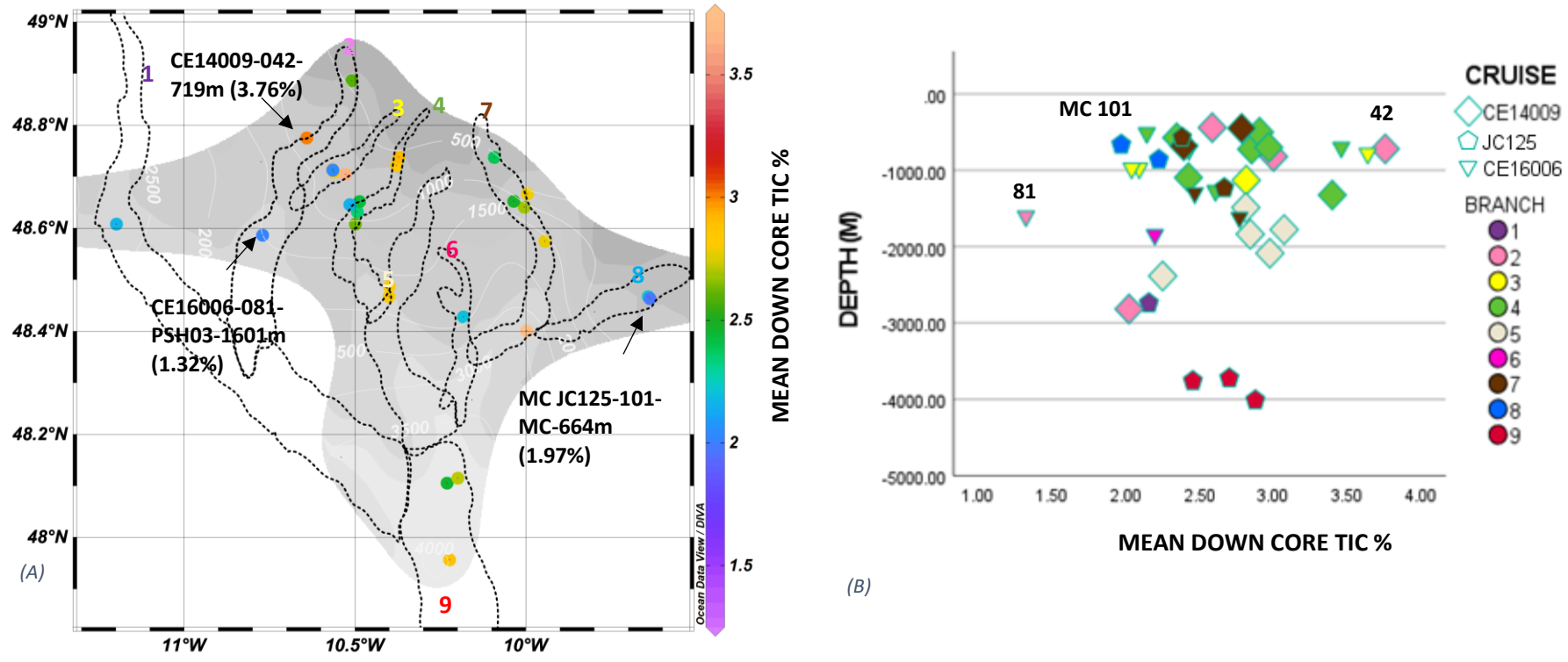

Figure 4:2 Surface plot and scatter diagram of mean TIC% down core across sites. Upper canyon 0-1000m ranges from 1.97% at the Explorer canyon to 3.76% at the Western Middle branch. Mid canyon 1000-2000m ranges from 1.32% at the Western Middle branch to 3.40% at the Eastern Middle branch. Lower canyon >2000m ranges from 2.02% at the Western Middle branch to 3.13% at the Main Channel. One-way ANOVA on ranks analyses showed that there was no significant difference in down core TIC% across branches or with depth ($p > 0.05$).

VII. *Spatial pattern of surficial TOC*

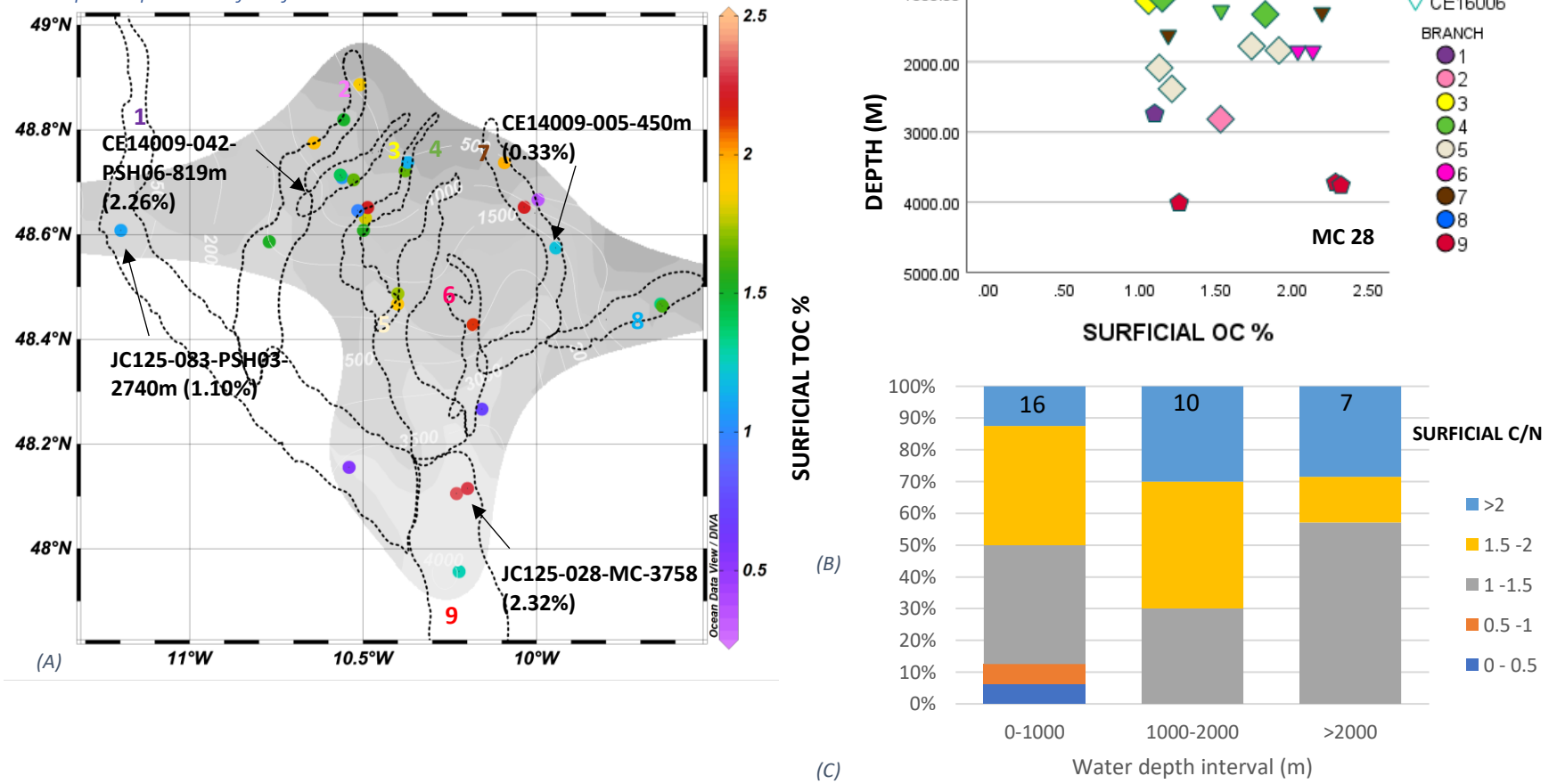

Figure 4:3 (A, B) Surface plot and scatter diagram of TOC% of the first-centimetre section across sites. Upper canyon 0-1000m ranges from 0.33% at the Eastern branch to 2.26% at the Western Middle branch. Mid canyon 1000-2000m ranges from 1.06% at the Acesta branch to 2.20% at the Eastern branch. Lower canyon >2000m ranges from 1.10% at the Western branch to 2.32% at the Main Channel. One-way ANOVA on ranks analyses revealed no significant difference in surficial mean TOC% across branches or with depth ($p > 0.05$). (C) Frequency distribution of TOC% in surface sediments (<1cm) of the Whittard Canyon (N 33) according to water depth interval. Organic enrichment is observed at all depths (>2%); however, the upper slopes down to 500m presents the lowest TOC% observed (0-0.5%). At depths between 3000 and 4000m, TOC contents higher than 2% were recorded, indicating possible increased input or burial.

VIII. *Spatial pattern of down core TOC*

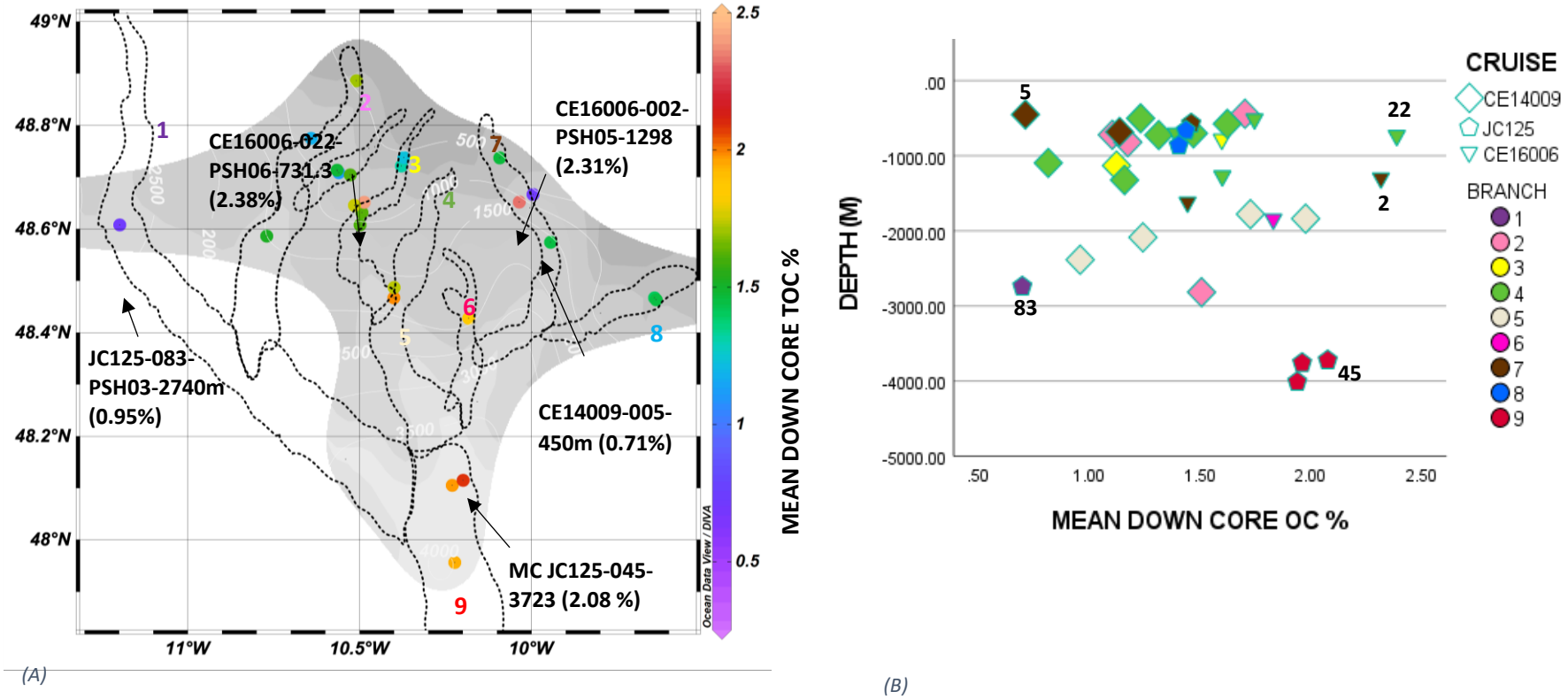

Figure 4:4 (A, B) Surface plot and scatter diagram of mean TOC% down core across sites. Upper canyon 0-1000m ranges from 0.71% at the Eastern branch to 2.38% at the Eastern Middle branch. Mid canyon 1000-2000m ranges from 1.15% at the Eastern Middle branch to 2.31% at the Eastern branch. Lower canyon >2000m ranges from 0.95% at the Western branch to 2.0 % at the Main Channel. One-way ANOVA on ranks analyses showed that there was no significant difference in down core mean TOC% and across branches or with depth ($p > 0.05$).

IX. *Down core total organic carbon*

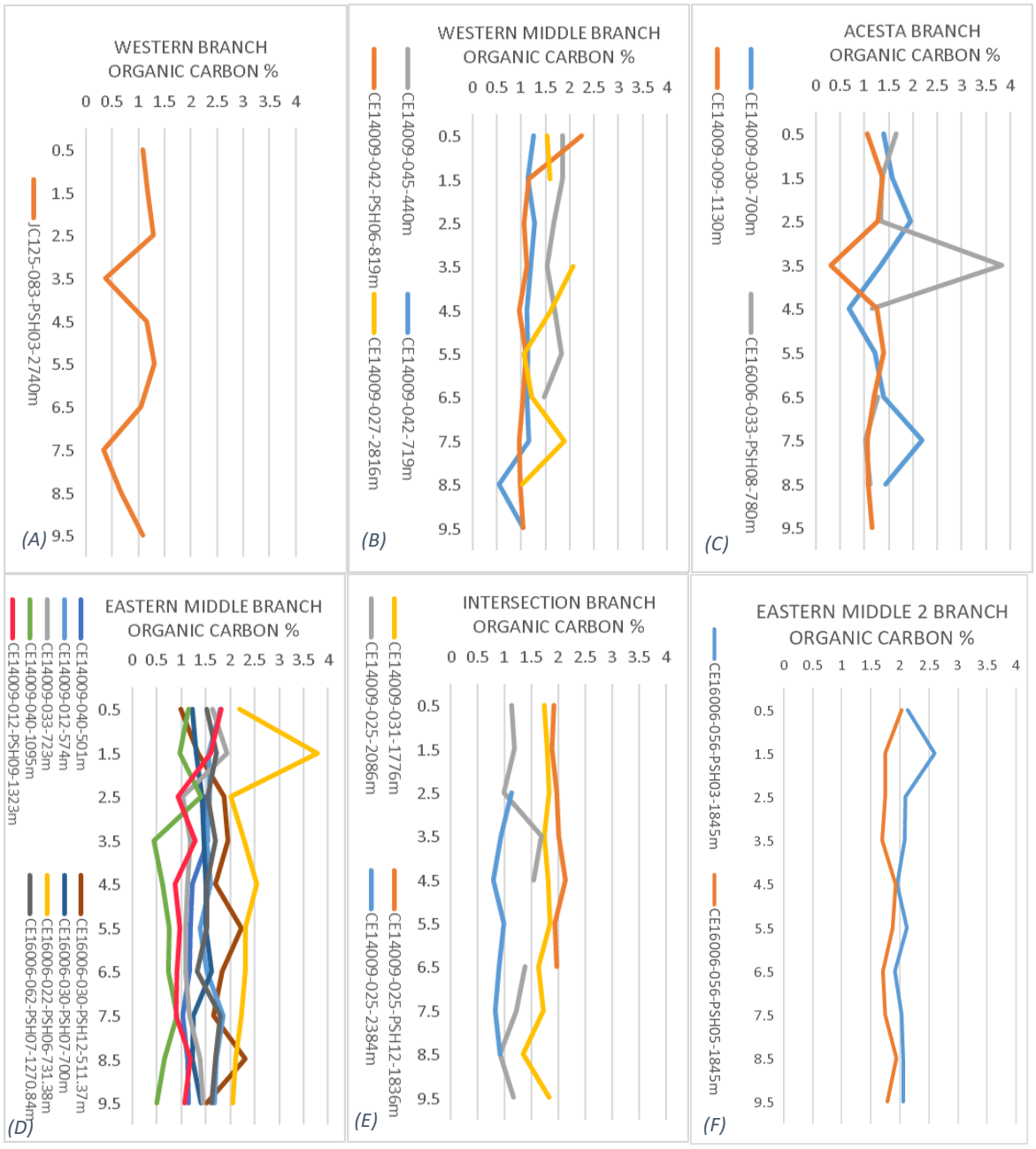

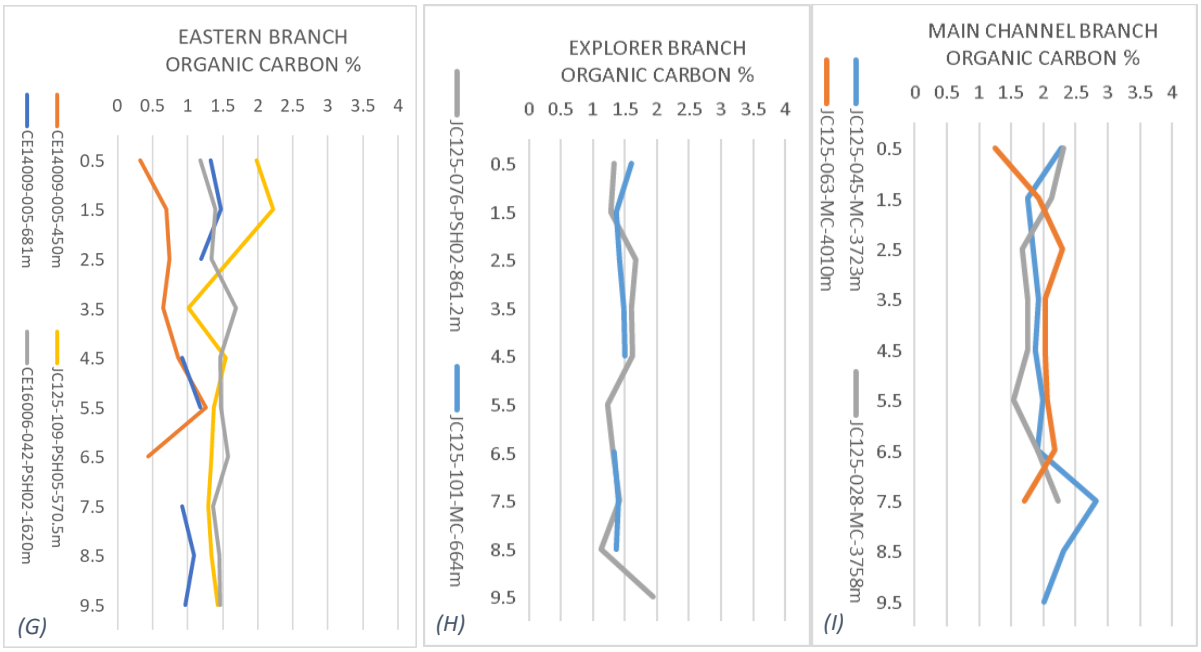

Figure 4:5 (A-I) TOC% down core plotted by branch. Sharp peaks of total organic carbon enrichment at the Acesta branch (CE16006-033-PSH08-780m) and Eastern Middle branch (CE16006-022-PSH06-731.38m).

X. *Spatial pattern of surficial molar C/N*

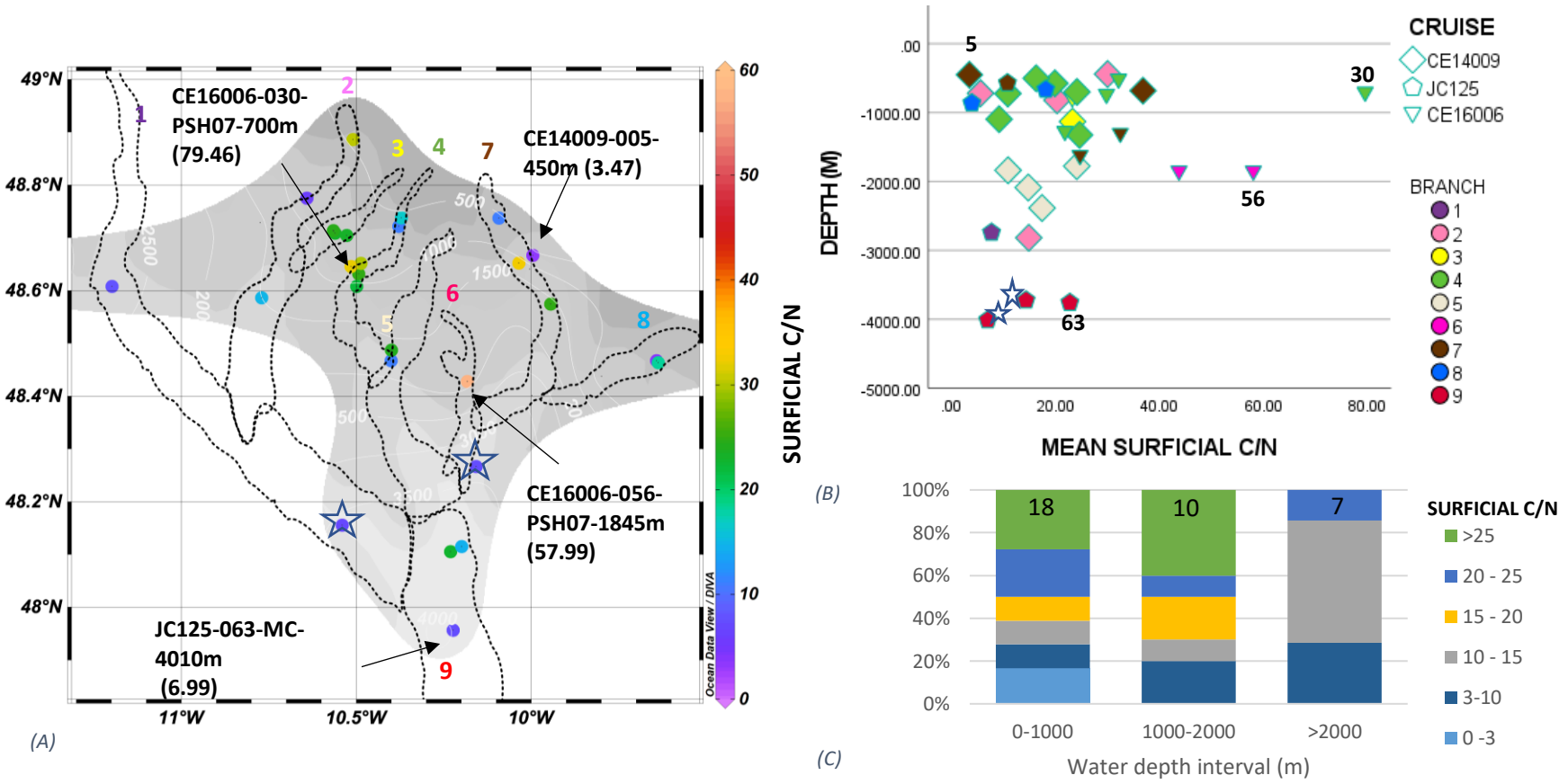

Figure 4:6 (A, B) Surface plot and scatter diagram of the C/N ratio of the first-centimetre section across sites. Most surficial samples analysed were within the range of 3 to 25 C/N. Upper canyon 0-1000m ranges from 3.47 at the Eastern branch to 79.46 at the Eastern Middle branch. Mid canyon 1000-2000m ranges from 9.17 at the Eastern Middle branch to 57.99 at the Eastern Middle 2 branch. Lower canyon >2000m ranges from 6.99 to 22.75 in the Main Channel. One-way ANOVA on ranks analyses revealed no significant difference in surficial mean molar C/N ratio across the branches or with depth ($p > 0.05$). R-squared linear correlation coefficient analysis revealed no significant linear relationship between depth and surficial mean molar C/N ratio. Stars represent data from Hunter et al. (2013). (C) Frequency distribution of molar C/N ratio in surface sediments (<1cm) of the Whittard Canyon (N 32) according to water depth interval. Typical marine signatures in the range of <3-10 where observed at all depths, excluding 3000-4000m. High values exceeding 25 were observed down to 2000m. Due to the distance from land, high C/N ratios likely indicate degradation and not a terrestrial contribution (Meyers, 1994).

XI. *Spatial pattern of down core molar C/N*

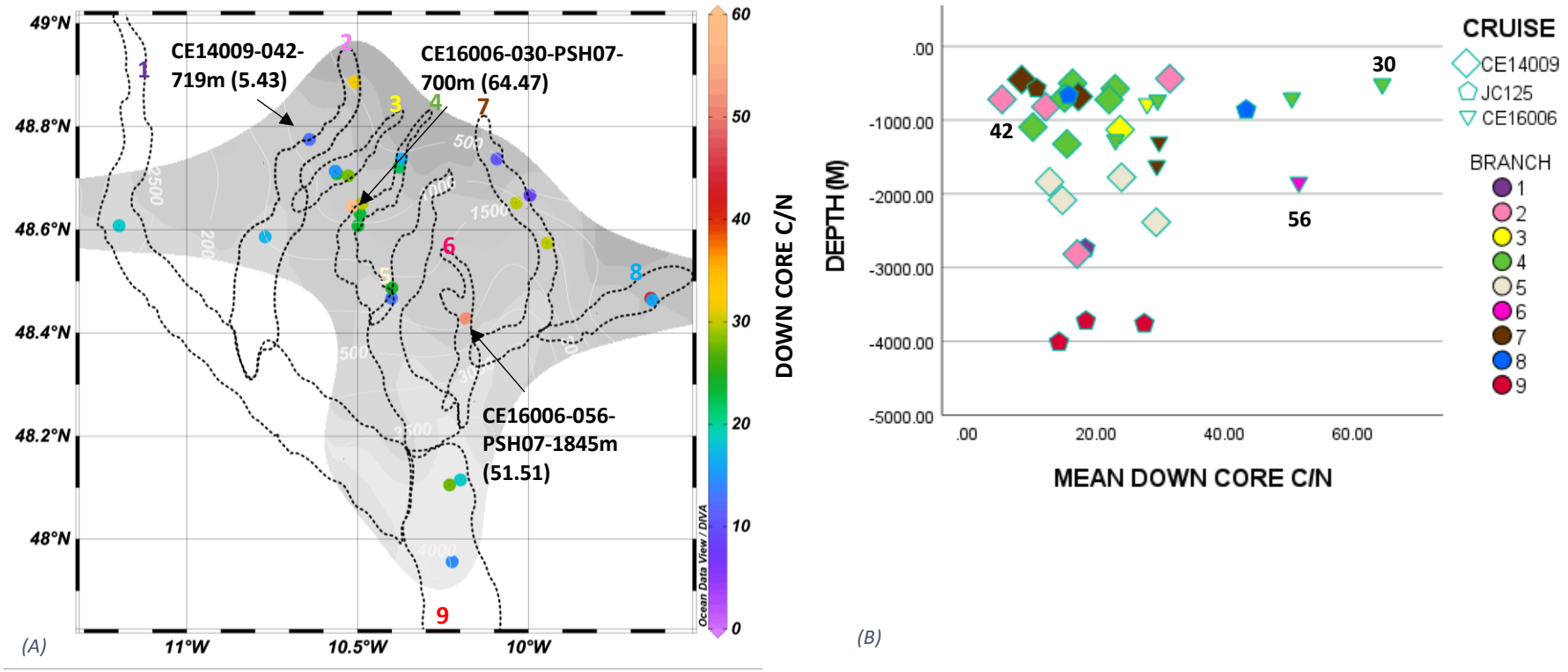

Figure 4:7 (A, B) Surface plot and scatter diagram of the down core mean molar C/N ratio across sites. Upper canyon 0-1000m ranges from 5.43 at the Western Middle branch to 64.47 at the Eastern Middle branch. Mid canyon 1000-2000m ranges from 10.22 at the Eastern Middle branch to 51.51 at the Eastern Middle 2 branch. Lower canyon >2000m ranges from 14.28 to 27.52 in the Main Channel. One-way ANOVA on ranks analyses showed that there was no significant difference in down core mean molar C/N ratio across the branches or with depth ($p > 0.05$). R-squared linear correlation coefficient analysis revealed no significant linear relationship between depth and down core mean molar C/N ratio %. Numbers are events.

4.4.2 Surficial stable isotopes $\delta^{13}C‰$, $\delta^{15}N‰$

$\delta^{13}C‰$ and $\delta^{15}N‰$ isotopes (Table 4:3) present a range of values across branches. However, One-way ANOVA on ranks analysis showed that there was no significant difference in stable isotopes across branches ($p > 0.05$). Likewise, no significant difference when compared across depth intervals (0-1000, 1000- 2000 and >2000m) was recorded ($p > 0.05$).

$\delta^{13}C‰$ ranged between -24.42‰ at the Explorer canyon (JC125-101-MC-664m) and -12.76‰ at the Eastern Middle branch (CE16006-030-PSH12-511.37m) (Figures 4:8 and 4:9). The majority of $\delta^{13}C‰$ values fell within the lighter isotopic range of ~-24‰ and ~-22‰, in line with previous research and indicating phytoplankton and zooplankton derived organic matter (Fry and Sherr, 1984; Levin and Michener, 2002; Hunter et al., 2013a). However, a heavier isotopic signature of -12.76‰ was recorded at the Eastern Middle branch (CE16006-030-PSH12-511.37m) which is indicative of sulfide-oxidized derived carbon that involves the form II Rubisco pathway (Levin and Michener, 2002).

The majority of $\delta^{15}N‰$ fell within the range of ~3 to ~4‰, just below the widely supported boundary value of ~5‰ for nitrate-derived organic matter production through algal primary productivity, and close to the value of <3‰ for sedimentary denitrification (Sigman and Casciotti, 2001; Sigman and Fripiat, 2019). The lightest reading of 1.30‰ was observed at the Western branch (JC125-083-PSH03-2740m) and the heaviest reading of 4.28‰ was recorded at the Explorer canyon (JC125-101-MC-664m). In the Western branch, the lightest isotopic reading of 1.30‰ coincided with a C/N ratio of 7.71 which is typical of fresh algal organic matter (Emerson and Hedges, 1988; Meyers, 1994). In the Explorer canyon, the heavier isotopic reading of 4.28‰ coincided with a carbon-rich C/N ratio of 18.12.

Table 4:4 Mean surficial values of stable isotopes ($\delta^{13}C$‰, $\delta^{15}N$‰) from 9 branches of the Whittard Canyon. Canyon branches are colour coded Purple (Western Branch), Pink (Western Middle Branch) Yellow (Acesta Branch), Green (Eastern Middle Branch), Cream (Intersection), Magenta (Eastern Mid 2), Brown (Eastern Branch), Blue (Explorer Canyon) and Red (Main channel). All data are presented in units (‰) relative to the international standard reference (Pee Dee Belemnite for $\delta^{13}C$ and Atmospheric Nitrogen for $\delta^{15}N$).

BRANCH	DEPTH (m)	CORE	$\delta^{13}C$ ‰	$\delta^{15}N$ ‰
Western	2740	JC125-083-PSH03-2740m	-22.27 ± 0.07	1.30 ± 0.48
Western Middle	440	CE14009-045-440m	-21.97 ± 0.14	3.81 ± 0.10
Western Middle	719	CE14009-042-719m	-23.83 ± 0.08	3.45 ± 0.06
Western Middle	1487	CE14009-027-1487m	ABSENT	4.03 ± 1.46
Western Middle	2816	CE14009-027-2816m	-22.54 ± 0.37	3.45 ± 0.02
Acesta	659	CE14009-030-659m	-22.57 ± 0.12	3.83 ± 0.19
Acesta	700	CE14009-030-700m	-22.59 ± 0.18	3.50 ± 0.40
Acesta	780	CE16006-033-PSH08-780m	-22.96 ± 0.15	3.88 ± 0.08
Acesta	1130	CE14009-009-1130m	-22.65 ± 0.09	3.34 ± 0.00
Eastern Middle	501	CE14009-040-501m	-23.40 ± 0.25	3.60 ± 0.12
Eastern Middle	511	CE16006-030-PSH12-511.37m	-12.76 ± 1.67	3.59 ± 0.19
Eastern Middle	574	CE14009-012-574m	-21.58 ± 1.72	3.66 ± 0.02
Eastern Middle	700	CE16006-030-PSH07-700m	-22.82 ± 0.00	1.50 ± 1.94
Eastern Middle	723	CE14009-033-723m	-22.65 ± 0.53	4.05 ± 0.42
Eastern Middle	1095	CE14009-040-1095m	-20.99 ± 1.84	3.95 ± 0.56
Eastern Middle	1271	CE16006-062-PSH07-1270.84m	-22.73 ± 0.01	2.65 ± 0.47
Eastern Middle	1323	CE14009-012-PSH09-1323m	ABSENT	2.82 ± 0.07
Intersection	1836	CE14009-025-PSH12-1836m	-23.07 ± 0.10	4.19 ± 0.04
Intersection	2086	CE14009-025-2086m	-22.87 ± 0.07	3.98 ± 0.41
Eastern Mid 2	1845	CE16006-056-PSH05-1845m	-22.15 ± 0.46	3.12 ± 0.69
Eastern Mid 2	1850	CE16006-056-PSH07-1850	-23.45 ± 0.14	2.34 ± 1.06
Eastern	450	CE14009-005-450m	-21.35 ± 0.39	3.65 ± 1.05
Eastern	571	JC125-109-PSH03-570.5m	-23.87 ± 1.14	4.05 ± 0.38
Eastern	681	CE14009-005-681m	-23.19 ± 0.11	3.67 ± 0.07
Eastern	1620	CE16006-042-PSH02-1620m	-22.50 ± 0.16	3.78 ± 0.29
Eastern	2979	JC125-091-PSH05-2979m	-23.08 ± 0.83	3.11 ± 0.39
Explorer	664	JC125-101-MC-664m	-24.42 ± 0.72	4.28 ± 0.15
Explorer	861	JC125-076-PSH02-861.2m	-24.95 ± 0.40	2.71 ± 0.15
Main Channel	3758	JC125-028-MC-3758m	-23.62 ± 0.45	3.57 ± 0.10

I. *Spatial pattern of surficial δ ^{13}C and δ ^{15}N*

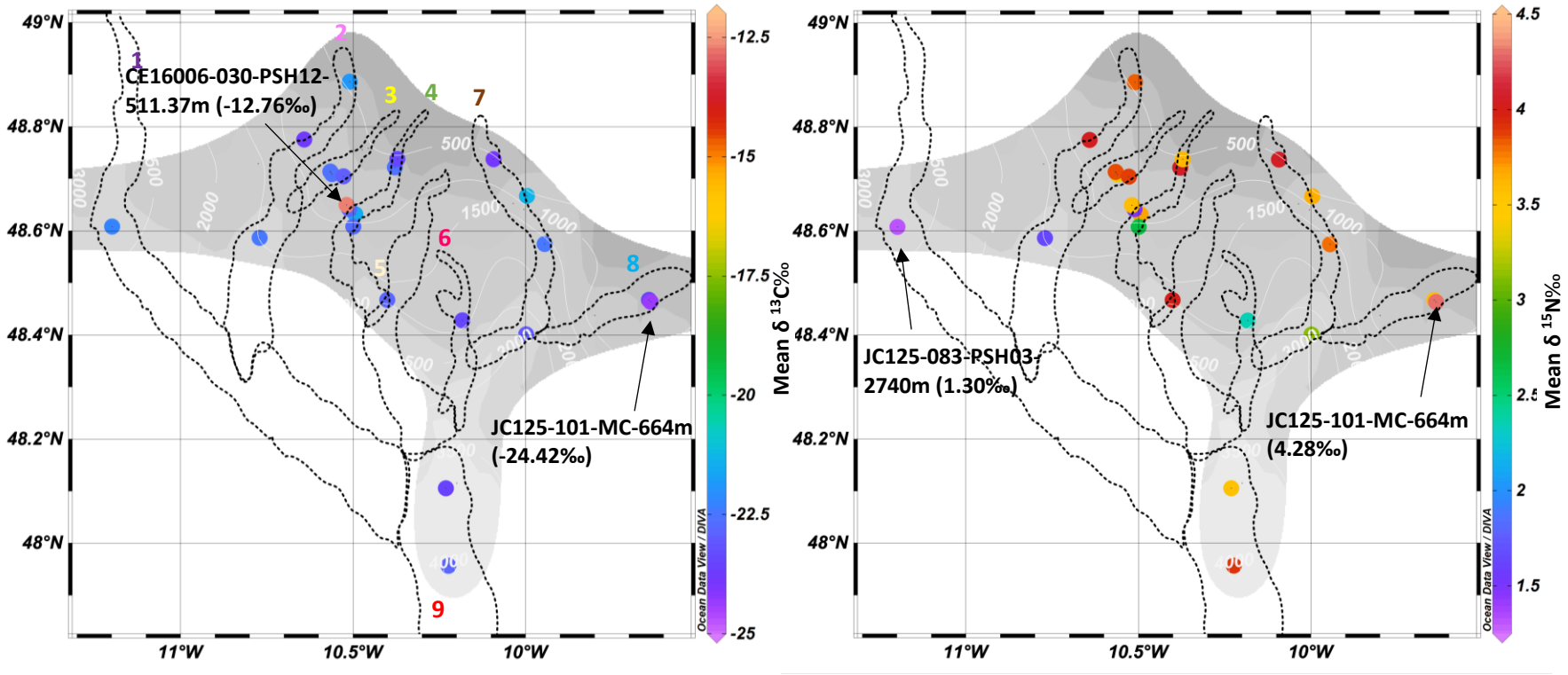

Figure 4:8 (A) Mean δ ^{13}C‰ of surficial 1cm section across all sampling sites. Lowest values of δ ^{13}C were observed within the Explorer canyon JC125-101-MC-664m (-24.42‰). The highest value was observed within the Eastern Middle branch CE16006-030-PSH12-511.37m (-12.76‰). (B) Mean δ ^{15}N‰ of surficial 1cm section across all sampling sites. The lowest value of δ ^{15}N was observed within the Western branch JC125-083-PSH03-2740m (1.30‰) and the highest was observed within the Explorer canyon JC125-101-MC-664m (4.28‰). One-way ANOVA on ranks analysis showed that there was no significant difference in stable isotopes across the branches (p > 0.05). All data are presented in units (‰) relative to the international standard reference (Pee Dee Belemnite for δ ^{13}C and Atmospheric Nitrogen for δ ^{15}N).

II. *Cross plot of δ ^{13}C and δ ^{15}N*

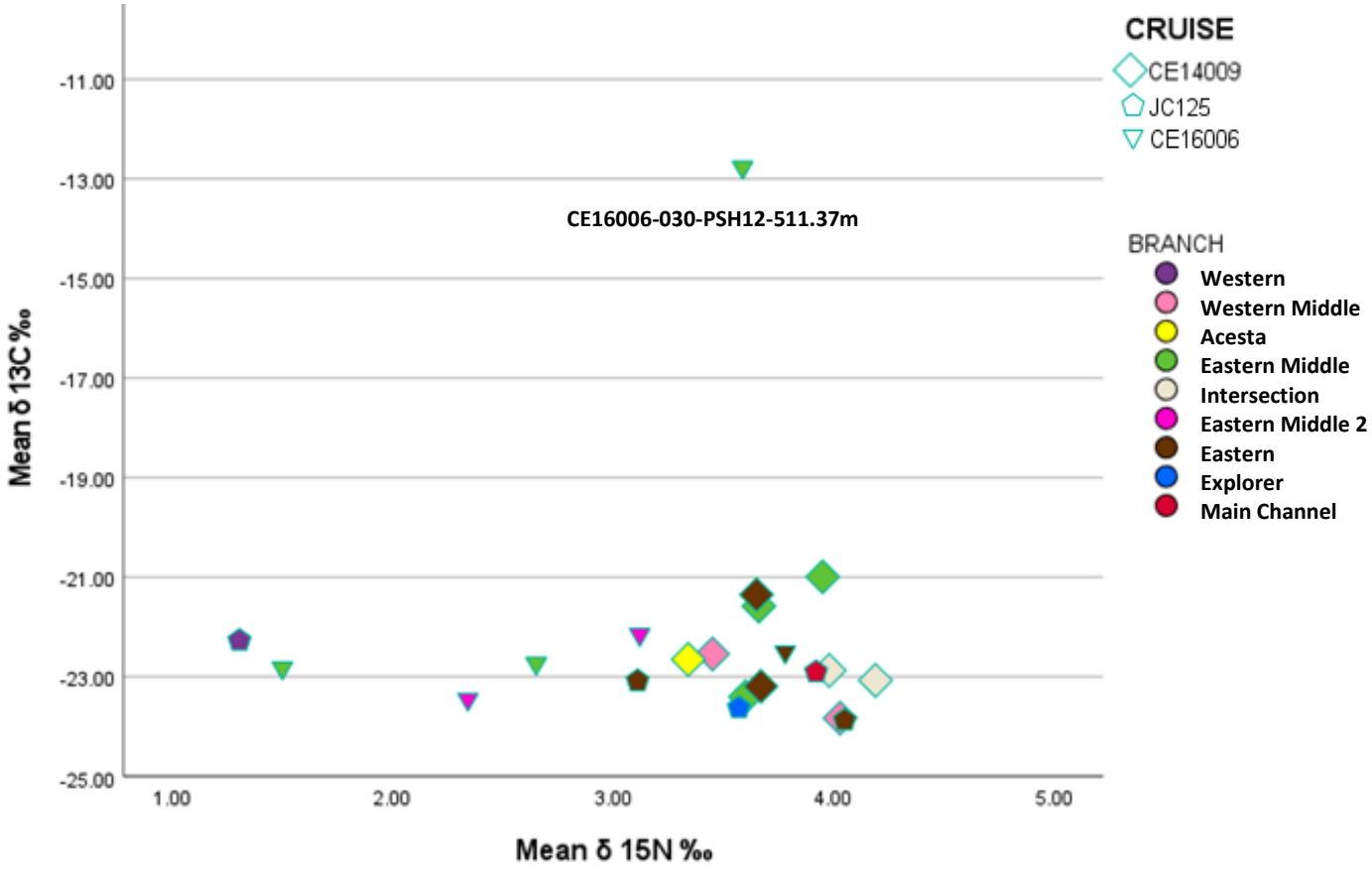

Figure 4:9 (A) Mean δ ^{13}C‰ and δ ^{15}N‰ of surficial 1cm section plotted with depth (m). Lowest values of δ ^{13}C were observed within the Explorer canyon JC125-101-MC-664m (-24.42‰). The highest value was observed within the Eastern Middle branch CE16006-030-PSH12-511.37m (-12.7‰6). Mean δ ^{15}N‰ of surficial 1cm section across all sampling sites. The lowest value of δ ^{15}N was observed within the Western branch JC125-083-PSH03-2740m (1.30‰) and the highest was observed within the Explorer canyon JC125-101-MC-664m (4.28‰) (Not seen as no δ ^{13}C value). One-way ANOVA on ranks analysis showed that there was no significant difference in stable isotopes across the branches ($p > 0.05$).

4.5 Discussion

The average surficial and down core TIC values across all sites were 2.62% ± 0.51 (*n* = 33) and 2.58% ± 0.53 (n= 37), respectively. Clustering of low TIC values was observed within the Explorer branch. In contrast, the Main Channel was characterized by higher TIC content. When transformed to $CaCO_3$, carbonates are spatially variable and not determined by depth. Spearman's rank correlation recorded no significant relationship with depth ($p > 0.05$). This suggests that dissolution processes do not influence the deposition of carbonate, though there are no microscopic observations to support this. However, the $CaCO_3$ depth is recorded as being >5000m within the North Atlantic, which suggests that it is not depth dependent at the targeted sites (Bickert, 2009). A moderate positive correlation was observed between TN% and $CaCO_3$% (r_s [35] = - .496, $p = 0.005$). The biological origin of both parameters may explain this. However, $CaCO_3$ only refers to calcareous production and does not account for the siliceous or other soft tissue contribution (e.g. flagellates/cyanobacteria) (Broecker, 2003). Furthermore, the lability and hence faster decomposition of N-containing organic matter and the potential incorporation of inorganic nitrogen in the sediments, may also be responsible for the moderate relationship observed (Walsh, 1991; Corman et al., 2015).

The average surficial and down core TOC values across all sites were 1.58% ± 0.47 (n= 33) and 1.47% ± 0.42 (n= 32), respectively. TOC content is enriched within the upper slopes of the canyon and to the East of the canyon. There is also a hotspot observed within the main channel. This suggests that the canyon may have the potential for efficient organic matter storage. TOC enrichments at increasing depths have also been observed within the morphologically complex Congo fan turbidite system, there values as high as 5% have been

recorded (Baudin et al., 2010). All sites, excluding the surficial sediment from site CE14009-005-450m of the Eastern branch, recorded TOC values > 0.5%, consequently exceeding the average organic content of open ocean marine sediments (Hedges and Keil, 1995). The lowest TOC% content was observed at site CE14009-005-450m, this site is characterized by the coarsest grain size observed across the canyon, which may explain the lowest TOC value noted. Generally, coarser-grained sediment increases oxygen exposure, penetration and thus oxidation of organic matter (Hedges and Keil, 1995) (See Chapter 5: Synthesis for interdisciplinary relationships). However, during the same dive event, at 681m, an enriched TOC signature of 1.33% was recorded, indicating that high organic matter may be more efficiently recycled at the shallower site and consequently not effectively buried.

The highest surficial TOC value of 2.32% was recorded within the Main Channel JC125-028-MC-3758m. A study of the Portuguese Nazaré Canyon recorded similar values of ~ 2% of organic carbon within canyon sediments (Masson et al., 2010a). At these depths, organic matter would likely have been subject to long degradation processes as it travelled through the water column. Therefore, rich eutrophic overlying waters, due to upwelling, is likely the reason for the enhanced TOC% content observed. Additionally, this indicates that the increased TOC content observed at this depth is a result of rapid sedimentation, transport and burial. Amaro et al. (2016a) suggested that an increase in TOC% content with depth may be explained by intermittent gravity flow events, whereby sediments rich with organic material are flushed down. While nonparametric testing found no correlation with depth and TOC% ($p < 0.05$). The highest average down core reading (2.38%) was observed within the Eastern Middle branch CE16006-022-PSH06-731.3, this could indicate high primary productivity in the overlying waters and the subsequent efficient burial of organic matter in

the seafloor sediments.

Higher macrofaunal abundance has been positively correlated with sedimentary total nitrogen, as increased total nitrogen values indicates better, more labile food quality (Cunha et al., 2011). Previously, Gunton et al. (2015) recorded significantly higher values of sedimentary total nitrogen in the Eastern branch, however One-Way ANOVA analysis showed no significant differences across branches or by water depth interval ($p > 0.5$). The average surficial and down core TN values across all sites were 0.11 ± 0.07 (*n* = 33) and 0.09 ± 0.04 (*n* = 33), respectively.

Bulk stable isotope values showed variation within and between branches (Table 4:4 and Figure 4:8). The average surficial value of $\delta^{13}C‰$ was -22.28‰ ± 2.25 (n = 22). Marine organic matter typically ranges between -20 to -22‰ (Meyers, 1994). This indicates that the carbon is likely derived from marine phytoplankton or zooplankton (Fry and Sherr, 1984; Petersen and Fry, 1987; Hayes, 1993; Meyers, 1994; Levin and Michener, 2002). While $\delta^{13}C$ values mainly range between -25 and -22.5‰, a heavier value was recorded at the connecting shelf of the Acesta and Eastern Middle branch CE16006-030-PSH12-511.37m (-12.76).

The average surficial and down core C/N ratios across all sites were 22.31 ± 15.60 (*n* = 33) and 23.55 ± 13.31 (n= 32), respectively. Amaro et al. (2015) recorded C/N ratios of 8.12 ± 1.23 and 8.80 ± 1.68 for the Western and Eastern branches. These lower ratios indicate organic matter of marine origin. Surficial C/N values between 3 and 10, indicating fresh algal organic matter rich in proteinaceous material, were observed to depths of >4000m (Meyers, 1994). Sites ranging from the upper slope to depths >4000m exhibited C/N values between 3 and 10 across the West, East and Main Channel. Therefore, it is possible that while there is

a marine contribution of organic matter, at extreme depths, this is subsequently recycled and degraded within the water column before depositing in the sediments (Meyers and Silliman, 1996). Lipid analyses undertaken by Huvenne et al. (2011) reported that phytoplankton or zooplankton derived docosahexaenoic acid (DHA) and eicosapentaenoic (EPA) acids were present in suspended particulate organic matter (SPOM) within the Eastern branch, which may provide the support that marine rich organic material is available within the Eastern branch. Several studies of marine sediments have shown increasing C/N ratios with increasing depth. Holm-Hansen et al. (1966) and Gordon (1971)) reported ratios close to the marine plankton signature in the upper few hundred meters of the water column, however, below 1000m the CN/N ratios were higher than 10, before increasing to values of around 15 in deeper sections. Within this study, high values >20 are observed down to depths of ~3500m. Due to the marine C/N signature and the distance from land, and unlikeliness of enhanced terrestrial input, high C/N ratios of organic matter, exported from the euphotic zone, is generally attributed to the preferential scavenging or nitrogen-rich compounds by bacteria. Thus, the high C/N ratios observed likely indicate extensively reworked and degraded material, removing much of the more labile N-containing organic matter (Müller, 1977; Kiriakoulakis et al., 2001, 2006). Wilson et al. (2015) recorded C/N ratios of 27 in the Eastern branch and suggested that this was because of trawl induced resuspension events, where the dilution of fresh rich organic material was mixed with degraded refractory material (Amaro et al., 2015). However, it remains unclear whether the differences are due to the modification of settling organic matter by benthic organisms or by dispersal of degraded organic matter from the shelf across the canyon.

The heaviest $\delta^{13}C$ signature of -12.76‰ was observed in the upper canyon, indicating

sulfide-oxidized carbon which is associated with the form II Rubisco pathway (Levin et al., 2001). Form II presents a low specificity factor, which is the measure of the ability of the enzyme to discriminate between CO_2 and O_2 at a given ratio. Thus, it is considered that form II is adapted to operate in low O_2 and high CO_2 surroundings (Badger and Bek, 2008; Tabita et al., 2008; Léniz et al., 2017). It is, therefore, possible, that this site is anoxic as a result of high primary productivity, low ventilation rates and high biological oxygen demand, due to high levels of organic matter respiration. At this site, grain size is characteristically silty with a mean down core grain size value of 37.11 ± 17.26µm, which could lead to low oxygen penetration. It is, therefore, possible, that the heavy isotopic value observed here is due to localised anoxic conditions, perhaps because of a pulse of organic matter being deposited in the area (See Chapter 5: Synthesis for interdisciplinary relationships). A study by Ingels et al. (2011) supports this theory, where it was suggested that the head of the canyon is oxygen-limited, creating possible sulphidic conditions.

The lighter $\delta^{13}C$ readings of -24 at the Explorer Canyon JC125-101-MC-664m and JC125-076-PSH02-861.2m, may indicate bacterial remineralisation of isotopically light mucus (~ -25‰ and -22‰) that is released into the water column by cold-water corals (Wild et al., 2008). This canyon is a marine conservation zone (MCZ), where cold-water corals exist, indicating that the isotopically light $\delta^{13}C$ values observed may indeed be because of a similar process occurring as observed by Wild et al. (2008) in the Australian Great Barrier Reef.

A study of ~2000 sites present the global $\delta^{15}N$‰ range of 2.5 to 16.6‰ for marine sediments. However, Tesdal et al. (2012) discovered that the majority of sites are positively skewed towards lower values of 4 and 6‰, highlighting the variability of marine sediments (Tesdal et al., 2012). Within this study, a mean $\delta^{15}N$ signature of 3.32‰ ± 0.84 falls just

below the deep-water average of ~5‰ value associated with internal cycling and assimilation by marine primary producers (Sigman and Casciotti, 2001). This is in line with previous research within the Whittard Canyon, where values of 4.09‰ ± 2.42 and 3.94‰ ± 0.67 for West and Eastern branches were recorded (Hunter et al., 2013a). All are below the oceanic deep water average, which may be a result of the lack of water column denitrification, previously recorded in the Atlantic ocean, or due to discrepancies in sampling techniques (Tesdal et al., 2012; Marconi et al., 2019). Low values, such 1.30‰ ± 0.48, recorded at the Westernmost site (JC125-083-PSH03-2740m) and 1.50‰ ± 1.94 at the Eastern Middle site (CE16006-030-PSH07-700m) may indicate deposited sediment where low fractionation has occurred, such as atmospheric nitrogen fixation by cyanobacteria in the surface waters (Sigman et al., 2000; Sigman and Casciotti, 2001; Sigman and Fripiat, 2019). Both sites were sampled within the summer season, and the reduced nitrogen signature may indicate the transition from nutrient-rich conditions, early in the phytoplankton bloom, to more oligotrophic conditions as the phytoplankton has ingested much of the fresh nitrogen (enriched in ^{15}N) and less nitrate is available. This may also result in marine phytoplankton utilizing recycled ammonia, which is typically depleted in ^{15}N— subsequently leading to low nitrogen isotopic values (Radke et al., 2017; Lu et al., 2020).

Oceanographic regimes observed by Huvenne et al. (2011) suggest that the Western branch receives less-frequent sedimentary inputs, therefore consequently less organic matter from the continental shelf. This may result in noticeable resource-limitation compared with other branches (Hunter et al., 2013a). Grain size characteristics support the observation of Huvenne et al. (2011) silty fine-grain sizes suggest a low energy depositional site (35.403µm ± 18.91). While fine-grained material may make oxygen penetration lower, the TOC value

here is the third-lowest observed (See Chapter 5: Synthesis for interdisciplinary relationships). Typically suboxic conditions are less efficient in breaking down organic matter, resulting in a corresponding increase in OC content (Winterer, 2012). However, this does not appear to be the case; thus, highlighting the complexity of the mechanisms occurring here.

Amaro et al. (2016) suggested that transport of labile OM, through gravity flows, is limited in the Whittard with fresh OM mainly arriving through vertical deposition and lateral transport of settling phytodetritus from phytoplankton blooms that occur during spring/summer. Hunter at al. (2013) found that macrofaunal assemblages differed across the Eastern and Western canyon branches. Furthermore, Amaro et al. (2016) found that foraminiferal abundance was higher in the upper parts of the canyon than the lower canyon, suggesting organic enrichment in the upper reaches of the canyon. This further highlights the complexity of the Whittard Canyon. However, questions remain on the small-scale spatial and temporal variability in these processes.

a) Upper slope 0-1000m

The largest range in biochemical parameters was observed in the upper slopes of the canyon (0 -1000m). Mean surficial and down core TOC values ranged between 0.33% - 2.26% and 0.71% - 2.38%, respectively. However, the largest percentage of TOC content down core of individual samples did exceed this. Within the Acesta branch, TOC peaked to 3.82% in the 3-4cm section (CE16006-033-PSH08-780m). Similarly, the Eastern Middle branch (CE16006-022-PSH06-731.38m) peaked to 3.78% down core at 1-2cm. The enriched organic carbon observed here may be due to increased sedimentation or burial (Amaro et al., 2016a). Due to it being characteristically out of the norm for the core profile, it may also

be due to an episodic event such as a gravity flow or another disturbance such as bioturbation; where an organism effectively subducts carbon from the surface sediment to deeper layers (Kiriakoulakis et al., 2004). Nepheloid layers have been observed within this branch, which may explain this enrichment (Wilson et al., 2015d; Daly et al., 2018) . Similar values have also been observed within the Angola basin; at the same bathymetric interval (0-1000), were TOC values were typically higher than 2%. This enrichment was attributed to coastal upwellings and lateral transport of organically enriched nepheloid layers that quickly deposit in the sediment (Inthorn et al., 2006; Baudin et al., 2017).

The lowest content of surficial TOC recorded (0.33%) at the Eastern branch (CE14009-005-450m) corresponded with the lowest surficial C/N value of 3.47, across all water depth intervals, and isotopic signatures of δ^{13}C ‰ -21.35‰ and δ^{15}N‰ 3.65‰. Low organic carbon content may be a result of increased internal cycling or low input. Amaro et al. (2016) suggested that at shallower sites (mainly < 600m) within the Eastern branch, there was a strong concentration of stained (living) foraminifera in the upper 0.5cm sediment layer, reflecting the shallow oxygen penetration depth associated with greater OM input. However, the permeable sandy material indicates an energetic regime and significant oxygen penetration, which may enhance remineralisation rates of TOC (Marchant et al., 2016; Ahmerkamp et al., 2017). This suggests that organisms are recycling TOC at this site. C/N ratios further support this. Where enhanced denitrification is expected when sediment is permeable, this does not appear to be the case. Instead, the nitrogen-rich C/N signature indicates that the organic matter is of marine origin and phytoplankton derived (Middelburg and Nieuwenhuize, 1998; Escobar-briones et al., 2009). While, it is also possible that nitrogen avoids being remineralized into the water column, by adsorption to the clay

surface, this is likely not the case in this instance as sediment from this site is characterized as fine sand with less than 5% of clay content present (Stevenson and Cheng, 1972; Suthhof et al., 2000). Stable isotopes provide further support that the organic matter is a consequence of phytoplankton or zooplankton contribution. Where $\delta^{13}C$ ‰ is -21.35‰, it is recognized that this is likely due to primary producers (Fry and Sherr, 1984; Levin and Michener, 2002).

The succeeding lowest TOC value does not display the same C/N relationship, as described previously. Instead, within the Eastern Middle branch (CE16006-030-PSH12-511.37m) where surficial TOC is 0.99 %, there is a high, carbon-rich, C/N ratio of 32.12 and isotopic values of $\delta^{13}C$ -12.76 ‰ and $\delta^{15}N$ 3.59 ‰. Due to distance from a terrestrial source, the high C/N value is indicative of the preferential loss of nitrogen-rich organic compounds, through degradation.

The lightest $\delta^{13}C$‰ value of -24.42‰ observed at the Explorer canyon (JC125-101-MC-664m) coincides with a carbon-rich C/N ratio of 18.12 and an organically enriched TOC value of 1.60%, higher than typical marine values of <0.5% (Archer et al., 2002; Emerson and Hedges, 2003). While the light carbon isotope is within the range for marine phytoplankton and zooplankton production (-25% to -15%), it may indicate bacterial remineralisation of isotopically light (~ -25‰ and -22‰) mucus that is released into the water column by cold-water corals (Rodelli et al., 1984; Wild et al., 2008). Vector ruggedness measurements, ROV observations and grain size statistics suggest a quiescent site with low rugosity, flat landscape and fine silty sediment 11.03 ± 4.52µm, which may preserve organic material more effectively. However, the high C/N ratio observed indicates that while the material is organically enriched, it is older and well degraded. As discussed earlier, the higher C/N ratio

of organic matter exported from the euphotic zone is generally attributed to the preferential scavenging of nitrogen-rich compounds by bacteria, indicating older reworked particles (Kiriakoulakis et al., 2006).

b) Mid canyon 1000-2000m

In the mid canyon water interval across all branches, surficial and down core TOC values range between 1.06% - 2.20% and 1.32% - 2.31%, respectively, indicating that all sites are relatively enriched in organic matter compared to the open ocean, where organic carbon content typically does not exceed 0.5% (Archer et al., 2002; Emerson and Hedges, 2003). Surficial and down core C/N values range between 9.17 - 57.99 and 10.22 - 51.51, highlighting large variability across branches. Fresh marine organic matter is generally believed to be ~6.6 which indicates that this organic matter is carbon-rich and nitrogen compounds have preferentially degraded (Kiriakoulakis et al., 2001; Burone et al., 2003; Escobar-briones et al., 2009; Sigman and Fripiat, 2019). Surficial isotopic signatures of $\delta^{13}C‰$ range between -23.07‰ and -20.99‰ and $\delta^{15}N‰$ range between 1.64‰ and 4.19‰. While $\delta^{13}C$ ‰ is typical of the marine environment (Meyers, 1994), lower $\delta^{15}N‰$ values indicate low fractionation occurring as discussed earlier.

c) Lower canyon > 2000m

Beyond 2000m, surficial and down core TOC values ranged between 1.10%- 2.32% and 0.70% - 2.08%. Surficial and down core C/N values ranged between 6.99 - 22.75 and 14.28 – 27.52, and isotopic signatures of $\delta^{13}C‰$ varied between -22.27‰ to -23.08‰, and $\delta^{15}N‰$ ranged between 1.30‰ - 3.98‰. The highest value of TOC (2.32%), across all water depth intervals, was detected at the Main channel (JC125-028-MC-3758m), suggesting an elevated

input of organic carbon to the site or improved burial (Masson et al., 2010a). Similarly, at similar depths within the Angola deep-sea fan, enrichment was observed at the abyssal depths and like the Whittard Canyon TOC values exceeding 2% were observed, relating to Congo turbidite deposits (Baudin et al., 2017). It is possible that the same thing is being observed within the JC125-028-MC-3758m because turbidite layers have been recorded at similar depths within the canyon (Zaragosi et al., 2006). A high C/N ratio of 22.75 is indicative of degraded organic carbon. At this depth, OM would likely have been reworked and recycled as it travelled through the water column before depositing; thus it may suggest that as it has survived this process, the remaining exposure to oxygenated pore water within the sediment is minimal (Masson et al., 2010b). While isotopic data was not available for this site, another main channel site (JC125-045-MC-3723m) detected high values of TOC% (2.29%) and isotopic signatures for δ^{13}C‰ and δ^{15}N‰ of -22.92‰ and 3.90‰, respectively, indicating phytoplankton and zooplankton derived carbon and internal cycling through assimilation (Michener and Kaufman, 2008; Sigman et al., 2010). The lightest nitrogen isotopic value of δ^{15}N 1.30‰ at the Western branch (JC125-083-PSH03-2740m) coincides with a nitrogen-rich C/N ratio of 7.71 and TOC value of 1.10%.

Through the biogeochemical analyses of deep-sea sediments through elemental and stable isotopes, insight into the quantity and quality of organic matter, reaching the ocean floor was expanded. While, One-way ANOVA on ranks analyses showed that there was no significant difference in biogeochemical parameters across branches or by water depth interval ($p > 0.05$), variability within branches and across canyon may be seen, suggesting that small-scale differences are important.

Chapter 5: Synthesis

While each chapter has attempted to describe variability across the canyon, relationships between geomorphological, sedimentological and biogeochemical parameters have yet to be investigated. This chapter will attempt to uncover relationships where they may exist through a series of multivariate statistical tests, providing further information on the processes that impact organic matter content across the canyon system.

5.1.1 Methods

For data preparation, please refer to Chapter 1. Methods.

I. *PCoA analysis*

Within Primer- E v7.0.13 software, principal coordinate analysis (PCoA), also known as multidimensional scaling, was undertaken to interpret the similarity, or dissimilarity of all geomorphological, sedimentological and biogeochemical parameters of surficial samples. The dataset was stripped back so that only sites that had a complete set of morphological, sedimentological and biogeochemical parameters would be assessed. Each parameter was assigned a location on a graphical plot, in a low-dimensional Euclidian space. The interpretation of a PCoA plot is as follows; objects located closer to one another are more similar than those located further away. Due to the resemblance measure being set to Euclidean distance, PCoA gives essentially the same results as principal component analysis (PCA). Pearson's correlation statistics were generated on the normalised data, and vectors of sedimentological and biogeochemical parameters were plotted if they returned a value <0.2.

Differences between the same variables across sample sites were examined using the non-

parametric Permutational Multivariate Analysis of Variance test (PERMANOVA) within Primer-E v7.0.13. PERMANOVA compares groups of variable and tests the hypothesis that the dispersion of the groups is equal for all groups. A rejection of the null hypothesis means that the spread of the variables is different across sample sites (Anderson et al., 2008). In other words, PERMANOVA analysis suggested that variable ranges differ across sample sites.

Splitting the data by water depth interval was done using the following rationale. Samples are placed in the following depth categories; 0-1000, 1000-2000 and >2000m. Depth intervals aim to separate the upper productive waters >1000m, the areas in which cold-water corals, such as *L.pertusa ,* may continue to persist >2000m and >2000m where nepheloid layers continue to occur but are a great distance from overlying productive waters. Amaro et al. (2015) found that foraminiferal assemblage composition on the adjacent slopes of the canyon changed according to these depth intervals, reflecting increasingly food-depleted conditions. This study aims to understand if the environmental parameters examined here follow similar trends.

One-way Analysis of Similarities (ANOSIM) was undertaken using Primer-E v7.0.13 on normalised data using the Euclidian distance matrix in order to determine the similarity of each variable across sites.

II. *DIVA data analysis*

While this study has an unprecedented amount of sampling sites, the Whittard canyon is vast and heterogeneous in nature. Thus, there is still likely to be under-sampling of the canyon variability. However, the sophisticated analysis tool Data Interpolating Variational

Analysis (DIVA) has been developed to optimize the use of limited in-situ data points. DIVA aims to estimate a continuous spatial field, of a given environmental or biological variable, from a discrete set of measurements, considering margin of errors attached to these measurements (Barth et al., 2016). DIVA uses a finite-element method to solve the variational principle, considering the following;

- The distance between analysis and data (observation constraint).
- The regularity of the analysis (smoothness constraint).
- The physical laws (behaviour constraint).

In comparison to standard optimal interpolation (OI), DIVA considers uncertainties on observations and when applied to ocean data, considers coastlines, sub-basins and advection because of its variational formulation on the real domain. Additionally, the numerical cost is not dependent on the number of data points, but instead on the number of degrees of freedom, relating to the size of the finite-element mesh model (Troupin et al., 2012). Sedimentological and biogeochemical data were plotted to predict spatial variability across the canyon extent according to the method by Troupin et al. (2012). Automatic scale lengths were used for the gridded field, and bad estimates were hidden according to a quality limit of 3.0. All ODV gridding methods assign for every estimate, at a given grid point (x, y), a dimensionless quality value. These values are based on the distances from the estimation point, measure in units of respective averaging scale lengths) of all the data points used for the estimate. A quality value larger than 3.0 indicates that the nearest measurement is more than two length-scales away from the estimation point, as such they are typically considered to be problematic. The domain selection map used was GEBCO

2014 30 X 30 sec. Nonlinear scaling was applied to visualize data effectively.

Gridded field DIVA interpolation maps indicate the spatial coverage of surficial sedimentological and biogeochemical values, highlighting hotspots. However, while this method of interpolation is useful when there are sparse data points, it must be noted that small scale or extreme features in the data may be altered or lost as a consequence of the gridding procedure (Schlitzer, 2011).

5.1.2 Results

I. *Multivariate PCoA*

PCoA analysis of surficial samples across the Whittard canyon. PC1 (33.3%) and PC2 (20.1%) account for 53.4% of the variation in environmental parameters between samples (Figure 5:1) The majority of samples group along the positive loading of PCO1 are driven by silt, and to a lesser degree, clay, $\delta^{15}N$, water depth, kurtosis and IC. However, there is a cluster of three sites that are negatively loaded along PC01, co-variances of sorting and skewness drive these, and to a lesser degree TN. The Western site (JC125-083-PSH03-2740m) varies from all sampled sites, while it is negatively loaded along PC01, it is positively loaded along PC02 and is driven by skewness S_{KG}. The Eastern branch reflects the largest variation in drivers of all the branches, with each site influenced by varying positive and negative loads of PC01 and PC02.

There is an apparent fluctuation in Acesta branch samples, with site CE16006-033-PSH08-780m negatively loaded. However, there is a cluster of two sites CE14009-009-1130m and CE14009-027-2816m loaded along site PC01, indicating the same drivers at these two sites. The Explorer branch also shows some variability, with site JC125-076-PSH02-861.2m

negatively loaded along PC01. However, the Eastern branch shows the most significant variability, with site CE14009-005-450m extremely positively loaded along PC02 and both negative and positive loadings for PCO1 observed at sites CE14009-005-681m and JC125-109-PSH05-570.5m. C/N and VRM appear to have a lower effect on all sites; however, weak correlations exist according to Pearson's statistic (>0.2).

The PCoA plot highlights correlations between variables. Positive correlations are observed between water depth, clay and silt content, and $\delta^{15}N$. Grain size µm and TOC are negatively correlated, as is silt, clay, $\delta^{15}N$, and water depth with sand. TOC is also negatively correlated with $\delta^{13}C$ and to a lesser degree sand content.

Sites tend to cluster towards the positive loading of PC01; however, the Acesta site CE16006-033-PSH08-780m is an exception and is driven by negative loading along PC01, indicating that skewness, sorting and TN are the main driving factors.

II. *PERMANOVA*

PERMANOVA testing showed no significant permutations (p = 0.598) between water depth interval where samples are placed in the following depth categories; 0-1000, 1000-2000 and >2000m. Depth intervals aim to separate the upper productive waters >1000m, the areas in which cold-water corals, such as *L.pertusa,* may continue to persist >2000m where nepheloid layers continue to occur but are a great distance from overlying productive waters. Additionally, there was no significant differences when samples were separated by branch (p = 0.135), North versus South (p = 0.58), or West versus East (p = 0.558) (for rationale please see Chapter 5.1.1 Methods).

III. *ANOSIM*

One-way ANOSIM testing for similarity highlighted the high similarity between variables across branches (R = 0.144), water depth interval (R = 0.104), North Versus South (R = 0.038) and West Versus East (R = 0.018).

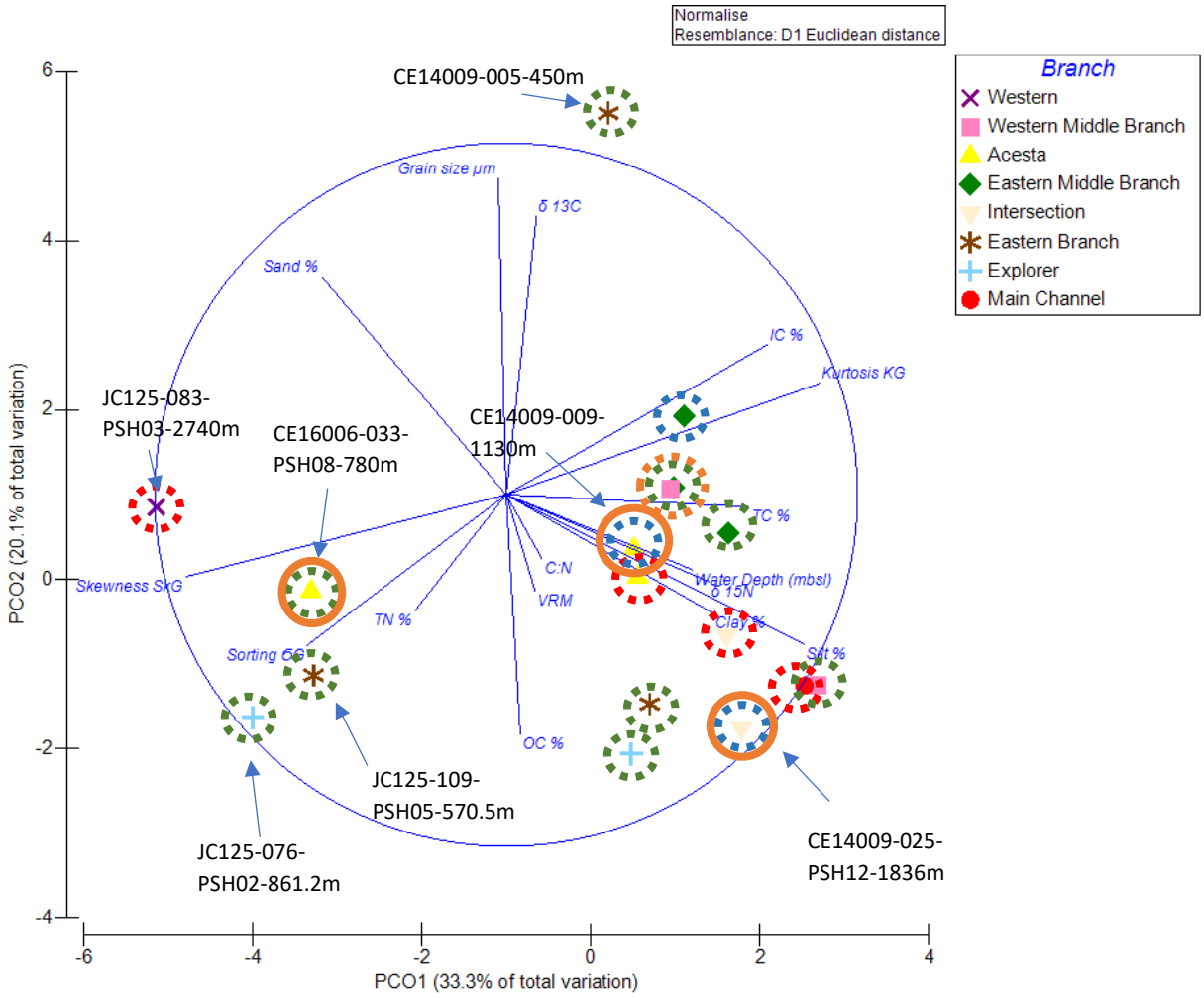

Figure 5:1 PCoA analysis of surficial samples across the Whittard canyon. PC1 (33.3%) and PC2 (20.1%) account for 53.4% of the variation in environmental parameters between samples. Environmental parameters with Pearson correlation of >0.2 are overlaid in blue with blue lines indicating eigenvector weighting of each parameter. Coloured symbols indicate samples. Samples that are clustered together indicate that they are driven by the co-variance of overlain environmental parameters (blue text). Dotted circles indicate water depth interval, where green is 0-1000m, blue is 1000-2000m and red is >2000m. Full orange circles indicate areas where enhanced nepheloid layers have been recorded. Dashed orange circles indicate dilute nepheloid layers (Wilson et al., 2015).

IV. *Relationships*

a) Spearman's rank correlation

Spearman's rank correlation was undertaken on non-parametric data to investigate relationships between geomorphological, sedimentological and biogeochemical data.

b) Surficial grain size

A moderate negative correlation was observed between surficial grain size and surficial OC (rs [33] =-0.408, p = 0.018). Furthermore, a strong positive correlation between $\delta^{13}C$ and surficial grain size was reported (rs [48] = 0.752, p = 0.000). Surficial grain size and depth presented a moderate negative correlation (rs [48] = -0.322, p = 0.029).

c) Skewness

Down core skewness positively correlated with down core IC (rs [48] = 0.338, p = 0.041).

d) Surficial total nitrogen

A strong negative correlation was reported between surficial TN and surficial C: N (rs [48] = -0.859, p = 0.000). A moderate negative correlation was reported between surficial TN and surficial IC (rs [30] = 0.446, p = 0.014).

A cross plot of nitrogen and carbon suggests that nitrogen may be preferentially degraded or trapped inorganic nitrogen could be present (see appendix 1).

e) AVG $\delta^{13}C$

Positive correlations were observed between $\delta^{13}C$ and surficial and down core grain size (rs [48] = 0.729, p = 0.000) and (rs [48] = 0.517, p = 0.009).

V. *DIVA interpolation*

a) Surficial sedimentological interpolation

DIVA interpolation plots of sedimentary parameters indicate that the upper canyon and Eastern Middle 2 branch is characterized by coarser grain sands, with finer material generally observed with increasing depth. While most of the sediments appear poorly sorted across the canyon, a hotspot of very poorly sorted material is indicated within the Explorer canyon. Near symmetrical mesokurtic sediments are hotspots throughout the central and western branches. Kurtosis values are typically lower within the central canyon (Figure 5:2).

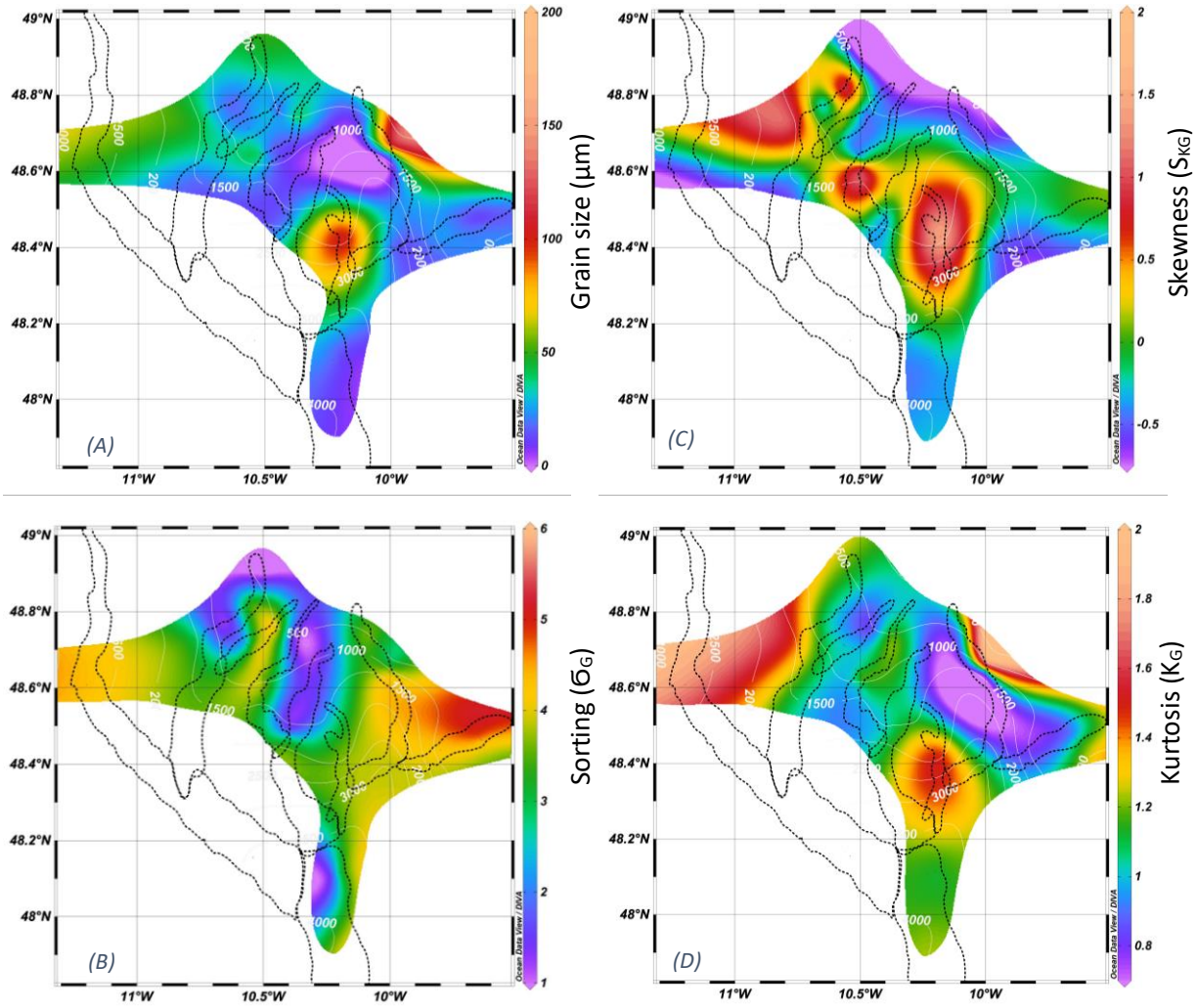

Figure 5:2 (A) Grain size (µm) (B) sorting (σ_G) (C) skewness (S_{KG}) and (D) kurtosis (K_G) for all surficial sediment samples across the Whittard canyon. Interpolations were produced in ODV 4.7.4 using Data Interpolating Variational Analysis (DIVA) gridding software according to the method by Troupin et al. 2012.

b) Surficial biogeochemical interpolation

DIVA interpolation reveals hotpots of enriched TOC at all water depths intervals of the canyon. The highest C/N ratio observed are within the Eastern branches. A hotspot of increased $\delta^{13}C$ values is seen between the Acesta and Eastern Middle branch, and $\delta^{15}N$ is lowest at the West of the canyon and within the Eastern middle 2 branches (Figure 5:3).

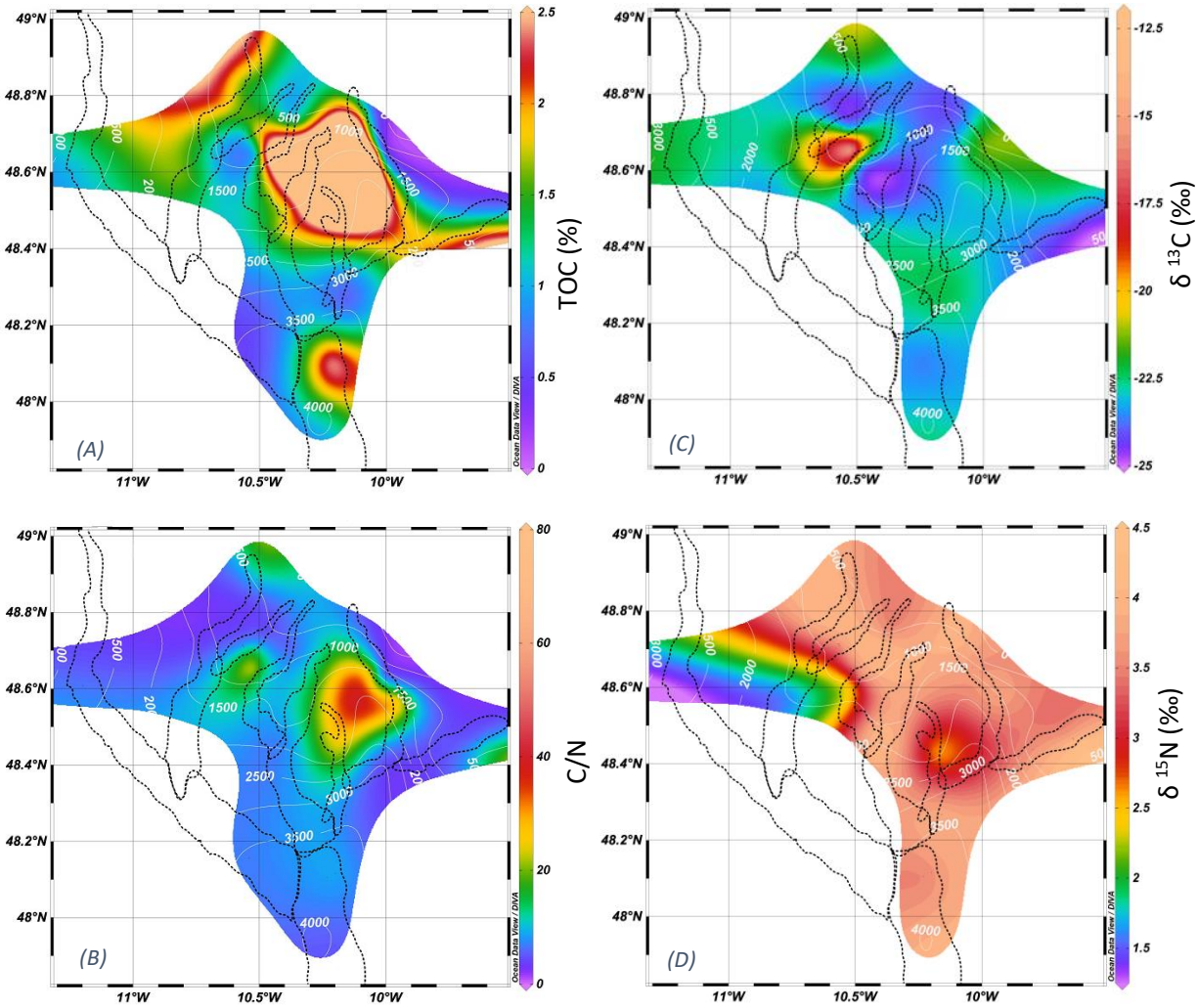

Figure 5:3 (A) TOC (%) (B) C/N (C) δ ^{13}C (‰) and (D) δ ^{15}N (‰) for all surficial sediment samples across the Whittard canyon. Interpolations were produced in ODV 4.7.4 using Data Interpolating Variational Analysis (DIVA) gridding software according to the method by Troupin et al. 2012.

5.1.3 Discussion

The highly varied morphology, sedimentology and biogeochemistry of the canyon is supported by PCoA analysis (Figure 5:1), which suggests that the number of environmental or chemical parameters may be driving the differences observed. However, just 53.4% of the variation is explained by PC01 and PC02, meaning that almost half of the variation is not described by principal coordinates analysis.

While some sites are influenced to greater degrees by differing variables, one-way ANOSIM testing for similarity, highlighted the high similarity of sedimentological and biogeochemical variables across groups; where an R-value close to 1.0 means dissimilarity between groups, and a value closer to 0 suggests an even distribution of high and low ranks between groups. R values between variables and groups are as follows; branches (R = 0.144), water depth interval (R = 0.104), North Versus South (R = 0.038) and West Versus East (R = 0.018). Additionally, when separated by water level, PERMANOVA testing showed no significant permutations, where the *P*-value is more than 0.05 (p = 0.598). Likewise, there were no significant differences when samples were divided by branch (p = 0.135), North versus South (p = 0.58), or West versus East (p = 0.558). However, this may be due to the grouping strategy, where differences may be lost due to the grouping procedure.

PCoA analysis displays clustering of sites, indicating similar processes occurring. Others are plotted independently such as the Acesta, Eastern and Explorer branches. The Eastern branch site CE14009-005-450m is unlike any other site recorded, where high sand content and grain size are the main drivers (positive PCO2). This suggests that while sedimentological and biogeochemical parameters may not differ a great deal when separated by water interval (0, 1000, >2000m). Across the canyon, individual sites are driven

by each parameter to a varying degree, indicating within branch and canyon patchiness.

The Eastern branch reflects the largest variation in drivers of all the branches, with each site influenced by varying PC01 and PC02 loads. This suggests that this branch is highly variable, further supported by the broad range of sedimentological and biogeochemical values recorded: wide-ranging VRM values and photographs support this (see Chapter 2). Steep bedded walls with dense coral, vertical chalky cliffs with stepped edges and overhangs, and flatter sandier areas are observed across the Eastern branch. Existing internal tide data has highlighted the high baroclinic energy generated southeast of the canyon along the Celtic shelf break. It is recognized that the Eastern branch is the focal point for this energy, with steep topography, driving higher energy fluxes within this branch than elsewhere in the canyon (Aslam et al., 2018). The increased energy may enable the transport and deposition of coarser material that is observed within this branch. End-member analysis further supports this, where a peak of coarse fraction, not seen in samples other than the Eastern Middle 2 branch, is recorded. This coarse fraction continues down to 9 cm, indicating the ongoing transport of shelf-derived coarse sediment to this site.

It has been suggested that the heterogeneity observed within the Eastern branch may be responsible for the increased total benthic polychaeta species richness recorded (Gunton et al., 2015). Many of these species have been described as opportunistic, benefitting from areas of high disturbance, and are not observed in as high numbers within other canyon branches (Paterson et al., 2011; Gunton et al., 2015).

Spearman's correlations between depth and surficial grain size presented a significant negative correlation. In other words, overall, the grain size reduces with increasing depth. PCoA statistics support this further. When normalised, Pearson's correlation testing

indicated a weak positive correlation between water depth, clay and silt content—suggesting that with increased depth, coarse material tends to deplete. However, fine sand at the Eastern Middle 2 site CE16006-056-PSH05-1845m (187.67µm) is observed at 1845 m, indicating a complex picture, where ongoing shelf derived coarse lithogenic material may contribute to the sediment component down to increased depth along the Western and Eastern Middle branches. While TIC and $CaCO_3$ values may loosely indicate the lithogenic fraction, a biogenic element may exist too, therefore this study cannot confirm this. While, some studies have found that coarse sediments dominate the upper canyon, and the lower canyon is predominantly covered in finer material, some research has reported vertical alterations in lithogenic fine sand and more carbonate-rich hemipelagic ooze, and have attributed this to episodic gravity flows within the canyon (Duros et al., 2011; Hunter et al., 2013b; Amaro et al., 2015).

PCoA analysis suggests that grain size and TOC are negatively correlated, as is silt, clay, $\delta^{15}N$, C/N and water depth with sand. In other words, as grain size increases, TOC, silt, clay, $\delta^{15}N$ and C/N decreases. This is supported by previous work, which suggests that where sediment is coarser, TOC is efficiently winnowed, lost, or remineralised quicker (Dauwe and Middelburg, 1998; Martín et al., 2014). This effect may be observed within the Eastern branch site (CE14009-005-450m), where the coarsest grain size fraction is recorded throughout the core profile, and the TOC is the lowest recorded in this study. Additionally, the $\delta^{15}N$ decreasing trend, as grain size increases, may be due to the residence time of the material in the water column. Large, fast-sinking particles are more likely to have a lower residence time than slow sinking fine particles. This results in increased oxygen exposure, a higher rate of microbial alteration, and the subsequent increase in $\delta^{15}N$, as the organic

matter decomposes and subsequently ^{15}N – depleted dissolved nitrogen is released (Altabet and Francois, 1994; Mintenbeck et al., 2007; Montes et al., 2013). PCoA analysis showed a strong inverse correlation between sediment grain size and C/N ratio. Furthermore, lower nitrogen levels associated with coarse particles may explain the increase in C/N (Figure 5:1) (Keil et al., 1994; Lesen, 2006).

Discrete measurements of organic enrichment levels have been recorded in the upper, middle and lower canyon, indicating that organic depocenters are seen at all bathymetric levels (Figure 4:3C). Typically, in the open ocean, as organic matter settles through the water column, it is almost entirely degraded back to dissolved chemicals and less than 1% of TOC reaches the seafloor (Archer et al., 2002; Emerson and Hedges, 2003). However, a significant enrichment in TOC is noted between 500-1000 m. At this bathymetric level, 6% of the study sites (33 data points) exhibited TOC values above 2%. Another enrichment was observed between 1000 and 2000m, here 9% of sites sampled presented TOC values above 2%. Below 2000 metres, TOC content decreases. A third enrichment was seen between 3000 and 4000m. Values as high as 2.08 % were observed, at a depth of 3723m (JC125-045-MC-3723m) This suggests that while depth is not the main factor in which controls TOC enrichment within the canyon, processes occurring within the canyon determine TOC content. Similar pulses of enriched organic matter have been observed within the West African Congo fan, where TOC values exceeding 3.5% were also recorded at abyssal depths (< 4000m). This has been attributed to the organically enriched Congo turbidite system, high sedimentation rates, and the high proportion of clay sediments that is prone to adsorption of organic matter (Savoye et al., 2009). Likewise, turbidite deposits have been documented within the deeper sections of the Whittard Canyon. However silt continues to dominate, so

it is possible that a reduced effect is being observed within the Whittard Canyon due to lower organic carbon adsorption (Zaragosi et al., 2006; Amaro et al., 2015). Sedimentary gravity flow events have been recorded at depths of ~4000m in the canyon, punctuated by increases in bottom water turbidity along with a strong increase in sediment deposition (Amaro et al., 2015). It is, therefore, possible that the organically enriched sediment observed at depth is a result of high sedimentation events, subsequently reducing the oxygen exposure of organic matter, such as has been observed at the Nazaré Canyon (Kiriakoulakis et al., 2011). Another explanation for the enrichment where the branches merge within the main channel may be due to the accumulation of organic matter transported by multiple canyon branches. This process has been suggested within the Barkley Canyon (NE Pacific), where organic carbon enrichments were also seen at depth (Campanyà-Llovet et al., 2018).

Surficial TOC is negatively correlated with surficial $\delta^{13}C$; in other words, increased TOC content leads to a decreased $\delta^{13}C$ value. A possible explanation for the changes in stable isotope values is that depleted $\delta^{13}C$ values may be due to the preferential removal of an organic fraction (carbohydrates and proteins) enriched in ^{13}C and ^{15}N; Whereby increased $\delta^{13}C$ and $\delta^{15}N$ values may be explained by the selective loss of organic matter components (lipids) depleted in ^{13}C and ^{15}N (Macko and Estep, 1984; Altabet, 1988; Montoya and Mccarthy, 1995; Altabet et al., 1999; Khim et al., 2018).

Where sites cluster towards the positive loading of PC01, enhanced nepheloid layers (ENLs) have been documented (Intersection branch CE14009-025-PSH12-1836m, Acesta branch CE14009-009-1130m) (Wilson et al., 2015d). The main drivers at these two sites, according to the PCoA plot, are the proportion of clay and silt content, water depth, $\delta^{15}N$, and to a

lesser degree TOC, VRM and C/N ratio. Wilson et al. (2015) established that the most turbid ENLs are present within the steeper mid-lower canyon branches, where dilute ENLs were present in the softer sloping upper reaches. While fishing is restricted to the smooth spurs, the steeper morphology of the canyon walls is believed to cause a large driving force and thus propagate more material, resulting in the more turbid ENLs observed here (Martín et al., 2014). While it is not confirmed that the sediment analysed here has been deposited from previous nepheloid occurrences, the raised $\delta^{15}N$ and TOC values in sedimentary material at sites were known ENLs had occurred a year prior (CE13008) may indicate deposition from these earlier events. Where, high TOC and high $\delta^{15}N$, suggest quickly transported organic-rich material from the upper reaches (Puig and Palanques, 1998; Sigman and Casciotti, 2001).

Furthermore, where an ENL is observed along the negative loading of PCO1, the increased TN content may be a signature of nitrogen-rich sedimentary material, transported rapidly within the nepheloid layer from overlying productive waters, subsequently escaping much of the remineralization and oxidation that would be expected with depth (Stein, 1990; Wakeham, 2002; Arzola et al., 2008). However, a contrasting effect has also been recorded, demonstrating the complexity of the system. Instead, molar C/N ratios of suspended organic matter exhibit high carbon, nitrogen-poor values, indicating the resuspension of well degraded superficial sediment and lithogenic material from the upper canyon (Wilson et al., 2015b).

5.2 Overall conclusions

Each discipline sought to determine if the canyon was homogenous throughout and to compare it to typical deep-sea values. Overall, geomorphological, sedimentological and biochemical analyses indicated that while most branches do not differ significantly from one another, some branches are more intervariable than others, and there is a divergence from typical oceanic values.

All disciplines agreed that the Eastern branch was notably different from the other branches, where the greatest range of parameters was observed for vector ruggedness measurements, grain size and total organic carbon- supporting and complementing previous findings. Amaro at al. (2015) indicated that megafauna and macrofauna were higher in the Eastern branch than the slope or western branches. Likewise, Gunton et al. (2015) highlighted the dissimilarity of the Eastern branches with the rest of the canyon, reporting that macrofaunal abundance was higher within this branch. These faunal patterns have been attributed to organic enrichment, different substrates, along with complex hydrodynamic activity and energy fluxes, that is influenced by the Eastern branch's complex topography and tidal regime. However, it remains unclear what the primary driver of these patterns are.

5.3 Further work

Though slope and vector ruggedness measures have improved the understanding of the context of each site, there is a limitation to how useful this information is alone. It does not provide insight into whether the site is an area of deposition or erosion. However, the use of Fine Bathymetric Positioning Indexing (FBPI) has been successfully applied by Campanyà-

Llovet et al. (2018) to determine convex or concave seafloor areas and, thus, areas of accumulation versus areas of resuspension. Indeed, the study by Campanyà-Llovet et al. (2018) found that the FBPI value was one of the main drivers of organic matter within the Barkley Canyon.

Although particle size analysis has provided some useful descriptives of the types of sediment available within the canyon, it has not quantified the lithogenic or biogenic fraction. As deep-sea sediments represent the largest carbon sink on Earth, it is important to understand what material is reaching the seafloor (Dutkiewicz et al., 2016).

Though it can be assumed that fluctuating sedimentological and biogeochemical values down core represent processes changing in time, without sedimentological rates it is not possible to determine if these changes were a result of seasonality, short-term disturbance events or representative of much longer-scale processes. Therefore, it is not possible to determine carbon rates. Carbon burial rates may help determine if the canyon is an efficient reservoir for carbon and to compare it with typical deep-ocean settings.

While there appears to be a connection between within-branch heterogeneity and biodiversity and abundance, this study cannot draw firm conclusions as to what the main casual factors are. Although total organic carbon has been useful in describing food quantity, C/N ratios have indicated organic matter origin (terrestrial or marine) and bulk stable isotopes have provided insight into the source and degradation state of organic matter, future lipid analysis would provide invaluable information about the origin and nutritional value of organic matter (Kiriakoulakis et al., 2005; Parrish, 2013). Within lipids, certain fatty acids (FAs), polyunsaturated fatty acids (PUFAs), and sterols are considered important drivers of ecosystem health and stability (Arts et al., 2001; Arts et al., 2009).

While fatty acids are a minor component of the organic matter in sediments, they provide the densest form of energy, yielding at least two-thirds more energy per gram than proteins or carbohydrates (Parrish, 2013). They can act as diagnostic indices (biomarkers), providing crucial information on the organic matter/carbon sources in the overlying ocean, trophic linkages, and diagenetic processes. Despite their importance, they remain the least well-understood nutrients for aquatic fauna, despite their role as essential nutrients (Parrish, 2013).

REFERENCES

Aberle, N. and Witte, U., (2003) Deep-sea macrofauna exposed to a simulated sedimentation event in the abyssal NE Atlantic: In situ pulse-chase experiments using 13C-labelled phytodetritus. *Marine Ecology Progress Series*, 251, pp.37–47.

Agrawal, Y.C., McCave, I.N. and Riley, J.B., (2010) Laser diffraction size analysis. In: *Principles, methods, and application of particle size analysis*. pp.119–128.

Ahmerkamp, S., Winter, C., Krämer, K., Beer, D. de, Janssen, F., Friedrich, J., Kuypers, M.M.M. and Holtappels, M., (2017) Regulation of benthic oxygen fluxes in permeable sediments of the coastal ocean. *Limnology and Oceanography*.

Alfaro, A.C., Thomas, F., Sergent, L. and Duxbury, M., (2006) Identification of trophic interactions within an estuarine food web (northern New Zealand) using fatty acid biomarkers and stable isotopes. *Estuarine, Coastal and Shelf Science*.

Allen, S.E. and Hickey, B.M., (2010) Dynamics of advection-driven upwelling over a shelf break submarine canyon. *Journal of Geophysical Research: Oceans*, 1158.

Altabet, M.A., (1988) Variations in nitrogen isotopic composition between sinking and suspended particles: implications for nitrogen cycling and particle transformation in the open ocean. *Deep Sea Research Part A, Oceanographic Research Papers*.

Altabet, M.A. and Francois, R., (1994) Sedimentary nitrogen isotopic ratio as a recorder for surface ocean nitrate utilization. *Global Biogeochemical Cycles*.

Altabet, M.A., Pilskaln, C., Thunell, R., Pride, C., Sigman, D., Chavez, F. and Francois, R., (1999) The nitrogen isotope biogeochemistry of sinking particles from the margin of the eastern North Pacific. *Deep-Sea Research Part I: Oceanographic Research Papers*.

Amaro, T., Huvenne, V.A.I., Allcock, A.L., Aslam, T., Davies, J.S., Danovaro, R., De Stigter, H.C., Duineveld, G.C.A., Gambi, C., Gooday, A.J., Gunton, L.M., Hall, R., Howell, K.L., Ingels, J., Kiriakoulakis, K., Kershaw, C.E., Lavaleye, M.S.S., Robert, K., Stewart, H., Van Rooij, D., White, M. and Wilson, A.M., (2016a) *The Whittard Canyon – A case study of submarine canyon processes*. *Progress in Oceanography*, .

Amaro, T., Huvenne, V.A.I., Allcock, A.L., Aslam, T., Davies, J.S., Danovaro, R., De Stigter, H.C., Duineveld, G.C.A., Gambi, C., Gooday, A.J., Gunton, L.M., Hall, R., Howell, K.L., Ingels, J., Kiriakoulakis, K., Kershaw, C.E., Lavaleye, M.S.S., Robert, K., Stewart, H., Van Rooij, D., White, M. and Wilson, A.M., (2016b) The Whittard Canyon – A case study of submarine canyon processes. *Progress in Oceanography*, [online] 146, pp.38–57. Available at: http://www.sciencedirect.com/science/article/pii/S0079661115300549 [Accessed 28 Apr. 2017].

Amaro, T., de Stigter, H., Lavaleye, M. and Duineveld, G., (2015) Organic matter enrichment in the Whittard Channel; its origin and possible effects on benthic megafauna. *Deep Sea Research Part I: Oceanographic Research Papers*, [online] 102, pp.90–100. Available at: http://linkinghub.elsevier.com/retrieve/pii/S0967063715000886.

Anderson, M.J., Gorley, R.N. and Clarke, K.R., (2008) PERMANOVA+ for PRIMER: Guide to Software and Statistical Methods. In: *Plymouth, UK*. pp.1–214.

Archer, D.E., Morford, J.L. and Emerson, S.R., (2002) A model of suboxic sedimentary diagenesis suitable for automatic tuning and gridded global domains. *Global Biogeochemical Cycles*.

Armstrong, R.A., Lee, C., Hedges, J.I., Honjo, S. and Wakeham, S.G., (2001) A new, mechanistic model for organic carbon fluxes in the ocean based on the quantitative association of POC with ballast minerals. *Deep-Sea Research Part II: Topical Studies in Oceanography*, 491–3, pp.219–236.

Arzola, R.G., Wynn, R.B., Lastras, G., Masson, D.G. and Weaver, P.P.E., (2008) Sedimentary features and processes in the Nazar?? and Set??bal submarine canyons, west Iberian margin. *Marine Geology*, 2501–2, pp.64–88.

Aslam, T., Hall, R.A. and Dye, S.R., (2018) Internal tides in a dendritic submarine canyon. *Progress in Oceanography*.

Badger, M.R. and Bek, E.J., (2008) Multiple Rubisco forms in proteobacteria: Their functional significance in relation to CO2 acquisition by the CBB cycle. In: *Journal of Experimental Botany*.

Barth, A., Watelet, S., Troupin, C., Alvera-Azcárate, A. and Beckers, J.-M., (2016) Analysis of Ocean in Situ Observations and Web-Based Visualization.

Baudin, F., Martinez, P., Dennielou, B., Charlier, K., Marsset, T., Droz, L. and Rabouille, C., (2017) Organic carbon accumulation in modern sediments of the Angola basin influenced by the Congo deep-sea fan. *Deep-Sea Research Part II: Topical Studies in Oceanography*.

Benn, A.R., Weaver, P.P., Billet, D.S.M., van den Hove, S., Murdock, A.P., Doneghan, G.B. and le Bas, T., (2010) Human activities on the deep seafloor in the North East Atlantic: An assessment of spatial extent. *PLoS ONE*, 59, pp.1–15.

Bergamaschi, B. a., Tsamakis, E., Keil, R.G., Eglinton, T.I., Montluçon, D.B. and Hedges, J.I., (1997) The effect of grain size and surface area on organic matter, lignin and carbohydrate concentration, and molecular compositions in Peru Margin sediments. *Geochimica et Cosmochimica Acta*, 616, pp.1247–1260.

Berner, R.A., (1982) Burial of organic carbon and pyrite sulfur in the modern ocean: Its geochemical and environmental significance. *American Journal of Science*, 2824, pp.451–473.

Bickert, T., (2009) Carbonate Compensation Depth. In: V. Gornitz, ed., *Encyclopedia of Paleoclimatology and Ancient Environments*. [online] Dordrecht: Springer Netherlands, pp.136–138. Available at: https://doi.org/10.1007/978-1-4020-4411-3_33.

Blott, S.J., Croft, D.J., Pye, K., Saye, S.E. and Wilson, H.E., (2004) Particle size analysis by laser diffraction. *Geological Society Special Publication*, 232, pp.63–73.

Blott, S.J. and Pye, K., (1986) Gradistat a Grain Size Distribution and statistics. *Developments in Water Science*, 26C, pp.1237–1248.

Blott, S.J. and Pye, K., (2001) Gradistat: A grain size distribution and statistics package for the analysis of unconsolidated sediments. *Earth Surface Processes and Landforms*, 2611, pp.1237–1248.

Bosley, K.L., Lavelle, J.W., Brodeur, R.D., Wakefield, W.W., Emmett, R.L., Baker, E.T. and Rehmke, K.M., (2004) Biological and physical processes in and around Astoria submarine Canyon, Oregon, USA. In: *Journal of Marine Systems*. pp.21–37.

Bourillet, J.F., Reynaud, J.Y., Baltzer, A. and Zaragosi, S., (2003) The 'Fleuve Manche': The submarine sedimentary features from the outer shelf to the deep-sea fans. *Journal of Quaternary Science*, 183–4, pp.261–282.

Bourillet, J.F., Zaragosi, S. and Mulder, T., (2006) The French Atlantic margin and deep-sea submarine systems. *Geo-Marine Letters*, 266, pp.311–315.

Boyd, P.W., Claustre, H., Levy, M., Siegel, D.A. and Weber, T., (2019) *Multi-faceted particle pumps*

drive carbon sequestration in the ocean. *Nature*, .

Broecker, W.S., (1982) Ocean chemistry during glacial time. *Geochim. Cosmochim. Acta*, 46, pp.1689–1705.

Broecker, W.S., (2003) The Oceanic CaCO3 Cycle. In: *Treatise on Geochemistry*.

Burone, L., Muniz, P., Pires-Vanin, A.M.S. and Rodrigues, M., (2003) Spatial distribution of organic matter in the surface sediments of Ubatuba Bay (Southeastern - Brazil). *Anais da Academia Brasileira de Ciencias*.

Burrough, P. a and McDonnell, R. a, (1998) Principles of Geographical Information Systems. *Economic Geography*, [online] 754, p.422. Available at: http://www.jstor.org/stable/144481?origin=crossref.

Calvert, S.E. and Fontugne, M.R., (1987) Stable carbon isotopic evidence for the marine origin of the organic matter in the holocene black sea sapropel. *Chemical Geology: Isotope Geoscience Section*, 663–4, pp.315–322.

Campanyà-Llovet, N., Snelgrove, P.V.R. and De Leo, F.C., (2018) Food quantity and quality in Barkley Canyon (NE Pacific) and its influence on macroinfaunal community structure. *Progress in Oceanography*. [online] Available at: https://www.sciencedirect.com/science/article/pii/S0079661117301842 [Accessed 14 May 2018].

Canals, M., Danovaro, R., Heussner, S., Lykousis, V., Puig, P., Trincardi, F., Calafat, A., Durrieu de Madron, X. and Palanques, A., (2009) Cascades in Mediterranean Submarine Grand Canyons. *Oceanography*, 221, pp.26–43.

Canfield, D.E., (1994) Factors Influencing Organic-Carbon Preservation in Marine- Sediments. *Chemical Geology*, 1143–4, pp.315–329.

Carpenter, E.J. and Capone, D.G., (2008) Nitrogen Fixation in the Marine Environment. In: *Nitrogen in the Marine Environment*. pp.141–198.

Cartapanis, O., Galbraith, E.D., Bianchi, D. and Jaccard, S.L., (2018) Carbon burial in deep-sea sediment and implications for oceanic inventories of carbon and alkalinity over the last glacial cycle. *Climate of the Past*, 1411, pp.1819–1850.

Carter, G.D.O., Huvenne, V.A.I., Gales, J.A., Lo Iacono, C., Marsh, L., Ougier-Simonin, A., Robert, K. and Wynn, R.B., (2018) Ongoing evolution of submarine canyon rockwalls; examples from the Whittard Canyon, Celtic Margin (NE Atlantic). *Progress in Oceanography*, 169, pp.79–88.

Catubig, N.R., Archer, D.E., Francois, R., DeMenocal, P., Howard, W. and Yu, E.F., (1998) Global deep-sea burial rate of calcium carbonate during the Last Glacial Maximum. *Paleoceanography*, 133, pp.298–310.

Cheetham, M.D., Keene, A.F., Bush, R.T., Sullivan, L.A. and Erskine, W.D., (2008) A comparison of grain-size analysis methods for sand-dominated fluvial sediments. *Sedimentology*, 556, pp.1905–1913.

Chisholm, J.R.M. and Barnes, D.J., (1998) Anomalies in coral reef community metabolism and their potential importance in the reef CO2 source-sink debate. *Proceedings of the National Academy of Sciences of the United States of America*, 9511, pp.6566–6569.

Clark, M.R. and Rowden, A.A., (2009) Effect of deepwater trawling on the macro-invertebrate assemblages of seamounts on the Chatham Rise, New Zealand. *Deep-Sea Research Part I: Oceanographic Research Papers*, 569, pp.1540–1554.

Conte, M.H., (2019) Oceanic Particle Flux. In: *Encyclopedia of Ocean Sciences*. pp.192–200.

Corman, J.R., Moody, E.K. and Elser, J.J., (2015) Stoichiometric impact of calcium carbonate deposition on nitrogen and phosphorus supplies in three montane streams. *Biogeochemistry*.

Cunha, M.R., Paterson, G.L.J., Amaro, T., Blackbird, S., de Stigter, H.C., Ferreira, C., Glover, A., Hilário, A., Kiriakoulakis, K., Neal, L., Ravara, A., Rodrigues, C.F., Tiago, Á. and Billett, D.S.M., (2011) Biodiversity of macrofaunal assemblages from three Portuguese submarine canyons (NE Atlantic). *Deep-Sea Research Part II: Topical Studies in Oceanography*, 5823–24, pp.2433–2447.

Cunningham, M.J., Hodgson, S., Masson, D.G. and Parson, L.M., (2005) An evaluation of along- and down-slope sediment transport processes between Goban Spur and Brenot Spur on the Celtic Margin of the Bay of Biscay. *Sedimentary Geology*, 1791–2, pp.99–116.

Daly, E., Johnson, M.P., Wilson, A.M., Gerritsen, H.D., Kiriakoulakis, K., Allcock, A.L. and White, M., (2018) Bottom trawling at Whittard Canyon: Evidence for seabed modification, trawl plumes and food source heterogeneity. *Progress in Oceanography*, 169, pp.227–240.

Dartnell, P. and Gardner, J. V., (2004) *Predicting seafloor facies from multibeam bathymetry and backscatter data*. *Photogrammetric Engineering and Remote Sensing*, .

Dauwe, B. and Middelburg, J.J., (1998) Amino acids and hexosamines as indicators of organic matter degradation state in North Sea sediments. *Limnology and Oceanography*.

Davies, A.J., Roberts, J.M. and Hall-Spencer, J., (2007) *Preserving deep-sea natural heritage: Emerging issues in offshore conservation and management*. *Biological Conservation*, .

Deacon, G.E.R., (1964) International Indian Ocean Expedition. *Nature*, 2014919, pp.561–562.

Deering, R., Bell, T., Forbes, D.L., Campbell, C. and Edinger, E., (2019) Morphological characterization of submarine slope failures in a semi-enclosed fjord, frobisher bay, eastern canadian arctic. *Geological Society Special Publication*, 4771, pp.367–376.

Dekas, A.E., Poretsky, R.S. and Orphan, V.J., (2009) Deep-Sea archaea fix and share nitrogen in methane-consuming microbial consortia. *Science*.

Van Dongen, B.E., Ashton, N.J. and Pattrick, R.A.D., (2014) The formation of ferromanganese nodules in the southwest Indian Ocean; an abiotic process. *Mineralogical Magazine*, 784, pp.941–955.

Van Dongen, B.E., Irene, W., Philippart, C.J.M., De Leeuw, J.W. and Sinninghe Damsté, J.S., (2000) Biomarkers in upper Holocene Eastern North Sea and Wadden Sea sediments. *Organic Geochemistry*, 3112, pp.1533–1543.

Douglas, R.G., (1978) Oceanic sediments. In: *Sedimentology*. [online] Berlin, Heidelberg: Springer Berlin Heidelberg, pp.785–802. Available at: https://doi.org/10.1007/3-540-31079-7_147.

Duineveld, G., Lavaleye, M., Berghuis, E. and De Wilde, P., (2001) Activity and composition of the benthic fauna in the Whittard Canyon and the adjacent continental slope (NE Atlantic). *Oceanologica Acta*.

Duineveld, G.C.A., Jeffreys, R.M., Lavaleye, M.S.S., Davies, A.J., Bergman, M.J.N., Watmough, T. and Witbaard, R., (2012) Spatial and tidal variation in food supply to shallow cold-water coral reefs of the Mingulay Reef complex (Outer Hebrides, Scotland). *Marine Ecology Progress Series*, 444, pp.97–115.

Dunlea, A.G., Scudder, R.P. and Murray, R.W., (2018) Marine sediment. In: *Encyclopedia of Earth Sciences Series*. pp.878–892.

Dunne, J.P., Sarmiento, J.L. and Gnanadesikan, A., (2007) A synthesis of global particle export from

the surface ocean and cycling through the ocean interior and on the seafloor. *Global Biogeochemical Cycles*, 214.

Duros, P., Fontanier, C., Metzger, E., Pusceddu, A., Cesbron, F., de Stigter, H.C., Bianchelli, S., Danovaro, R. and Jorissen, F.J., (2011) Live (stained) benthic foraminifera in the Whittard Canyon, Celtic margin (NE Atlantic). *Deep-Sea Research Part I: Oceanographic Research Papers*, 582, pp.128–146.

Dutkiewicz, A., O'Callaghan, S. and Müller, R.D., (2016) Controls on the distribution of deep-sea sediments. *Geochemistry, Geophysics, Geosystems*.

Emerson, S. and Hedges, J., (2003) Sediment Diagenesis and Benthic Flux. In: *Treatise on Geochemistry*.

Emerson, S. and Hedges, J., (2008) *Chemical oceanography and the marine carbon cycle*. *Chemical Oceanography and the Marine Carbon Cycle*.

Emerson, S. and Hedges, J.I., (1988) Processes controlling the organic carbon content of open ocean sediments. *Paleoceanography*.

Escobar-briones, E., García-villalobos, F.J., Nacional, U., México, A. De, Ciencias, I. De, Académica, U. and Marina, D.E., (2009) Distribution of total organic carbon and total nitrogen in deep-sea sediments from the southwestern Gulf of Mexico. *Boletín de la Sociedad …*, [online] 611, pp.73–86. Available at: http://scielo.unam.mx/pdf/bsgm/v61n1/v61n1a8.pdf.

Fettweis, M., Baeye, M., Lee, B.J., Chen, P. and Yu, J.C.S., (2012) Hydro-meteorological influences and multimodal suspended particle size distributions in the Belgian nearshore area (southern North Sea). *Geo-Marine Letters*, 322, pp.123–137.

Fleitmann, D., Foster, G. and Kageyama, M., (2013) IPCC AR5. WG1. Chap. 5. Information from paleoclimate archives. *Climate Change 2013 the Physical Science Basis: Working Group I Contribution to the Fifth Assessment Report of the Intergovernmental Panel on Climate Change*, 9781107057, pp.383–464.

Folk, R.L. and Ward, W.C., (1957) Brazos River bar [Texas]; a study in the significance of grain size parameters. *Journal of Sedimentary Research*, [online] 271, pp.3–26. Available at: http://jsedres.sepmonline.org/cgi/doi/10.1306/74D70646-2B21-11D7-8648000102C1865D.

Foster, R.A., Kuypers, M.M.M., Vagner, T., Paerl, R.W., Musat, N. and Zehr, J.P., (2011) Nitrogen fixation and transfer in open ocean diatom-cyanobacterial symbioses. *ISME Journal*.

Francois, R., Honjo, S., Krishfield, R. and Manganini, S., (2002) Factors controlling the flux of organic carbon to the bathypelagic zone of the ocean. *Global Biogeochemical Cycles*, 164, pp.34-1-34–20.

Fry, B. and Sherr, E.B., (1984) delta super(13)C measurements as indicators of carbon flow in marine and freshwater ecosystems. *Contrib. Mar. Sci.*

Gage, J.D. and Tyler, P.A., (1992) *Deep-Sea Biology. A natural history of organims at the deep-sea floor*. *Geobios*, .

Gambi, C. and Danovaro, R., (2016) Biodiversity and life strategies of deep-sea meiofauna and nematode assemblages in the Whittard Canyon (Celtic margin, NE Atlantic Ocean). *Deep-Sea Research Part I: Oceanographic Research Papers*.

Garcia, R., Koho, K.A., De Stigter, H.C., Epping, E., Koning, E. and Thomsen, L., (2007) Distribution of meiobenthos in the Nazar?? canyon and adjacent slope (western Iberian Margin) in relation to sedimentary composition. *Marine Ecology Progress Series*, 340, pp.207–220.

García, R., van Oevelen, D., Soetaert, K., Thomsen, L., De Stigter, H.C. and Epping, E., (2008) Deposition rates, mixing intensity and organic content in two contrasting submarine canyons. *Progress in Oceanography*, 762, pp.192–215.

Gardner, W.D., (1989) Baltimore Canyon as a modern conduit of sediment to the deep sea. *Deep Sea Research Part A, Oceanographic Research Papers*, 363, pp.323–358.

Gearing, J.N., (1991) The Study of Diet and Trophic Relationships through Natural Abundance 13C. In: *Carbon Isotope Techniques*.

Genin, A., (2004) Bio-physical coupling in the formation of zooplankton and fish aggregations over abrupt topographies. *Journal of Marine Systems*, 501–2, pp.3–20.

Gerald M. Friedman, (1967) Dynamic Processes and Statistical Parameters Compared for Size Frequency Distribution of Beach and River Sands. *SEPM Journal of Sedimentary Research*.

Gerritsen, H.D. and Lordan, C., (2014) *Atlas of Commercial Fisheries around Ireland*. Available at: http://hdl.handle.net/10793/958.

Gordon, D.C., (1971) Distribution of particulate organic carbon and nitrogen at an oceanic station in the central Pacific. *Deep-Sea Research and Oceanographic Abstracts*.

Gruber, N. and Galloway, J.N., (2008) *An Earth-system perspective of the global nitrogen cycle*. *Nature*.

Gunton, L.M., Neal, L., Gooday, A.J., Bett, B.J. and Glover, A.G., (2015) Benthic polychaete diversity patterns and community structure in the Whittard Canyon system and adjacent slope (NE Atlantic). *Deep-Sea Research Part I: Oceanographic Research Papers*.

Hall, P., Brunnegård, J., Hulthe, G., Martin, W., Stahl, J. and Tengberg, A., (2007) Dissolved organic matter in abyssal sediments: Core recovery artifacts. *Limnology and Oceanography - LIMNOL OCEANOGR*, 52, pp.19–31.

Hall, R.A., Aslam, T. and Huvenne, V.A.I., (2017) Partly standing internal tides in a dendritic submarine canyon observed by an ocean glider. *Deep-Sea Research Part I: Oceanographic Research Papers*, 126, pp.73–84.

Harris, P. and Baker, E., (2012) *Seafloor Geomorphology as Benthic Habitat*. *Seafloor Geomorphology as Benthic Habitat*.

Harris, P.T., Macmillan-Lawler, M., Rupp, J. and Baker, E.K., (2014a) Geomorphology of the oceans. *Marine Geology*, 352, pp.4–24.

Harris, P.T., Macmillan-Lawler, M., Rupp, J. and Baker, E.K., (2014b) GHarris, P. T., et al. "Geomorphology of the Oceans." Marine Geology, vol. 352, Elsevier, June 2014, pp. 4–24, doi:10.1016/J.MARGEO.2014.01.011.eomorphology of the oceans. *Marine Geology*, [online] 352, pp.4–24. Available at: https://www.sciencedirect.com/science/article/pii/S0025322714000310.

Harris, P.T. and Whiteway, T., (2011) Global distribution of large submarine canyons: Geomorphic differences between active and passive continental margins. *Mar. Geol.*, 285, pp.69–86.

Hayes, B.J., (1993) Stable Carbon Isotope Geochemistry Stable Carbon Isotopes. *In Organic Geochemistry Mar. Geol. Plant Physiol. Carbon Isotope Fractionation in Plants. Phytochem. @BULLET Fry B. and Sherr E.B. Contrib. Mar. Sci. @BULLET Gearing P., Plucker F.E. and Parker P.L. Mar. Chem. @BULLET Bromley B. Anal. Biochem*, 113126, pp.73–98.

Hedges, J.I. and Keil, R.G., (1995) Sedimentary organic matter preservation: an assessment and speculative synthesis. *Marine Chemistry*, 492–3, pp.81–115.

Henson, S.A., Sanders, R., Madsen, E., Morris, P.J., Le Moigne, F. and Quartly, G.D., (2011) A reduced estimate of the strength of the ocean's biological carbon pump. *Geophysical Research Letters*, 384.

Hjulstrom, F., (1939) *Transportation of Detritus by Moving Water: Part 1. Transportation*. *Recent Marine Sediments*.

Hobson, R.D., (2019) Surface roughness in topography: Quantitative approach. In: *Spatial Analysis in Geomorphology*. pp.221–245.

Holcomb, Z.C., Cox, K.S., Holcomb, Z.C. and Cox, K.S., (2018) One-Way ANOVA. In: *Interpreting Basic Statistics*. pp.154–157.

Holm-Hansen, O., Strickland, J.D.H. and Williams, P.M., (1966) A DETAILED ANALYSIS OF BIOLOGICALLY IMPORTANT SUBSTANCES IN A PROFILE OFF SOUTHERN CALIFORNIA. *Limnology and Oceanography*.

Hotchkiss, F.S. and Wunsch, C., (1982) Internal waves in Hudson Canyon with possible geological implications. *Deep Sea Research Part A, Oceanographic Research Papers*, 294, pp.415–442.

Hunter, W.R., Jamieson, A., Huvenne, V.A.I. and Witte, U., (2013a) Sediment community responses to marine vs. terrigenous organic matter in a submarine canyon. *Biogeosciences*, 101, pp.67–80.

Hunter, W.R., Jamieson, A., Huvenne, V.A.I. and Witte, U., (2013b) Sediment community responses to marine vs. terrigenous organic matter in a submarine canyon. *Biogeosciences*.

Huvenne, V.A.I., Tyler, P.A., Masson, D.G., Fisher, E.H., Hauton, C., Hühnerbach, V., Bas, T.P. and Wolff, G.A., (2011) A picture on the wall: Innovative mapping reveals cold-water coral refuge in submarine canyon. *PLoS ONE*, 612.

Ingels, J., Tchesunov, A. V. and Vanreusel, A., (2011) Meiofauna in the gollum channels and the whittard canyon, celtic margin-how local environmental conditions shape nematode structure and function. *PLoS ONE*, 65.

Inthorn, M., Mohrholz, V. and Zabel, M., (2006) Nepheloid layer distribution in the Benguela upwelling area offshore Namibia. *Deep-Sea Research Part I: Oceanographic Research Papers*.

IPCC, (2012) *Climate Change IPCC 2013*. *Southeast Asian Journal of Tropical Medicine and Public Health*, .

Ishiwatari, R. and Uzaki, M., (1987) Diagenetic changes of lignin compounds in a more than 0.6 million-year-old lacustrine sediment (Lake Biwa, Japan). *Geochimica et Cosmochimica Acta*, 512, pp.321–328.

Jannasch, H. and Taylor, C., (1984) Deep-sea microbiology. *Annual review of microbiology*, 18, pp.487–514.

Jiang, H., Wan, S., Ma, X., Zhong, N. and Zhao, D., (2017) End-member modeling of the grain-size record of Sikouzi fine sediments in Ningxia (China) and implications for temperature control of Neogene evolution of East Asian winter monsoon. *PLoS ONE*, 1210.

Johnson, M.P., White, M., Wilson, A., Würzberg, L., Schwabe, E., Folch, H. and Allcock, A.L., (2013a) A vertical wall dominated by Acesta excavata and Neopycnodonte zibrowii, part of an undersampled group of deep-sea habitats. *PLoS ONE*.

Johnson, M.P., White, M., Wilson, A., Würzberg, L., Schwabe, E., Folch, H. and Allcock, A.L., (2013b) A vertical wall dominated by Acesta excavata and Neopycnodonte zibrowii, part of an undersampled group of deep-sea habitats. *PLoS ONE*, 811.

Johnson, T.C., Hamilton, E.L. and Berger, W.H., (1977) Physical properties of calcareous ooze: Control by dissolution at depth. *Marine Geology*.

Kaiser, M.J., Collie, J.S., Hall, S.J., Jennings, S. and Poiner, I.R., (2002) Modification of marine habitats by trawling activities: Prognosis and solutions. *Fish and Fisheries*, 32, pp.114–136.

Kang, H.S., Won, E.J., Shin, K.H. and Yoon, H. Il, (2007) Organic carbon and nitrogen composition in the sediment of the Kara Sea, Arctic Ocean during the Last Glacial Maximum to Holocene times. *Geophysical Research Letters*, 3412.

Karl, H.A., (2006) Sediment of the Sea Floor. *United States Geological Survey: Boulder, CO, USA,*.

Keil, R.G., Tsamakis, E., Fuh, C.B., Giddings, J.C. and Hedges, J.I., (1994) Mineralogical and textural controls on the organic composition of coastal marine sediments: Hydrodynamic separation using SPLITT-fractionation. *Geochimica et Cosmochimica Acta*, 582, pp.879–893.

Keir, R.S., Greinert, J., Rhein, M., Petrick, G., Sültenfuß, J. and Fürhaupter, K., (2005) Methane and methane carbon isotope ratios in the Northeast Atlantic including the Mid-Atlantic Ridge (50°N). *Deep-Sea Research Part I: Oceanographic Research Papers*.

Khim, B.K., Otosaka, S., Park, K.A. and Noriki, S., (2018) δ13C and δ15N Values of Sediment-trap Particles in the Japan and Yamato Basins and Comparison with the Core-top Values in the East/Japan Sea. *Ocean Science Journal*.

Kiriakoulakis, K., Bett, B.J., White, M. and Wolff, G.A., (2004) Organic biogeochemistry of the Darwin Mounds, a deep-water coral ecosystem, of the NE Atlantic. *Deep-Sea Research Part I: Oceanographic Research Papers*, 5112, pp.1937–1954.

Kiriakoulakis, K., Blackbird, S., Ingels, J., Vanreusel, A. and Wolff, G.A., (2011) Organic geochemistry of submarine canyons: The Portuguese Margin. *Deep-Sea Research Part II: Topical Studies in Oceanography*, 5823–24, pp.2477–2488.

Kiriakoulakis, K., Fisher, E.L., Wolff, G.A., Freiwald, A., Grehan, A., Roberts, J.M., Grehand, A. and Roberts, J.M., (2005) Lipids and nitrogen isotopes of two deep-water corals from the North-East Atlantic: initial results and implications for their nutrition. In: A. Freiwald and J.M. Roberts, eds., *Cold-water Corals and Ecosystems*. Berlin: Springer-Verlag, pp.715–729.

Kiriakoulakis, K., Freiwald, A. and Fisher, E., (2006) Organic matter quality and supply to deep-water coral/mound systems of the NW European Continental Margin. *International Journal of Earth Sciences*.

Kiriakoulakis, K., Stutt, E., Rowland, S.J., Vangriesheim, A., Lampitt, R.S. and Wolff, G.A., (2001) *Controls on the organic chemical composition of settling particles in the Northeast Atlantic Ocean*. *Progress in Oceanography*.

Klaas, C. and Archer, D.E., (2002) Association of sinking organic matter with various types of mineral ballast in the deep sea: Implications for the rain ratio. *Global Biogeochemical Cycles*, 164, pp.63-1-63–14.

De La Rocha, C.L., Nowald, N. and Passow, U., (2008) Interactions between diatom aggregates, minerals, particulate organic carbon, and dissolved organic matter: Further implications for the ballast hypothesis. *Global Biogeochemical Cycles*, 224.

Lambeck, K., (1996) Glaciation and sea-level change for Ireland and the Irish Sea since Late Devensian/Midlandian time. *Journal of the Geological Society*, [online] 1536, pp.853–872. Available at: https://doi.org/10.1144/gsjgs.153.6.0853.

Layman, C.A., Araujo, M.S., Boucek, R., Hammerschlag-Peyer, C.M., Harrison, E., Jud, Z.R., Matich, P.,

Rosenblatt, A.E., Vaudo, J.J., Yeager, L.A., Post, D.M. and Bearhop, S., (2012) *Applying stable isotopes to examine food-web structure: An overview of analytical tools*. *Biological Reviews*, .

Lecours, V., Devillers, R., Simms, A.E., Lucieer, V.L. and Brown, C.J., (2017) Towards a framework for terrain attribute selection in environmental studies. *Environmental Modelling and Software*, 89, pp.19–30.

Lecours, V., Dolan, M.F.J., Micallef, A. and Lucieer, V.L., (2016) *A review of marine geomorphometry, the quantitative study of the seafloor*. *Hydrology and Earth System Sciences*, .

Lee, B.J., Toorman, E. and Fettweis, M., (2014) Multimodal particle size distributions of fine-grained sediments: Mathematical modeling and field investigation. *Ocean Dynamics*, 643, pp.429–441.

Léniz, B., Murillo, A.A., Ramírez-Flandes, S. and Ulloa, O., (2017) Diversity and transcriptional levels of RuBisCO form II of sulfur-oxidizing γ-proteobacteria in coastal-upwelling waters with seasonal anoxia. *Frontiers in Marine Science*.

DE Leo, F.C., Smith, C.R., Rowden, A.A., Bowden, D.A., Clark, M.R. and Soc, P.R., (2010) Submarine canyons : hotspots of benthic biomass and productivity in the deep sea Subject collections Submarine canyons : hotspots of benthic biomass and productivity in the deep sea. *Proceeding of the Royal Society of Biological Science*, May, pp.1–11.

Lesen, A.E., (2006) Sediment organic matter composition and dynamics in San Francisco Bay, California, USA: Seasonal variation and interactions between water column chlorophyll and the benthos. *Estuarine, Coastal and Shelf Science*.

Levin, L.A., Etter, R.J., Rex, M.A., Gooday, A.J., Smith, C.R., Pineda, J., Stuart, C.T., Hessler, R.R. and Pawson, D., (2001) Environmental Influences on Regional Deep-Sea Species Diversity. *Annual Review of Ecology and Systematics*, [online] 321, pp.51–93. Available at: http://www.annualreviews.org/doi/10.1146/annurev.ecolsys.32.081501.114002.

Levin, L.A. and Michener, R.H., (2002) Isotopic evidence for chemosynthesis-based nutrition of macrobenthos: The lightness of being at Pacific methane seeps. *Limnology and Oceanography*.

Libes. M.S, (1992) S.M. Libes An introduction to marine biogeochemistry. xv, 734 p. John Wiley and Sons, 1992. Price £45–95. *Journal of the Marine Biological Association of the United Kingdom*, 723, pp.731–731.

Locat, J., (2001) Instabilities along ocean margins: A geomorphological and geotechnical perspective. *Marine and Petroleum Geology*, 184, pp.503–512.

Lu, X., Zhou, F., Chen, F., Lao, Q., Zhu, Q., Meng, Y. and Chen, C., (2020) Spatial and seasonal variations of sedimentary organic matter in a subtropical bay: Implication for human interventions. *International Journal of Environmental Research and Public Health*.

Lundblad, E.R., Wright, D.J., Miller, J., Larkin, E.M., Rinehart, R., Naar, D.F., Donahue, B.T., Anderson, S.M. and Battista, T., (2006) A benthic terrain classification scheme for American Samoa. *Marine Geodesy*, 292, pp.89–111.

Lykousis, V., Collins, M., Polymenakou, P.N., Pusceddu, A., Tselepides, A., Polychronaki, T., Giannakourou, A., Fiordelmondo, C., Hatziyanni, E. and Danovaro, R., (2005) Benthic microbial abundance and activities in an intensively trawled ecosystem (Thermaikos Gulf, Aegean Sea). *Continental Shelf Research*, [online] 2519, pp.2570–2584. Available at: http://www.sciencedirect.com/science/article/pii/S0278434305001470.

Mackin, J.E. and Aller, R.C., (1984) Diagenesis of dissolved aluminum in organic-rich estuarine sediments. *Geochimica et Cosmochimica Acta*, 482, pp.299–313.

Macko, S.A. and Estep, M.L.F., (1984) Microbial alteration of stable nitrogen and carbon isotopic compositions of organic matter. *Organic Geochemistry*.

MacMillan, R.A. and Shary, P.A., (2009) *Landforms and landform elements in geomorphometry*. *Developments in Soil Science*, .

Marchant, H.K., Holtappels, M., Lavik, G., Ahmerkamp, S., Winter, C. and Kuypers, M.M.M., (2016) Coupled nitrification-denitrification leads to extensive N loss in subtidal permeable sediments. *Limnology and Oceanography*.

Marconi, D., Weigand, M.A. and Sigman, D.M., (2019) Nitrate isotopic gradients in the North Atlantic Ocean and the nitrogen isotopic composition of sinking organic matter. *Deep-Sea Research Part I: Oceanographic Research Papers*.

Martín, J., Puig, P., Masqué, P., Palanques, A. and Sánchez-Gómez, A., (2014) Impact of bottom trawling on deep-sea sediment properties along the flanks of a submarine canyon. *PLoS ONE*, 98.

Martins, I. and Hope E, O., (2020) Ancient Deposition Environment, Mechanism of Deposition and Textural attributes of Ajali Formation, Western Flank of the Anambra Basin, Nigeria. *Case Studies in Chemical and Environmental Engineering*.

Maslin, M.A. and Swann, G.E.A., (2006) ISOTOPES IN MARINE SEDIMENTS. In: *Isotopes in Palaeoenvironmental Research*. pp.227–290.

Masson, D.G., Huvenne, V.A.I., de Stigter, H.C., Wolff, G.A., Kiriakoulakis, K., Arzola, R.G. and Blackbird, S., (2010a) Efficient burial of carbon in a submarine canyon. *Geology*, 389, pp.831–834.

Masson, D.G., Huvenne, V.A.I., de Stigter, H.C., Wolff, G.A., Kiriakoulakis, K., Arzola, R.G. and Blackbird, S., (2010b) Efficient burial of carbon in a submarine canyon. *Geology*.

McCave, I.N. and Syvitski, J.P.M., (2010) Principles and methods of geological particle size analysis. In: *Principles, methods, and application of particle size analysis*. pp.3–21.

McDonnell, A.M.P., (2011) *Marine particle dynamics : sinking velocities, size distributions, fluxes, and microbial degradation rates*. *Marine particle dynamics : sinking velocities, size distributions, fluxes, and microbial degradation rates*.

McDonnell, A.M.P. and Buesseler, K.O., (2010) Variability in the average sinking velocity of marine particles. *Limnology and Oceanography*, 555, pp.2085–2096.

McLaren, P., (1981) An interpretation of trends in grain size measures. *Journal of Sedimentary Petrology*.

Meyers, P.A., (1994) Preservation of elemental and isotopic source identification of sedimentary organic matter. *Chemical Geology*, 1143–4, pp.289–302.

Meyers, P.A. and Silliman, J.E., (1996) Organic matter in Pleistocene to Quaternary turbidites from Site 897, 898, 899, and 900, Iberia Abyssal Plain. In: *Proceedings of the Ocean Drilling Program, 149 Scientific Results*.

Michener, R.H. and Kaufman, L., (2008) Stable Isotope Ratios as Tracers in Marine Food Webs: An Update. In: *Stable Isotopes in Ecology and Environmental Science: Second Edition*.

Middelburg, J.J., (2014) Stable isotopes dissect aquatic food webs from the top to the bottom. *Biogeosciences*.

Middelburg, J.J. and Nieuwenhuize, J., (1998) Carbon and nitrogen stable isotopes in suspended matter and sediments from the Schelde Estuary. *Marine Chemistry*, 603–4, pp.217–225.

Middleton, G. V., (1962) On Sorting, Sorting Coefficients, and the Lognormality of the Grain-Size Distribution of Sandstones: A Discussion. *The Journal of Geology*, 706, pp.754–756.

Minagawa, M. and Wada, E., (1984) Stepwise enrichment of 15N along food chains: Further evidence and the relation between δ15N and animal age. *Geochimica et Cosmochimica Acta*.

Mintenbeck, K., Jacob, U., Knust, R., Arntz, W.E. and Brey, T., (2007) Depth-dependence in stable isotope ratio δ15N of benthic POM consumers: The role of particle dynamics and organism trophic guild. *Deep-Sea Research Part I: Oceanographic Research Papers*.

Mohn, C. and Beckmann, A., (2002) Numerical studies on flow amplification at an isolated shelfbreak bank, with application to Porcupine Bank. *Continental Shelf Research*, 229, pp.1325–1338.

Montes, E., Thunell, R., Muller-Karger, F.E., Lorenzoni, L., Tappa, E., Troccoli, L., Astor, Y. and Varela, R., (2013) Sources of δ15N variability in sinking particulate nitrogen in the Cariaco Basin, Venezuela. *Deep-Sea Research Part II: Topical Studies in Oceanography*.

Montoya, J.P. and Mccarthy, J.J., (1995) Isotopic fractionation during nitrate uptake by phytoplankton grown in continuous culture. *Journal of Plankton Research*.

Morris, K.J., Tyler, P.A., Masson, D.G., Huvenne, V.I.A. and Rogers, A.D., (2013a) Distribution of cold-water corals in the Whittard Canyon, NE Atlantic Ocean. *Deep-Sea Research Part II: Topical Studies in Oceanography*.

Morris, K.J., Tyler, P.A., Masson, D.G., Huvenne, V.I.A. and Rogers, A.D., (2013b) Distribution of cold-water corals in the Whittard Canyon, NE Atlantic Ocean. *Deep-Sea Research Part II: Topical Studies in Oceanography*, 92, pp.136–144.

Morris, K.J., Tyler, P.A., Masson, D.G., Huvenne, V.I.A. and Rogers, A.D., (2013c) Distribution of cold-water corals in the Whittard Canyon, NE Atlantic Ocean. *Deep Sea Research Part II: Topical Studies in Oceanography*, [online] 92, pp.136–144. Available at: http://www.sciencedirect.com/science/article/pii/S0967064513001343 [Accessed 12 May 2017].

Mountjoy, J. and Micallef, A., (2018) Submarine Landslides. In: *Springer Geology*. pp.235–250.

Mulder, T., Zaragosi, S., Garlan, T., Mavel, J., Cremer, M., Sottolichio, A., Sénéchal, N. and Schmidt, S., (2012) Present deep-submarine canyons activity in the Bay of Biscay (NE Atlantic). *Marine Geology*, 295–298, pp.113–127.

Müller, P.J., (1977) C N ratios in Pacific deep-sea sediments: Effect of inorganic ammonium and organic nitrogen compounds sorbed by clays. *Geochimica et Cosmochimica Acta*, 416, pp.765–776.

Nicholas, J.R.J., (2003) *Grain Size Analysis of the Sediments of Spurn Head, Yorkshire, England*. [online] University of Cincinnati. Available at: http://rave.ohiolink.edu/etdc/view?acc_num=ucin1043959373.

Novaczek, E., Devillers, R. and Edinger, E., (2019) Generating higher resolution regional seafloor maps from crowd-sourced bathymetry. *PLoS ONE*, 146.

Oberle, F., Puig, P. and Martín, J., (2017) Submarine Geomorphology: Fishing Activities. In: *Submarine Geomorphology*. pp.503–534.

Oberle, F.K.J., Swarzenski, P.W., Reddy, C.M., Nelson, R.K., Baasch, B. and Hanebuth, T.J.J., (2016) Deciphering the lithological consequences of bottom trawling to sedimentary habitats on the shelf. *Journal of Marine Systems*, 159, pp.120–131.

Van Oevelen, D., Soetaert, K., Garcia, R., de Stigter, H.C., Cunha, M.R., Pusceddu, A. and Danovaro, R., (2011) Canyon conditions impact carbon flows in food webs of three sections of the Nazar??

canyon. *Deep-Sea Research Part II: Topical Studies in Oceanography*, 5823–24, pp.2461–2476.

Opdyke, B.N. and Walker, J.C.G., (1992) Return of the coral reef hypothesis: basin to shelf partitioning of CaCO 3 and its effect on atmospheric CO 2. *Geology*, 208, pp.733–736.

Palanques, A., Martín, J., Puig, P., Guillén, J., Company, J.B. and Sardà, F., (2006) Evidence of sediment gravity flows induced by trawling in the Palamós (Fonera) submarine canyon (northwestern Mediterranean). *Deep-Sea Research Part I: Oceanographic Research Papers*, 532, pp.201–214.

Palanques, A., Puig, P., Durrieu de Madron, X., Sanchez-Vidal, A., Pasqual, C., Martín, J., Calafat, A., Heussner, S. and Canals, M., (2012) Sediment transport to the deep canyons and open-slope of the western Gulf of Lions during the 2006 intense cascading and open-sea convection period. *Progress in Oceanography*, 106, pp.1–15.

Paradis, S., Pusceddu, A., Masqué, P., Puig, P., Moccia, D., Russo, T. and Iacono, C. Lo, (2019) Organic matter contents and degradation in a highly trawled area during fresh particle inputs (Gulf of Castellammare, southwestern Mediterranean). *Biogeosciences*, 1621, pp.4307–4320.

Parrish, C.C., (2013) Lipids in Marine Ecosystems. *ISRN Oceanography*, 2013, pp.1–16.

Passega, R., (1957) Texture as Characteristic of Clastic Deposition. *AAPG Bulletin*, 419, pp.1952–1984.

Passega, R., (1964) Grain size representation by CM patterns as a geologic tool. *Journal of Sedimentary Research*, [online] 344, pp.830–847. Available at: https://pubs.geoscienceworld.org/jsedres/article/34/4/830-847/95793.

Passega, R., (2003) Grain size representation by CM patterns as a geologic tool. *Journal of Sedimentary Research*, 344, pp.830–847.

PASSEGA, R. and BYRAMJEE, R., (1969) GRAIN-SIZE IMAGE OF CLASTIC DEPOSITS. *Sedimentology*, 133–4, pp.233–252.

Paterson, G.A. and Heslop, D., (2015) New methods for unmixing sediment grain size data. *Geochemistry, Geophysics, Geosystems*, 1612, pp.4494–4506.

Paterson, G.L.J., Glover, A.G., Cunha, M.R., Neal, L., de Stigter, H.C., Kiriakoulakis, K., Billett, D.S.M., Wolff, G.A., Tiago, A., Ravara, A., Lamont, P. and Tyler, P., (2011) Disturbance, productivity and diversity in deep-sea canyons: A worm's eye view. *Deep-Sea Research Part II: Topical Studies in Oceanography*.

Pedrosa-Pàmies, R., Parinos, C., Sanchez-Vidal, A., Gogou, A., Calafat, A., Canals, M., Bouloubassi, I. and Lampadariou, N., (2015) *Composition and sources of sedimentary organic matter in the deep Eastern Mediterranean Sea*. *Biogeosciences Discussions*, .

Pérenne, N., Haidvogel, D.B. and Boyer, D.L., (2001) Laboratory-numerical model comparison of flow over a coastal canyon. *Journal of Atmospheric and Oceanic Technology*, 182, pp.235–255.

Petersen, B.J. and Fry, B., (1987) Stable Isotopes in Ecosystem Studies. *Annu Rev Ecol Syst*, [online] 181987, pp.293–320. Available at: http://www.annualreviews.org/doi/10.1146/annurev.es.18.110187.001453%5Cnhttp://www.ncbi.nlm.nih.gov/entrez/query.fcgi?db=pubmed&cmd=Retrieve&dopt=AbstractPlus&list_uids=A1987K958800013.

Peterson, B.J. and Fry, B., (1987) Stable isotopes in ecosystem studies. *Annual review of ecology and systematics. Vol. 18*.

Petsch, S.T., (2013) Weathering of Organic Carbon. In: *Treatise on Geochemistry: Second Edition*.

Pike, R.J., Evans, I.S. and Hengl, T., (2009) *Geomorphometry: A brief guide*. *Developments in Soil Science*, .

Pinet, P.R., (2009) *Invitation to Oceanography*. [online] *Jones and Bartlett Publishers*. Available at: http://books.google.com/books?id=h-eWVhoxtmUC&pgis=1.

Praeg, D., McCarron, S., Dove, D., Ó Cofaigh, C., Scott, G., Monteys, X., Facchin, L., Romeo, R. and Coxon, P., (2015) Ice sheet extension to the Celtic Sea shelf edge at the Last Glacial Maximum. *Quaternary Science Reviews*.

Du Preez, C., (2015) A new arc–chord ratio (ACR) rugosity index for quantifying three-dimensional landscape structural complexity. *Landscape Ecology*, 301, pp.181–192.

Puig, P., Canals, M., Company, J.B., Martín, J., Amblas, D., Lastras, G., Palanques, A. and Calafat, A.M., (2012) Ploughing the deep sea floor. *Nature*, 4897415, pp.286–289.

Puig, P. and Palanques, A., (1998) Temporal variability and composition of settling particle fluxes on the Barcelona continental margin (Northwestern Mediterranean). *Journal of Marine Research*, 563, pp.639–654.

Puig, P., Palanques, A. and Martín, J., (2014) Contemporary Sediment-Transport Processes in Submarine Canyons. *Annual Review of Marine Science*, 61, pp.53–77.

Pusceddu, A., Fiordelmondo, C., Polymenakou, P., Polychronaki, T., Tselepides, A. and Danovaro, R., (2005) Effects of bottom trawling on the quantity and biochemical composition of organic matter in coastal marine sediments (Thermaikos Gulf, northwestern Aegean Sea). *Continental Shelf Research*, 2519–20, pp.2491–2505.

Radke, L., Nicholas, T., Thompson, P.A., Li, J., Raes, E., Carey, M., Atkinson, I., Huang, Z., Trafford, J. and Nichol, S., (2017) Baseline biogeochemical data from Australia's continental margin links seabed sediments to water column characteristics. *Marine and Freshwater Research*.

Rajganapathi, V.C., Jitheshkumar, N., Sundararajan, M., Bhat, K.H. and Velusamy, S., (2013) Grain size analysis and characterization of sedimentary environment along Thiruchendur coast, Tamilnadu, India. *Arabian Journal of Geosciences*, 612, pp.4717–4728.

Rajput, S., Thakur, N.K., Rajput, S. and Thakur, N.K., (2016) Chapter 3 – Sedimentation Pattern. In: *Geological Controls for Gas Hydrate Formations and Unconventionals*. pp.69–106.

Redfield, A.C., (1958) The biological control of chemical factors in the environment. *American Scientist*, 463, p.230A–221.

Reid, G.S. and Hamilton, D., (1990) A reconnaissance survey of the Whittard Sea Fan, Southwestern Approaches, British Isles. *Marine Geology*, 921–2, pp.69–86.

Ridgwell, A. and Arndt, S., (2015) Why Dissolved Organics Matter: DOC in Ancient Oceans and Past Climate Change. In: *Biogeochemistry of Marine Dissolved Organic Matter: Second Edition*.

Robert, K., Jones, D.O.B., Tyler, P.A., Van Rooij, D. and Huvenne, V.A.I., (2015) Finding the hotspots within a biodiversity hotspot: Fine-scale biological predictions within a submarine canyon using high-resolution acoustic mapping techniques. *Marine Ecology*, 364, pp.1256–1276.

Rodelli, M.R., Gearing, J.N., Gearing, P.J., Marshall, N. and Sasekumar, A., (1984) Stable isotope ratio as a tracer of mangrove carbon in Malaysian ecosystems. *Oecologia*.

Rounick, J.S., Winterbourn, M.J. and Lyon, G.L., (1982) Differential Utilization of Allochthonous and

Autochthonous Inputs by Aquatic Invertebrates in Some New Zealand Streams: A Stable Carbon Isotope Study. *Oikos*.

Rovere, M., Gamberi, F., Mercorella, A. and Leidi, E., (2014) Geomorphometry of a submarine mass-transport complex and relationships with active faults in a rapidly uplifting margin (Gioia Basin, NE Sicily margin). *Marine Geology*, 356, pp.31–43.

Rowe, G.T. and Staresinic, N., (1979) Sources of Organic Matter to the Deep-Sea Benthos. *Ambio Special Report*, 6, p.19.

Ryan. John P., Chavez, F.P. and Bellingham, J.G., (2005) Physical-biological coupling in Monterey Bay, California: Topographic influences on phytoplankton ecology. *Marine Ecology Progress Series*, [online] 287, p.23. Available at: ryjo@mbari.org.

Sañé, E., Martín, J., Puig, P. and Palanques, A., (2013) Organic biomarkers in deep-sea regions affected by bottom trawling: Pigments, fatty acids, amino acids and carbohydrates in surface sediments from the la Fonera (Palamós) Canyon, NW Mediterranean Sea. *Biogeosciences*, 1012, pp.8093–8108.

Sappington, J.M., Longshore, K.M. and Thompson, D.B., (2007) Quantifying Landscape Ruggedness for Animal Habitat Analysis: A Case Study Using Bighorn Sheep in the Mojave Desert. *Journal of Wildlife Management*, 715, pp.1419–1426.

Sarmiento, J.L., Dunne, J., Gnanadesikan, A., Key, R.M., Matsumoto, K. and Slater, R., (2002) A new estimate of the CaCO 3 to organic carbon export ratio . *Global Biogeochemical Cycles*, 164, pp.54-1-54–12.

Savoye, B., Babonneau, N., Dennielou, B. and Bez, M., (2009) Geological overview of the Angola-Congo margin, the Congo deep-sea fan and its submarine valleys. *Deep-Sea Research Part II: Topical Studies in Oceanography*, [online] 5623, pp.2169–2182. Available at: Nathalie.Babonneau@univ-brest.fr.

Schlitzer, R., (2011) Ocean Data View User's Guide. *Contract*.

Schmiedl, G., Pfeilsticker, M., Hemleben, C. and Mackensen, A., (2004) Environmental and biological effects on the stable isotope composition of recent deep-sea benthic foraminifera from the western Mediterranean Sea. *Marine Micropaleontology*, 511–2, pp.129–152.

Schumacher, B. a, (2002) Methods for the Determination of Total Organic Carbon in Soils and Sediments. *Carbon*, 32April, p.25.

Scourse, J., Uehara, K. and Wainwright, A., (2009) Celtic Sea linear tidal sand ridges, the Irish Sea Ice Stream and the Fleuve Manche: Palaeotidal modelling of a transitional passive margin depositional system. *Marine Geology*.

Seiter, K., Hensen, C., Schröter, J. and Zabel, M., (2004) Organic carbon content in surface sediments - Defining regional provinces. *Deep-Sea Research Part I: Oceanographic Research Papers*, 5112, pp.2001–2026.

Selvaraj, K., Lee, T.Y., Yang, J.Y.T., Canuel, E.A., Huang, J.C., Dai, M., Liu, J.T. and Kao, S.J., (2015) Stable isotopic and biomarker evidence of terrigenous organic matter export to the deep sea during tropical storms. *Marine Geology*, [online] 364, pp.32–42. Available at: http://www.sciencedirect.com/science/article/pii/S0025322715000729 [Accessed 6 Apr. 2016].

Sharples, J., Scott, B.E. and Inall, M.E., (2013) *From physics to fishing over a shelf sea bank*. *Progress in Oceanography*, .

Shepard, F.P. and Dill, R.F., (1966) *Submarine canyons and other sea valleys*. *Rand McNally geology*

series, .

Sigman, D.M., Altabet, M.A., McCorkle, D.C., Francois, R. and Fischer, G., (2000) The δ 15 N of nitrate in the Southern Ocean: Nitrogen cycling and circulation in the ocean interior . *Journal of Geophysical Research: Oceans*, 105C8, pp.19599–19614.

Sigman, D.M. and Boyle, E.A., (2000) *Glacial/interglacial variations in atmospheric carbon dioxide*. *Nature*, .

Sigman, D.M. and Casciotti, K.L., (2001) Nitrogen Isotopes in the Ocean. In: *Encyclopedia of Ocean Sciences*.

Sigman, D.M. and Fripiat, F., (2019) Nitrogen isotopes in the ocean. In: *Encyclopedia of Ocean Sciences*. pp.263–278.

Sigman, D.M. and Hain, M.P., (2012) The Biological Productivity of the Ocean | Learn Science at Scitable. *Nature Education Knowledge*.

Sigman, D.M., Karsh, K.L. and Casciotti, K.L., (2010) Nitrogen Isotopes in the Ocean. In: *Encyclopedia of Ocean Sciences*. pp.40–54.

Smith, K.L., Ruhl, H.A., Bett, B.J., Billett, D.S.M., Lampitt, R.S. and Kaufmann, R.S., (2009) *Climate, carbon cycling, and deep-ocean ecosystems*. *Proceedings of the National Academy of Sciences of the United States of America*, .

Soliman, Y.S. and Rowe, G.T., (2008) Secondary production of Ampelisca mississippiana Soliman and Wicksten 2007 (Amphipoda, Crustacea) in the head of the Mississippi Canyon, northern Gulf of Mexico. *Deep-Sea Research Part II: Topical Studies in Oceanography*, 5524–26, pp.2692–2698.

Di Stefano, M. and Mayer, L.A., (2018) An automatic procedure for the quantitative characterization of submarine bedforms. *Geosciences (Switzerland)*, 81.

Stein, R., (1990) *Accumulation of organic carbon in marine sediments*. *Lecture Notes in Earth Sciences*, .

Stevenson, F.J. and Cheng, C.N., (1972) Organic geochemistry of the Argentine Basin sediments: Carbon-nitrogen relationships and Quaternary correlations. *Geochimica et Cosmochimica Acta*.

Stewart, H.A., Davies, J.S., Guinan, J. and Howell, K.L., (2014) The Dangeard and Explorer canyons, South Western Approaches UK: Geology, sedimentology and newly discovered cold-water coral mini-mounds. *Deep-Sea Research Part II: Topical Studies in Oceanography*, 104, pp.230–244.

de Stigter, H.C., Boer, W., de Jesus Mendes, P.A., Jesus, C.C., Thomsen, L., van den Bergh, G.D. and van Weering, T.C.E., (2007) Recent sediment transport and deposition in the Nazaré Canyon, Portuguese continental margin. *Marine Geology*, 2462–4, pp.144–164.

Stoffers, P., Plÿger, W. and Walter, P., (1984) Geochemistry and mineralogy of continental margin sediments from Westland, New Zealand. *New Zealand Journal of Geology and Geophysics*, 273, pp.351–365.

Suess, E., (1980) Particulate organic carbon flux in the oceans—surface productivity and oxygen utilization. *Nature*, 2885788, pp.260–263.

Sundborg, Å. and Sundborg, A., (1956) The River Klaralven: A Study of Fluvial Processes. *Geografiska Annaler*.

Suthhof, A., Jennerjahn, T.C., Schäfer, P. and Ittekkot, V., (2000) Nature of organic matter in surface sediments from the Pakistan continental margin and the deep Arabian Sea: Amino acids. *Deep-Sea*

Research Part II: Topical Studies in Oceanography.

Switzer, A.D. and Pile, J., (2015) Grain size analysis. In: *Handbook of Sea-Level Research*. pp.331–346.

Tabita, F.R., Hanson, T.E., Satagopan, S., Witte, B.H. and Kreel, N.E., (2008) Phylogenetic and evolutionary relationships of RubisCO and the RubisCO-like proteins and the functional lessons provided by diverse molecular forms. In: *Philosophical Transactions of the Royal Society B: Biological Sciences*.

Tesdal, J.E., Galbraith, E.D. and Kienast, M., (2012) The marine sedimentary nitrogen isotope record. *Biogeosciences Discussions*.

Toucanne, S., Zaragosi, S., Bourillet, J.F., Cremer, M., Eynaud, F., Van Vliet-Lano??, B., Penaud, A., Fontanier, C., Turon, J.L., Cortijo, E. and Gibbard, P.L., (2009) Timing of massive 'Fleuve Manche' discharges over the last 350 kyr: insights into the European ice-sheet oscillations and the European drainage network from MIS 10 to 2. *Quaternary Science Reviews*, 2813–14, pp.1238–1256.

Troupin, C., Barth, A., Sirjacobs, D., Ouberdous, M., Brankart, J.M., Brasseur, P., Rixen, M., Alvera-Azcárate, A., Belounis, M., Capet, A., Lenartz, F., Toussaint, M.E. and Beckers, J.M., (2012) Generation of analysis and consistent error fields using the Data Interpolating Variational Analysis (DIVA). *Ocean Modelling*.

Turnewitsch, R., Reyss, J.L., Nycander, J., Waniek, J.J. and Lampitt, R.S., (2008) Internal tides and sediment dynamics in the deep sea-Evidence from radioactive 234Th/238U disequilibria. *Deep-Sea Research Part I: Oceanographic Research Papers*, 5512, pp.1727–1747.

Twenhofel, W.H., (1933) Treatise on Sedimentation. *The Journal of Physical Chemistry*, 372, pp.261–262.

Tyler, P., Amaro, T., Arzola, R., Cunha, M.R., de Stigter, H., Gooday, A., Huvenne, V., Ingels, J., Kiriakoulakis, K., Lastras, G., Masson, D., Oliveira, A., Pattenden, A., Vanreusel, A., Van Weering, T., Vitorino, J., Witte, U. and Wolff, G., (2009a) Europe's Grand Canyon: Nazaré Submarine Canyon. *Oceanography*, [online] 221, pp.46–57. Available at: http://www.tos.org/oceanography/issues/current.html.

Tyler, P.A., Amaro, T., Arzola, R., Cunha, M.R., de Stigter, H., Gooday, A.J., Huvenne, V., Ingels, J., Kiriakoulakis, K., Lastras, G., Masson, D., Oliveira, A., Pattenden, A., Vanreusel, A., van Weering, T.C.E., Vitorino, J., Witte, U. and Wolff, G.A., (2009b) Europe's Grand Canyon Nazare submarine canyon. *Oceanography*, 221, pp.46–57.

Uk, D.F., Uk, G.F., Zealand, N. and France, M.K., (2013) IPCC AR5. WG1. Chap. 5. Information from paleoclimate archives. *Climate Change 2013 the Physical Science Basis: Working Group I Contribution to the Fifth Assessment Report of the Intergovernmental Panel on Climate Change*, 9781107057, pp.383–464.

Vetter, E.W. and Dayton, P.K., (1999) Organic enrichment by macrophyte detritus, and abundance patterns of megafaunal populations in submarine canyons. *Marine Ecology Progress Series*, 186, pp.137–148.

Vlasenko, V., Stashchuk, N., Inall, M.E. and Hopkins, J.E., (2014) Tidal energy conversion in a global hot spot: On the 3-D dynamics of baroclinic tides at the Celtic Sea shelf break. *Journal of Geophysical Research: Oceans*, 1196, pp.3249–3265.

Voelker, D., (2016) Abyssal plains. In: *Encyclopedia of Earth Sciences Series*. pp.1–5.

Voss, M., Bange, H.W., Dippner, J.W., Middelburg, J.J., Montoya, J.P. and Ward, B., (2013) The marine nitrogen cycle: Recent discoveries, uncertaintiesand the potential relevance of climate

change. *Philosophical Transactions of the Royal Society B: Biological Sciences*.

Wagner, S., Schubotz, F., Kaiser, K., Hallmann, C., Waska, H., Rossel, P.E., Hansman, R., Elvert, M., Middelburg, J.J., Engel, A., Blattmann, T.M., Catalá, T.S., Lennartz, S.T., Gomez-Saez, G. V., Pantoja-Gutiérrez, S., Bao, R. and Galy, V., (2020) *Soothsaying DOM: A Current Perspective on the Future of Oceanic Dissolved Organic Carbon*. *Frontiers in Marine Science*.

Wakeham, S., (2002) Diagenesis of Organic Matter at the Water-Sediment Interface BT - Chemistry of Marine Water and Sediments. In: A. Gianguzza, E. Pelizzetti and S. Sammartano, eds. [online] Berlin, Heidelberg: Springer Berlin Heidelberg, pp.147–164. Available at: https://doi.org/10.1007/978-3-662-04935-8_6.

Wakeham, S.G. and Lee, C., (1989) Organic geochemistry of particulate matter in the ocean : The role of particles in oceanic sedimentary cycles. *Organic Geochemistry*, 14I, pp.83–96.

Walbridge, S., Slocum, N., Pobuda, M. and Wright, D., (2018) *Unified Geomorphological Analysis Workflows with Benthic Terrain Modeler*. *Geosciences (Switzerland)*, .

Wallmann, K., Schneider, B. and Sarnthein, M., (2016) Effects of eustatic sea-level change, ocean dynamics, and nutrient utilization on atmospheric pCO2 and seawater composition over the last 130 000 years: A model study. *Climate of the Past*, 122, pp.339–375.

Walsh, J.J., (1991) Importance of continental margins in the marine biogeochemical cycling of carbon and nitrogen. *Nature*, 3506313, pp.53–55.

Watling, L. and Norse, E.A., (1998) Disturbance of the seabed by mobile fishing gear: A comparison to forest clearcutting. *Conservation Biology*, 126, pp.1180–1197.

Weart, S., (2003) The Carbon Dioxide Greenhouse Effect. In: *The Discovery of Global Warming*. p.240.

van Weering, T., Thomsen, L., Heerwaarden, J., Koster, B. and Viergutz, T., (2000) A seabed lander and new techniques for long term in situ study of deep-sea near bed dynamics. *Sea Technology*, 41, pp.17–27.

Welhan, J.A., (1988) Origins of methane in hydrothermal systems. *Chemical Geology*.

Weltje, G.J., (1997) End-member modeling of compositional data: Numerical-statistical algorithms for solving the explicit mixing problem. *Mathematical Geology*, [online] 294, pp.503–549. Available at: http://link.springer.com/10.1007/BF02775085.

Wentworth, C.K., (1922) A Scale of Grade and Class Terms for Clastic Sediments. *The Journal of Geology*, 305, pp.377–392.

White, H.K., Hsing, P.-Y., Cho, W., Shank, T.M., Cordes, E.E., Quattrini, A.M., Nelson, R.K., Camilli, R., Demopoulos, A.W.J., German, C.R., Brooks, J.M., Roberts, H.H., Shedd, W., Reddy, C.M. and Fisher, C.R., (2012) Impact of the Deepwater Horizon oil spill on a deep-water coral community in the Gulf of Mexico. *Proceedings of the National Academy of Sciences of the United States of America*, 10950, pp.20303–20308.

Wild, C., Jantzen, C., Struck, U., Hoegh-Guldberg, O. and Huettel, M., (2008) Biogeochemical responses following coral mass spawning on the Great Barrier Reef: Pelagic-benthic coupling. *Coral Reefs*.

Wilson, A.M., Kiriakoulakis, K., Raine, R., Gerritsen, H.D., Blackbird, S., Allcock, A.L. and White, M., (2015a) Anthropogenic influence on sediment transport in the Whittard Canyon, NE Atlantic. *Marine pollution bulletin*.

Wilson, A.M., Kiriakoulakis, K., Raine, R., Gerritsen, H.D., Blackbird, S., Allcock, A.L. and White, M., (2015b) Anthropogenic influence on sediment transport in the Whittard Canyon, NE Atlantic. *Marine Pollution Bulletin*, [online] 1011, pp.320–329. Available at: http://linkinghub.elsevier.com/retrieve/pii/S0025326X15301405 [Accessed 9 Mar. 2017].

Wilson, A.M., Raine, R., Mohn, C. and White, M., (2015c) Nepheloid layer distribution in the Whittard Canyon, NE Atlantic Margin. *Marine Geology*, [online] 367, pp.130–142. Available at: http://www.sciencedirect.com/science/article/pii/S0025322715001243.

Wilson, A.M., Raine, R., Mohn, C. and White, M., (2015d) Nepheloid layer distribution in the Whittard Canyon, NE Atlantic Margin. *Marine Geology*.

Wilson, M.F.J., O'Connell, B., Brown, C., Guinan, J.C. and Grehan, A.J., (2007) Multiscale terrain analysis of multibeam bathymetry data for habitat mapping on the continental slope. *Marine Geodesy*, 301–2, pp.3–35.

Winterer, E.L., (2012) 19 - Pelagic realms. In: D.G. Roberts and A.W.B.T.-R.G. and T.P. of G.A. Bally, eds. [online] Amsterdam: Elsevier, pp.538–551. Available at: http://www.sciencedirect.com/science/article/pii/B9780444530424000194.

Wölfl, A.C., Snaith, H., Amirebrahimi, S., Devey, C.W., Dorschel, B., Ferrini, V., Huvenne, V.A.I., Jakobsson, M., Jencks, J., Johnston, G., Lamarche, G., Mayer, L., Millar, D., Pedersen, T.H., Picard, K., Reitz, A., Schmitt, T., Visbeck, M., Weatherall, P. and Wigley, R., (2019) *Seafloor mapping - The challenge of a truly global ocean bathymetry*. *Frontiers in Marine Science*, .

Woosley, R.J., (2018) Carbonate Compensation Depth. In: W.M. White, ed., *Encyclopedia of Geochemistry: A Comprehensive Reference Source on the Chemistry of the Earth*. Cham: Springer International Publishing, pp.204–205.

Yu, S.Y., Colman, S.M. and Li, L., (2016) BEMMA: A Hierarchical Bayesian End-Member Modeling Analysis of Sediment Grain-Size Distributions. *Mathematical Geosciences*, 486, pp.723–741.

Zaragosi, S., Bourillet, J.F., Eynaud, F., Toucanne, S., Denhard, B., Van Toer, A. and Lanfumey, V., (2006) The impact of the last European deglaciation on the deep-sea turbidite systems of the Celtic-Armorican margin (Bay of Biscay). *Geo-Marine Letters*.

APPENDIX 1

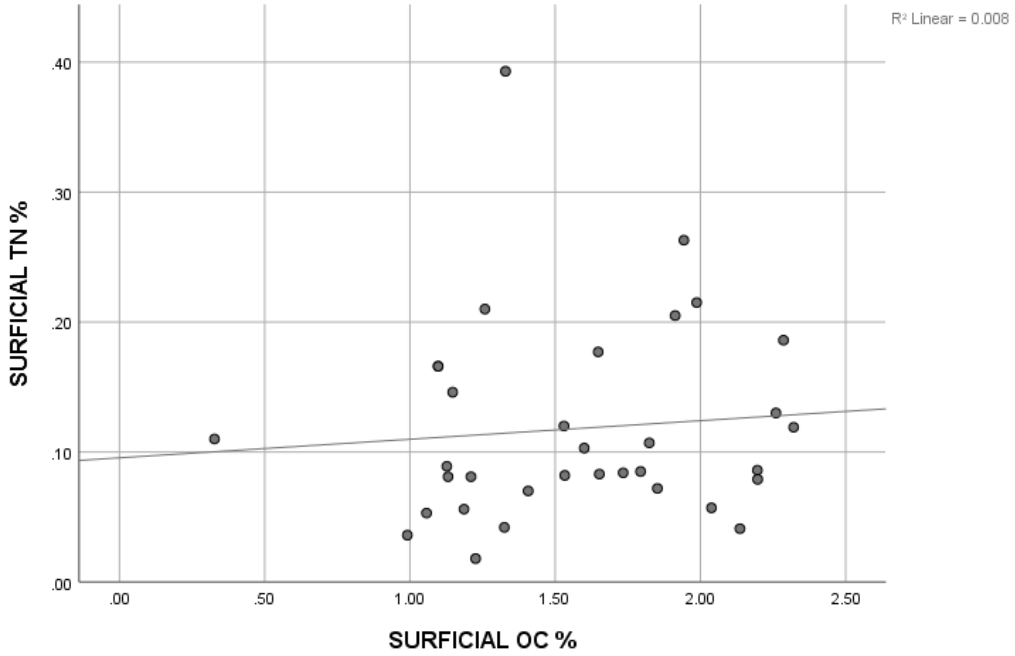

Appendix 1 Cross plot that indicates possible preferential degradation of nitrogen or trapped inorganic nitrogen.